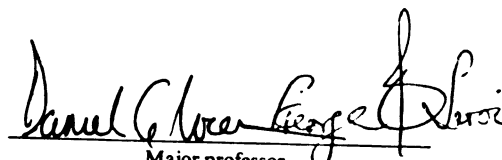This is to certify that the

dissertation entitled

Luminescent Cyclodextrin Supramolecular Recognition
Sites for Optical Chemosensing

presented by

Wanda K. Hartmann

has been accepted towards fulfillment
of the requirements for

_____Ph.D._____ degree in ___Chemistry___

_____
Major professor

Date___29 July 1997_____

0-12771

LIBRARY
Michigan State
University

DATE DUE	DATE DUE	DATE DUE

LUMINESCENT CYCLODEXTRIN SUPRAMOLCULAR RECOGNITION SITES
FOR OPTICAL CHEMOSENSING

By

Wanda K. Hartmann

A DISSERTATION

Submitted to
Michigan State University
in partial fulfillment of the requirements
for the degree of

DOCTOR OF PHILOSOPHY

Department of Chemistry

1997

ABSTRACT

LUMINESCENT CYCLODEXTRIN SUPRAMOLCULAR RECOGNITION SITES FOR OPTICAL CHEMOSENSING

By

Wanda K. Hartmann

Novel physical and chemical processes can be studied with supramolecular assemblies. Molecular recognition allows one to design an active site in a supramolecular assembly to target an analyte for chemical sensing applications. Supramolecular assemblies can be designed for chemical sensing that ranges from monitoring of environmental contaminants such as benzene to medically relevant analytes such as glucose, pH, and blood gases. One class of molecule that is useful in designing a supramolecular assembly is a cyclodextrin (CD); CDs have a hydrophobic cavity that binds molecules that are insoluble in water. We have used the hydrophobic pocket to bind chromophores and lumophores that are used for triggering a luminescent optical signal in the presence of analytes. One supramolecule designed in our laboratory triggers phosphorescence of 1-bromonaphthalene (1-BrNp) upon formation of a ternary complex with hydrogen-bonding substrates (alcohols) and cyclodextrin (Chapters 2-4). A second active site that is suitable for an optical sensor for sensing of aromatic hydrocarbons (benzene, toluene, xylene, biphenyl, naphthalene) is also discussed in detail (Chapters 5 and 6).

To my brother and parents.

ACKNOWLEDGMENTS

The Nocera and Leroi group, Adrian, Al Barney, Ann, Claudia, Dan, Dimitris, Eric, Janice, Jean, Jeff, Jerry, JP, Jude, Mark Mortellaro, Mark Torgerson, Niels, Sara, Tom, Zoe and, most of all, Jim have been a very supportive research group. First and foremost I would like to thank Adrian Ponce, who taught me the tools of the trade. Mark and Jude were also especially helpful in teaching me organic chemistry and cyclodextrin synthesis. I am especially indebted to them. Thanks to my other coworkers Professor Peter Wong (Andrews University), Jeong-Uk Kim, and undergraduates, Mike Gray and John Flenner. Last and most importantly, Jim has helped me through the most difficult times in graduate school and helped me to believe in myself.

I would like to give a personal thanks to my cousin Theresa, my godmother Maria Weiner and all of my aunts (especially Cathy, Margie, Marie and Betty) and especially my uncles Richard and Larry. I would like to thank my friends Lisa, Natsuko, Marie, Melissa and Tara and all the friends I made at M.S.U. My father and brother have always encouraged me to do my best. I am fortunate to have a wonderful family.

Lastly, I would like to acknowledge all those family members and friends who have passed away, especially Chris Serafin and my mother, both of whom died at the very young age of 35. I will always remember how hard my mother fought in her battle against lung cancer and the courage that she inspired in me.

TABLE OF CONTENTS

LIST OF FIGURES

LIST OF TABLES

CHAPTER 1

INTRODUCTION

The modern world has seen an explosion of the chemical industry as it responds to an increased global population. With industrialization, humankind has put an enormous environmental demand on the global ecosystem, resulting in significant levels of air, water and soil pollution [1]. In the past few decades, significant efforts have been devoted to seeking out and remediating geographical areas polluted by gaseous emissions, organic waste, heavy metals and pesticides from manufacturing and other sources. The Comprehensive Environmental Response, Compensation and Liability Act or "Superfund" of 1980 was signed into law to address the issue of cleaning up inactive hazardous waste sites [2].

Of the contaminants found in land pollution, some of the largest contributions are from industrial solvents and wastes including polycyclic aromatic hydrocarbons (PAHs), polychlorinated biphenyls (PCBs), trichloroethylene (TCE), benzene, toluene, xylene

(BTX), and halogenated hydrocarbons [3]. The common properties of these molecules are their hydrophobicity and the presence, generally, of a halogen heavy atom (F, Cl). A goal of this dissertation is to exploit these properties to selectively design active recognition sites to detect these environmental contaminants by optical transduction means.

Chemosensing extends beyond the realm of environmental applications. Another potential application for optical chemical sensors is for the control of advanced systems [4]. Industrial processes require monitoring of manufacturing, processing and operation of large plants. A wide variety of sensors can be implemented to monitor these processes. For instance, a modern automobile requires a great deal of technology that is related to sensors. There are over 24 sensing functions that measure operations of only the engine and the transmission of an automobile [5]. In addition to physical sensors found in the engine, some of the chemicals of interest in sensing applications are alcohols such as ethanol and methanol used in fuel blends; also concentrations of exhaust gas oxygen (EGO) must be monitored. Although there are currently sensors available for oxygen based on zirconia [6] and titania [7], these sensors are based on electrical signals (voltage is proportional to a logarithmic function of oxygen partial pressures between exhaust gas and ambient air) and indicate only the transition from oxygen rich to oxygen lean fuel burning; i.e., they do not give an indication of the concentration of oxygen present in the exhaust gas. Ideally, one would like to be able to determine the exact oxygen to fuel ratio. Given the electrically noisy environment of an automobile, it is also preferable to use an electrically quiet transduction mechanism.

A chemical sensing active site (sometimes called chemosensor) can be classified by the property used to detect the target molecule. The word sensor is derived from the human senses of sight, taste, touch and smell. More specifically, a sensor is referred to as a transducer, "a device which provides a usable output in response to a specified measurand [8]." The output is typically an electrical quantity and the measurand is a physical quantity, property or condition. Chemical sensing can be achieved by various transduction methods involving conductivites, potentials, capacities, heats and masses of a sensor when an analyte is present. However, with the advent of advanced fiber optic technologies, spurred by advances in the communications industry, potentially the most powerful transduction mechanism for chemical sensors is optical [9-10].

Molecule-based optical sensing schemes can report on nanometer-length scales with nanosecond time responses and continuously monitor analytes and their influences in real-time. They possess an inherently large bandwidth (and hence information capacity), feature intrinsic selectivity owing to choices of wavelength and polarization, and can be married to a variety of imaging technologies, including optical wave guides, the most important of which are optical fibers. The latter issue has been the primary driving force behind the emergence of optical sensing schemes in recent years [11-13]. Fiber optic sensors (sometimes called optodes) permit "wireless" communication between the detection element and the analyte, making them particularly attractive for *in situ* remote sensing applications. Moreover, because signals of many different wavelengths can propagate in either direction within a optical fiber, sensor arrays with multiple sensing capabilities may be constructed.

Optical Sensing: Turn On vs. Quenching Detection of Light from Excited States

Optical sensing is based on physical and chemical properties of excited states. Molecules normally reside in dark or ground states and enter excited states upon absorption of energy from the environment. Electronic excited states result typically from absorption of ultraviolet or visible light. They are generally very reactive and will eventually return to the original ground state or react photochemically, resulting in a different product ground state molecule (P) (in Figure 1). The departure of the molecule from the excited state may occur in the absence of a reacting partner molecule (intramolecular decay) or in the presence of a second molecule (intermolecular decay). Because emitted light is more easily detected than changes in transmitted light, luminescence detection schemes are generally implemented with greater facility than absorption schemes, especially when the signal is proportional to the intensity of the light [14,15].

Figure 1 shows the intramolecular decay processes for an isolated excited state molecule (M^*). Competing thermal emission and photon emission pathways for the overall excited state decay are described by the non-radiative and radiative rate constants, k_{nr} and k_r, respectively. The radiative rate constant is an intrinsic property of the molecule itself and is related to the absorption cross-section [16]. All decay pathways that do not lead to photon emission are included in the non-radiative rate constant. Typically, non-radiative decay entails the conversion of the electronic energy of the excited state into high energy vibrations of the ground state molecule. Relaxation to the vibrationally equilibrated ground state molecule is accompanied by the concomitant release of heat (k_{nr}); alternatively, the excess vibrational energy may be manifested in the creation of a
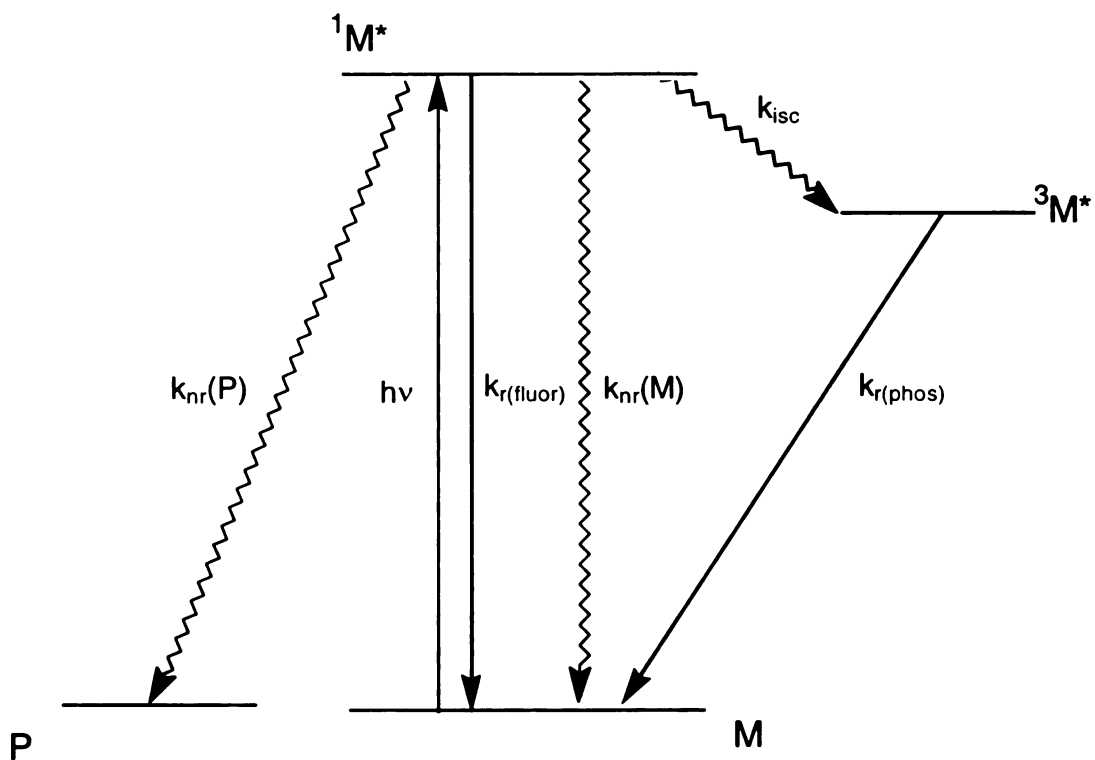
Figure 1. Electronic state diagram. M, ^{1}M* and ^{3}M* and denote the ground, singlet excited state and triplet excited state of a molecule, respectively. The photochemical product is P.

different ground state molecule ($k_{nr}(P)$). The overall non-radiative decay rate constant, k_{nr}, is simply the sum of $k_{nr}(M)$ and $k_{nr}(P)$.

The radiative and non-radiative rate constants are important because they define the fundamental properties of molecules in excited states [16]. The intensity of luminescence, I_e, is directly dependent on the luminescence efficiency, usually called the emission quantum yield, ϕ_e, which is the ratio of the number of photons emitted per photons absorbed. The emission quantum yield is directly related to k_r and k_{nr} by the following expression,

$$I_e \approx \phi_e = \frac{k_r}{k_r + k_{nr}} = k_r \tau_0 \tag{1}$$

where τ_0 is the observed lifetime of the electronic excited state. Usually, the non-radiative relaxation pathways dominate, $k_{nr} >> k_r$, and as can be seen from Eq. (1) molecules remain dark upon excitation. However, when thermal emission is inefficient with respect to photon emission, excited states will literally light up or luminescence. The excited state molecule is termed a lumophore, which is a general term for an emissive molecule.

In the presence of a reacting partner, the emission intensity of the excited state of the indicator molecule, I_e, is related to the quantum yield, ϕ_e, by the following equation [17, 18]:

$$I_e \approx \phi_e = \frac{k_r}{k_r + k_{nr} + k_q[Q]} \tag{2}$$

where k_r is the radiative rate constant, k_{nr} the non-radiative rate constant, k_q the quenching rate constant of the excited state molecule and $[Q]$ is the concentration of the quencher molecule. Many chemosensing schemes detect the presence of an analyte by quenching

the luminescence of an active site. Detection occurs when the last term in the denominator ($k_q[Q]$) increases in the presence of an analyte. This leads to an overall attenuation of visible light signal in the presence of increasing concentrations of analyte [19]. Consequently, schemes whose function is derived from quenching mechanisms are hampered by the necessity to detect small differences in luminescence intensity relative to a high background. In addition, selectivity is compromised because excited states are highly energetic and thus may be quenched by a variety of analytes.

A goal of our research in recent years has been to generalize the design of chemosensing schemes based on a triggered luminescence response so that the approach can be used to detect a variety of neutral and charged analytes. Our strategy centers on synthesizing supramolecules containing multiple sites of complementary function. The analyte is detecting an increase in visible phosphorescence or luminescence from a dark background [20]. At one site is a photoactive center capable of emitting visible light; at the other is a docking site for the analyte. Our work is based on perturbing the rate processes of an excited state center by an analyte. The fundamental parameters governing the luminescence intensity of the photoactive center are manipulated such that the molecular recognition of the analyte at the docking site causes $k_r \gg k_{nr}$ and k_q; this condition is met by increasing the effective k_r, decreasing k_{nr} or decreasing k_q upon the molecular recognition of analyte by the supramolecule. In this manner, ϕ_e approaches its theoretical limiting value of unity, and thus bright luminescence from the photoactive center heralds the presence of an analyte in the supramolecule's environment.

Intersystem Crossing of Excited States

The photoactive molecules used in our optical sensing schemes are organic aromatic systems. The first excited state of most organic molecules is a singlet state, where there are no unpaired electron spins. The radiative emission from a singlet excited state, fluorescence, is very short lived (nanoseconds) and typically occurs in the ultraviolet (higher energy) region of the electromagnetic spectrum. For these two reasons, optical sensing by detection of fluorescence is not desirable. Our approach uses longer lived and visible (500 – 700 nm) phosphorescence from supramolecular assemblies to detect analytes. However, to reach triplet excited states (electronic states with two electrons possessing parallel spins) and higher order spin states (luminescent states) an excited state molecule typically passes through the singlet state, and one or more electrons must undergo a spin flip. This non-radiative processes of an excited state molecule traveling between electronic excited states of different spin multiplicities is termed intersystem crossing.

The rates of intersystem crossing must be faster than fluorescence in order to promote population of excited states that will lead to phosphorescence or luminescence. However, aromatic hydrocarbons such as PAHs and BTXs, have comparatively slow intersystem crossing rates (k_{ST} = 10^8 - 10^6 s^{-1}), which are considerably smaller in magnitude than the values for molecules with a "heavy atom" (k_{ST}(bromonaphthalene) = $10^9 s^{-1}$) or n,π* excited states (k_{ST}(benzophenone) = 10^{11} s^{-1}) [21]. The three factors that contribute to the magnitude of the intersystem crossing rate are the electronic configuration of the two states, the energy gap between the two states (S_1 and T_1)

involved in the non-radiative transition, and the spin-orbit coupling between the two states.

Coulombic and exchange interactions are responsible for the energy gap between the triplet and singlet states. The energy gap is inversely related to the magnitude of intersystem crossing rates, as is true for many radiationless processes. The energies of the ground state, first excited singlet and first excited triplet of a generic aromatic hydrocarbon with π,π^* states are given below [17,21]:

$$E(S_0)=0 \tag{3}$$

$$E(S_1)= E(\pi,\pi^*) + J(\pi,\pi^*) + K(\pi,\pi^*) \tag{4}$$

$$E(T_1)= E(\pi,\pi^*) + J(\pi,\pi^*) - K(\pi,\pi^*) \tag{5}$$

where J is the coulombic repulsion and K is the electron exchange repulsion. Therefore, $\Delta E(S_1-T_1) = 2K(\pi,\pi^*) > 0$. The smaller splittings for n,π^* states compared to π,π^* states is one explanation for faster intersystem crossing in aromatic hydrocarbons containing a ketone group such acetylacetonates and carboxylates. The singlet-triplet excited state energy gap decreases and the rate of intersystem crossing increases along the series: benzene ($\Delta E(S_1-T_1)$ = 40 kcal/mol), naphthalene (35 kcal/mol) and anthracene (30 kcal/mol) [17].

In addition to the effects of the energy gap between the singlet and triplet states, spin-orbit coupling of internal and external heavy atoms will increase intersystem crossing. Spin-orbit coupling arises when a magnetic moment is created from the intrinsic

spin of an electron. The Hamiltonian for spin-orbit coupling in a many-electron field is given by the sum of the terms for the individual electrons [21],

$$H_{SO} = \sum_i \frac{Ze^2}{4m^2c^2} \frac{1}{r_i^3} l_i s_i \tag{6}$$

where Z is the atomic number, e is the charge of an electron, m is the electronic mass, c is the velocity of light, r is the distance between the heavy atom and the electron being perturbed, and l and s are the electron's orbital and spin quantum numbers. The dependence on Z is the heavy atom effect and is dependent on the Coulomb nature of the field created.

The rates of intersystem crossing via spin-orbit coupling of aromatic hydrocarbons (BTXs, PAHs, phosphor active sites) can be affected by an internal heavy atom (e.g. bromine or iodine) or external heavy atom (e.g. lanthanide ions). Heavy halogens (Cl, Br, I) and lanthanide ions such as Eu^{3+}, Gd^{3+} and Tb^{3+} promote intersystem crossing through a spin-orbit coupling process. In general, the heavy atom effect will act to decrease ϕ_F (fluorescence quantum yield) and increase ϕ_{isc} if the rate of intersystem crossing is comparable to the rate of fluorescence. However, the increase or decrease of ϕ_P (phosphorescence quantum yield) and ϕ_{TS} (triplet to singlet quantum yield) will depend on how k_P and k_{TS} (rate of triplet conversion to ground state) are influenced by the heavy atom. The maximum heavy atom effect that can be induced by bromine substitution is k_{isc} = 10^8 - 10^9 s^{-1} [17]. We will use the heavy atom bromine to induce intersystem crossing in our phosphor supramolecular assembly for alcohol detection.

Supramolecular Assemblies

Our approach to designing optical sensors is to build a supramolecular assembly where different molecular structural sites have an complimentary optical functions. Jean-Marie Lehn, one of the founders of the field of supramolecular chemistry, defines the field as encompassing the study of "chemical species of greater complexity than molecules themselves, that are held together and organized by means of intermolecular (non-covalent) binding interactions [22]." Because a supramolecule is held together by intermolecular bonds this imparts selective binding and molecular recognition of substrates by a molecular receptor. The receptors are designed to posses steric and electronic features that complement the target substrate molecule, balancing enough flexibility for the function to be performed. Molecular recognition implies binding and selection of a substrate by a receptor, which in most cases leads to a specific function. Some of the functions are changes in the electronic, ionic, optical or conformational properties, thereby generating a signal at the molecular level.

There are many sizes and shapes of receptor molecules ranging from spherical to tetrahedral, linear to branched, charged to neutral, organic to inorganic to biological. Chemists have learned to sculpt molecules into shapes ranging from molecular bracelets to tiny pagodas. Some of the exotic molecules are (Figure 2): boxes [23], butterflies [24], calixes [25], carcerands [26], cavitands [27], clefts [28], crowns [29], cryptands [30], cyclophanes [31], footballene [32], gondolas [33], hinges [34], ladders [35], octopus [36], pagodanes [37], scorpiands [38], sepulchrands [39], speleands [40], spherands [41],torands [42], tweezers [43-44], vessels [27] and wires [45].

a

b

c

d

e

f

g

h
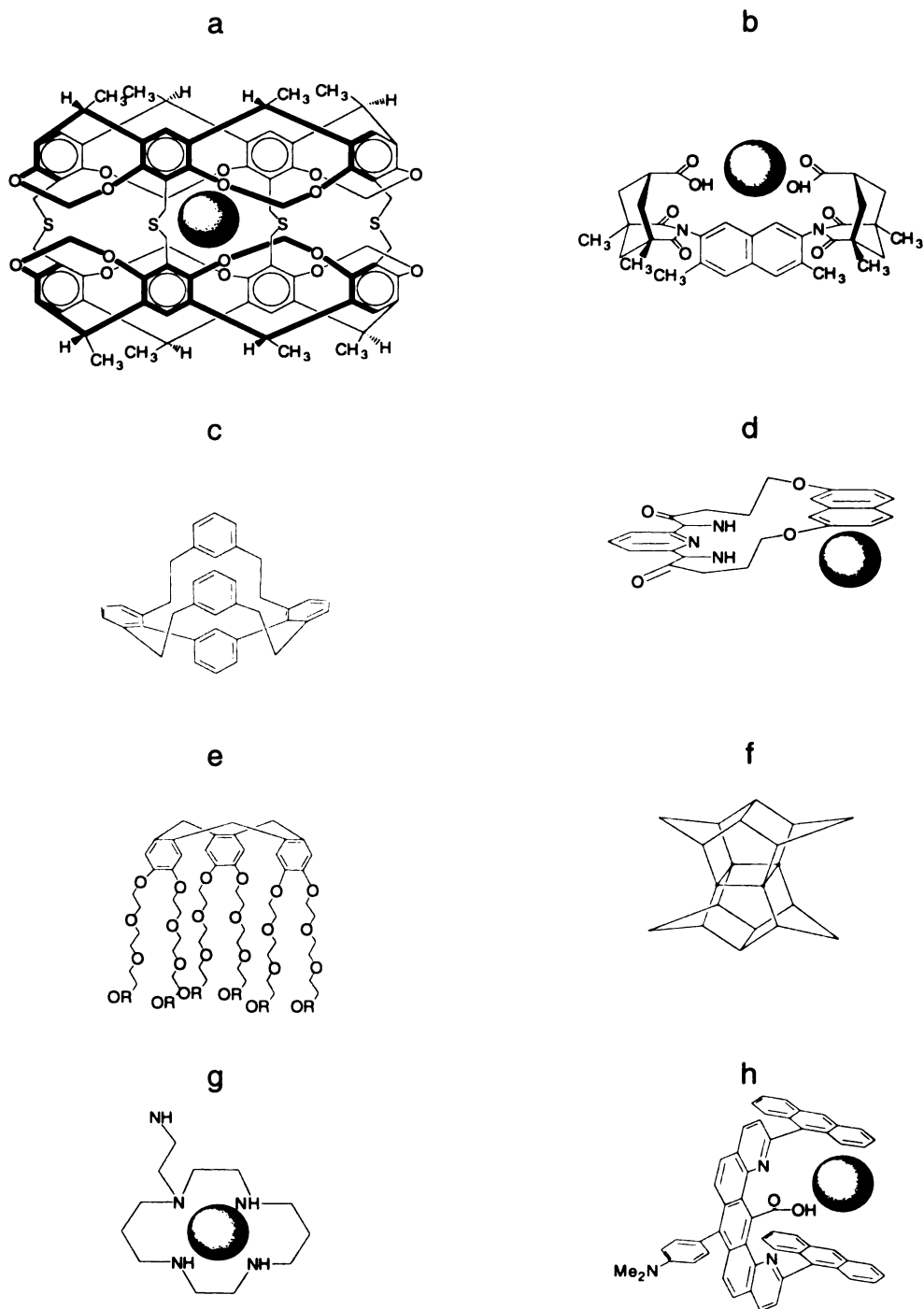
Figure 2. Supramolecules: (a) carcerand with a guest molecule in the cavity shown in gray (b) molecular cleft with guest molecule (c) molecular gondola (d) molecular hinge with host (e) molecular octopus (f) pagodane ($C_{20}H_{20}$) (g) scorpiand with guest (h) molecular tweezer with guest.

Whereas some of these molecules are merely attractive (such as the pagodane), others can act as receptors for guests by relying on an elaborate network of intermolecular bonds. For instance, the carcerand is a hollow cylindrically shaped host molecule that possesses an interior cavity that may trap simple organic molecules, gases and inorganic ions (Figure 2a). This cavity provides an interesting environment with unique physical and chemical properties.

Various types of substrates can be recognized by deliberate design of the supramolecular assembly. The assemblies are held together by hydrogen bonding, hydrophobic and electrostatic interactions. Tetrahedral, anionic, cationic, linear and multiple recognition sites can be fused into the supramolecular backbone. Several examples are given in Figure 3. The top four molecules of this figure are derivatives of cryptands. The smaller cryptands can host small cations such as the tetrahedral ammonium ion or spherical sodium cation, or they can host ellipsoidal negative ions N_3^-. In some cases cryptands have enough space and coordination sites for two metal cation guests (Figure 3d). The speleand shown in Figure 3e optimizes two sites, an aromatic portion which supplies a hydrophobic interaction and an aza crown ether providing a site for binding a positive charge. These two recognition sites are ideal for binding molecules such as methyl amine. Lastly, the cyclophane derivative shown in Figure 3f combines binding by intercalation and electrostatic charge [22].

Other supramolecules converge to provide a platform for guest molecules. The molecular cleft (Figure 2b) can interact via its carboxylic acid groups thereby to bind molecules by hydrogen bonding interactions. Metal ions and neutral substrates will also

a

b

c

d

e

f
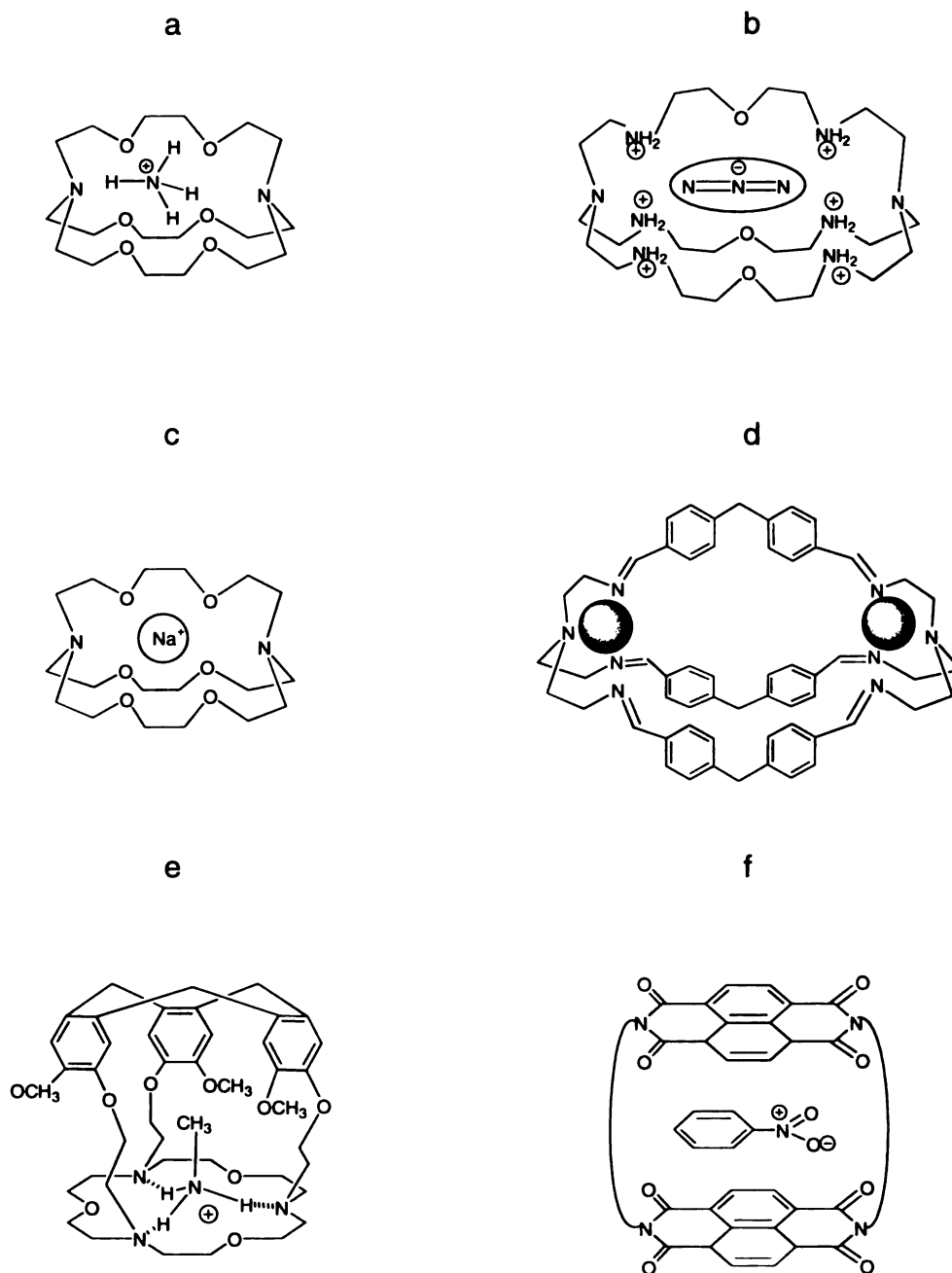
Figure 3. Supramolecular encapsulation of a tetrahedral ammonium ion, N_3^-, sodium ion and multiple ions in cryptands (a-d). Methylamine guests in an amphiphilic speleand and nitrobenzene cyclointercaland in a cyclophane (e-f).

bind to the cleft. The size of the cleft can be made larger or smaller by substituting the naphthyl ring with a benzyl or anthryl ring to impart size selectivity. Molecular hinges and tweezers (Figure 2 d,h) also recognize substrates by hydrogen bonding as well as π-stacking intercalating interactions. Nucleic acid guests, such as 1-butyl-thymine and adenine, bind to the molecular hinges and clefts. Molecules such as the gondola, octopus scorpiand and (Figure 2 c,e,g) are closely related to the cyclophane, cryptand and speleand supramolecules shown in Figure 3 and can also be used to capture guest molecules.

Supramolecular assemblies can be used to make molecular devices based on the manipulation of photons, electrons and ions, incorporate photosensitive groups for light conversion and charge separation, be employed as catalysts, use redox active moieties to make molecular wires and ion channels, form helices and other higher order structures based on self-assembly, and finally supramolecules can be used for recognition reaction, translocation, transformation and regulation [22c]. Supramolecular species can transport amino acids, metal cations, anions across membranes, transport electrons in a redox gradient and protons in pH gradients and drive light transport. Our interest centers on controlling and manipulating light transport to design optical based chemical sensors, where the substrate is the analyte of interest and the receptor is the active site of the sensor. The structure of the chemical sensor is critical in determining the outcome of the function, because it triggers the visible optical signal.

The most prolific work on chemical sensor design, which incorporates highly specific membranes and selective receptors, comes from the laboratories of Göpel and coworkers [46]. Some examples of such sensors are those that operate by chemically

sensitive field effect transistors (CHEMFET) [47] and light-addressable potentiometry (LAP) [48]. Sensor arrays and neural networks are also being developed that will target a collection of substrates, with a specific pattern for each compound [46c-d]. Self-assembled monolayers of cavitand receptors on gold surfaces have been examined that are selective for perchloroethylene (C_2Cl_4) [22a]. Many of the supramolecular chemosensors operate by transduction of electrical and mass signals, which are subject to more noise interferences than the optical methods being investigated in our laboratory.

Building a Supramolecule from a Cyclodextrin Bucket

Supramolecular chemosensors must be built around the receptacle that will capture the substrate. This container must be invisible to light, to avoid an interfering signal emanating from this component of the supramolecule. Because we are interested in chemosensing of hydrophobic molecules (PAHs and BTXs) as well as those involving hydrogen-bonding substrates (alcohols), we require a molecule whose structure will bind the analyte with hydrophobic and/or hydrogen-bonding interactions. There are many molecules that have a hydrophobic cavity (calixarenes, cavitands, hemicarcerands, speleands, and cyclodextrins). However, there are few that meet our specification of optical transparency. One such supramolecular template is a cyclodextrin (CD).

There are many reviews of cyclodextrins and 7000 publications between 1979 and 1994 [49-52] as well as two texts [53,54]. Cyclodextrins are simple and inexpensive to produce by the fermentation of starch and are soluble in methanol, ethanol, dimethyl sulfoxide, dimethylformamide, N,N-dimethylacetamide, pyridine and, most importantly, in water. They are versatile molecules because they are chemically stable, non-reducing,

non-toxic, biodegradable and chiral. Cyclodextrins are active catalysts, used to study weak interactions and are used to encapsulate drugs, perfumes and flavorings.

A cyclodextrin is one of the few molecules that has, in addition to the hydrophobic pocket, hydrophilic rims available for hydrogen-bonding and water solublization, and can be modified regioselectively on the primary or secondary side (see Figure 4). There are three sizes of cyclodextrins, α-, β-, and γ-CD, which have 6-, 7-, and 8-glucose units. We have chosen the mid-sized β-CD for designing a chemosensor site for an optical sensor, as it is an ideal size for mono- and bicyclic aromatic hydrocarbons. The narrow primary hydroxyl rim has seven hydroxyl groups (on carbon number 6, C6, of the glucose group) available for functionalization, whereas the wider secondary side has 14 hydroxyl groups attached to secondary carbons (C2 and C3). If we desire further size selectivity, we can use the α-CD for monocyclic aromatic hydrocarbons (BTXs) and the γ-CD for larger PAHs. In the first study described in this dissertation, glucosyl-β-CD was used as a cyclodextrin host. β-CD derivatized with a glucosyl (Gβ-CD) attached to the primary hydroxyl rim via a 1-6 linkage is a better host structure than underivatized β-CD because of its increased (40-fold) water solubility [55]. The binding of guests to the glucosyl derivatized CD cup is only marginally attenuated when compared with underivatized β-CD.

A cyclodextrin is transparent to excitation in the ultraviolet and visible regions of the electromagnetic spectrum, as it is replete with saturated carbon-carbon bonds.
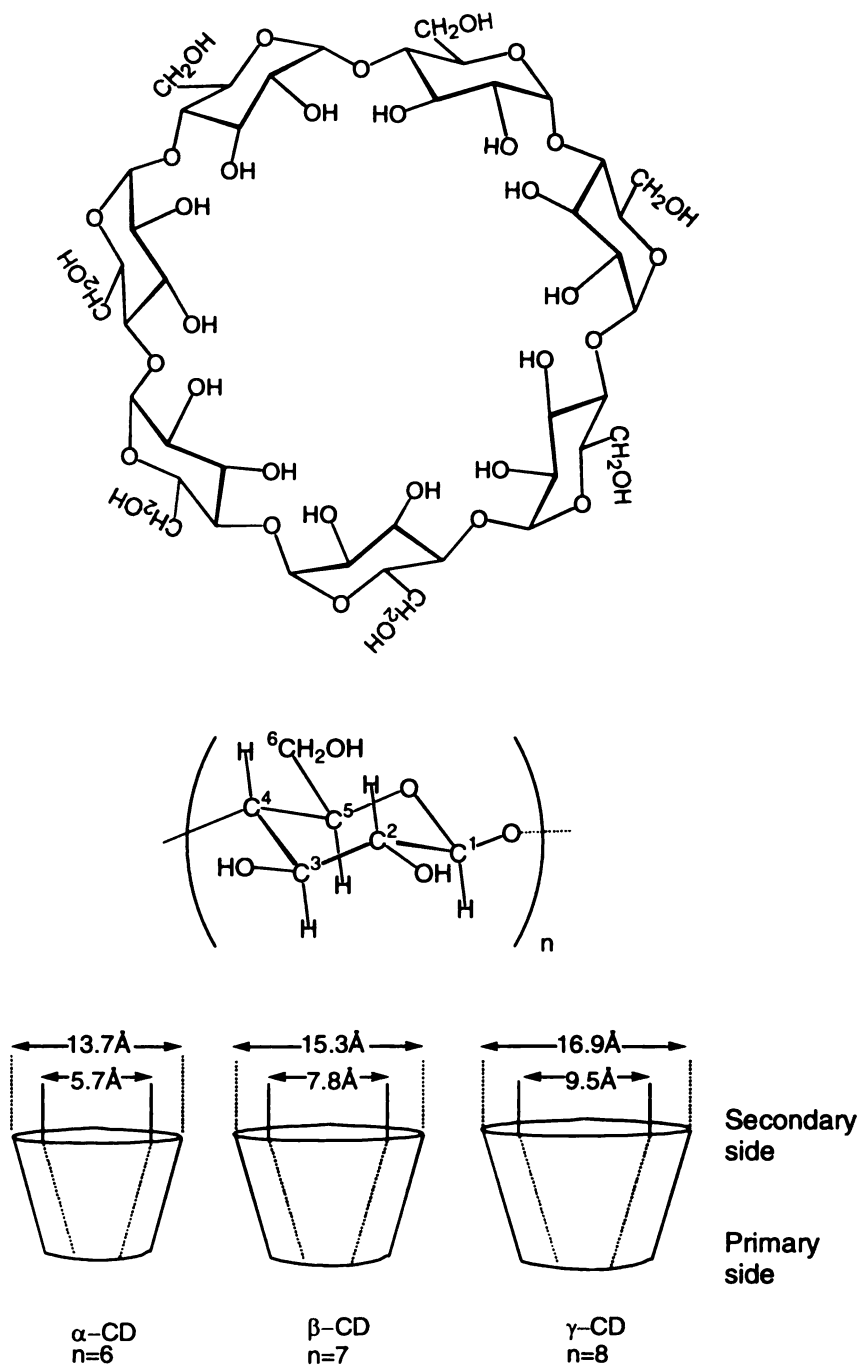
Figure 4. Cyclodextrins with a hydrophobic cavity, hydrophilic rims and three sizes of cavities. Shown in the middle is the glucose unit with the carbon atoms labeled with the standard notation.

This property is advantageous in our studies of photophysical properties of supramolecular assemblies that employ components that will absorb and emit light in ultraviolet and visible wavelengths. Yet another advantageous property of a cyclodextrin supramolecular system is the distance constraint imposed when several chemical species are brought together by intermolecular forces. In solution, the distance over which these interactions can dominate is too long to be efficient. We plan to use the distance restrictions of a cyclodextrin to enforce properties that are distance dependent, such as spin-orbit coupling from external heavy atoms and electronic energy transfer.

Guest molecules form inclusion complexes with cyclodextrins upon binding to the hydrophobic cavity. The driving force for binding is the expulsion of energetic water molecules from the CD cavity and replacement by a guest molecule. Although they bind neutral molecules, cyclodextrins are polar molecules, where β-CD has a dipole moment two-thirds the magnitude of α-CD (12-13 D) [56-57]. Cyclodextrins are electrophilic molecules, and nucleophilic bases bind to their cavities. The strongest bases form the most stable complexes with CDs. However, apolar molecules will also bind to the cavity, as inclusion will induce a dipole moment in the guest molecule. Polarizability is a crucial factor in determining complex formation. Inclusion complexes of photoactive molecules such as methyl orange [58], crystal violet [59], methylene blue [60], dansyl [61] and 1-anilinonaphthalene-8-sulfonate (ANS) [62] have been examined with cyclodextrin. The binding of dye molecules causes a change in the absorption spectrum as well as change in the pH.

Two Optical Strategies for Chemical Sensing

Schematic diagrams of two optical strategies we have designed for use as active sites in optical chemosensors are shown in Figure 5. At the top of the figure is the template for an AICE (Absorption-Intersystem Crossing-Emission) process used for optical sensing of alcohols. The supramolecular chemosensor is based on self-assembly of a ternary system. The foundation of the supramolecule is a water soluble glucosyl-β-CD with a cavity size that is ideal for inclusion of a phosphor molecule. The glucosyl attachment imparts water solubility to an otherwise less soluble β-CD. A hydrophobic interaction holds the phosphor in the water repelling cavity. The phosphor is directly excited with ultraviolet light to create a singlet excited state. Although the phosphor has an inherently large intersystem crossing rate between the singlet and triplet states, oxygen gas present in aerated aqueous solutions is able to quench the vulnerable phosphor excited state at primary and secondary openings of the cyclodextrin basket. Migrating at the rate of diffusion ($k_D = 10^9$ s^{-1}), oxygen non-radiatively quenches or steals the phospor's excited state energy before it arrives at the ground state by radiative decay. Phosphorescence (emission from the first triplet state to the ground singlet state) is typically a slow process, as the electronic transition is dipole forbidden. Thus, the phosphor, although included in the cyclodextrin cavity, is unable to emit light due to the rapidity of oxygen quenching. We have exploited the shortcomings of the phosphor cyclodextrin complex by adding a third molecule that inhibits diffusion of oxygen to the phosphor. The third molecule is an alcohol substrate, which is recognized by the cyclodextrin rims by an intermolecular hydrogen bond. The structure of the alcohol allows bitopic or two-site recognition by the cyclodextrin receptor.

Components   *Processes*

hv

Binding Properties

Binding Site for
Phosphor

Topology of Complex

Cyclodextrin

hv'

Quantum Yield of Phosphor

Binding Site for Alcohol
or other substrate

RX

X

Oxygen Quenching Rate Constant

$^3O_2$ $^1O_2$

Components   *Processes*

hv

Binding Properties

Binding Site for
Aromatic Hydrocarbon

Absorption of aromatic donor

Cyclodextrin

Energy Transfer

Binding Site for
Lanthanide Ion

Photophysics of Ln^{3+} acceptor

hv'

Figure 5. Three component multiprocess supramolecular assemblies for optical sensing (a) Absorption-Intersystem Crossing-Emission (AICE), where RX is a hydrogen-bonding substrate. (b) Absorption-Energy Transfer-Emission (AETE).

The unique structure of this molecular basket results in bright, glowing emission from the phosphor, which can efficiently radiate energy from the triplet state, and results in a triggered photonic signal. The lock and key structure of the ternary complex permits us to effect an optical functionality. These results will be described in Chapters 2-4.

Chapters 5 and 6 describe another molecular architecture that has been designed for optical chemosensing derived from a β-cyclodextrin (Figure 5b). The specific cyclodextrin receptor used for sensing of BTXs and PAHs also has a bitopic structure that allows recognition of the analyte substrate and of a lumophore. The hydrophobic cavity in this case does not hold the lumophore, but instead acts to capture the substrate, a light absorber. On the narrow end of the cyclodextrin bucket, a macrocyclic ligand containing chelating nitrogens and oxygens has been tethered. This ligand acts as a binding site for metal lumophore ions. The macrocycle also prevents water from entering the coordination sphere of the ion, thereby decreasing k_{nr} of the lumophore. The metal ion coordinated to the cyclodextrin macrocycle has an intrinsically low absorption cross-section, and therefore, when it is directly excited with ultraviolet light, the excited state luminesces weakly. Molecular recognition of a BTX or PAH by the cyclodextrin's cavity greatly enhances the population of the upper state of the lumophore by energy transfer, and intense triggered excited state emission is observed. This process of absorption by the BTX, energy transfer across the interior cavity of the cyclodextrin, and emission by the lumophore ion is termed AETE (Absorption-Energy Transfer-Emission). The shortened distance between the aromatic hydrocarbons and the lumophore imposed by the cyclodextrin cavity allows ultraviolet light energy absorbed by the aromatic analyte to be transferred non-radiatively to the lumophore. Therefore, the analyte of interest must have

a sufficient absorption cross-section and the lumophore should have a large quantum yield of emission. We have chosen the lanthanide ions, terbium (III) and europium(III) as the lumophores in our cyclodextrin AETE system.

CHAPTER 2

OPTICAL CHEMOSENSING OF ALCOHOLS BY AN ABSORPTION INTERSYSTEM CROSSING EMISSION PROCESS

Introduction

Alcohol (ethanol) is one of the most prevalent molecules in our society. We consume it in alcoholic beverages, use it as a fuel additive or as an industrial solvent. As an alternative fuel additive with the promise for reduced level of emissions produced by combustion, ethanol and methanol need to be detected in hydrocarbon backgrounds [5]. To enable automobiles to burn mixed fuel efficiently, the engine must have information about the relative percentages of gasoline and alcohol. Chemosensors for simple alcohols, ethanol and methanol, are therefore highly desirable [63]. Ethanol sensing is useful for many biotechnological processes as well [64,65]. Techniques that have been employed to determine ethanol concentration include electronic absorption, infrared spectroscopy, fuel cells, refractive index changes, piezoelectrics, electrochemical techniques, semiconductors and enzymatic reactions. The latter has been mostly successful, yet these

measurements indirectly monitor ethanol by oxygen consumption by alcohol oxidase [66,67] or NADH production by alcohol dehydrogenase [68-72]. However, there is a need for more selective optical sensors for alcohol sensing, especially for fuel composition measurements, in order to improve vehicle performance and public acceptance of alternative fuels. Our laboratory is interested in developing a direct ethanol sensor based on triggered luminescence for monitoring fuel composition.

Optical methods for alcohol detection are prominent for selective applications such as measuring blood alcohol concentrations. Determining if a driver is under the influence of alcohol has been a challenge for law enforcement for many years [73]. The Breathalyzer, a well-known ethanol sensor, is based on absorption spectroscopy. The concentration of ethanol is determined by reduction of potassium dichromate by ethanol and a subsequent change in the absorption spectrum as orange chromium(V) is reduced to green Cr(III). The reaction is given schematically below:

primary   orange
alcohol

RCH_2OH + $Cr_2O_7^{2-}$ ⟶ R—C $\overset{H}{\underset{O}{<}}$ + Cr^{3+}
                                                                        pale green

$\downarrow$ $Cr_2O_7^{2-}$

R—C $\overset{OH}{\underset{O}{<}}$ + Cr^{3+}
                                        pale green
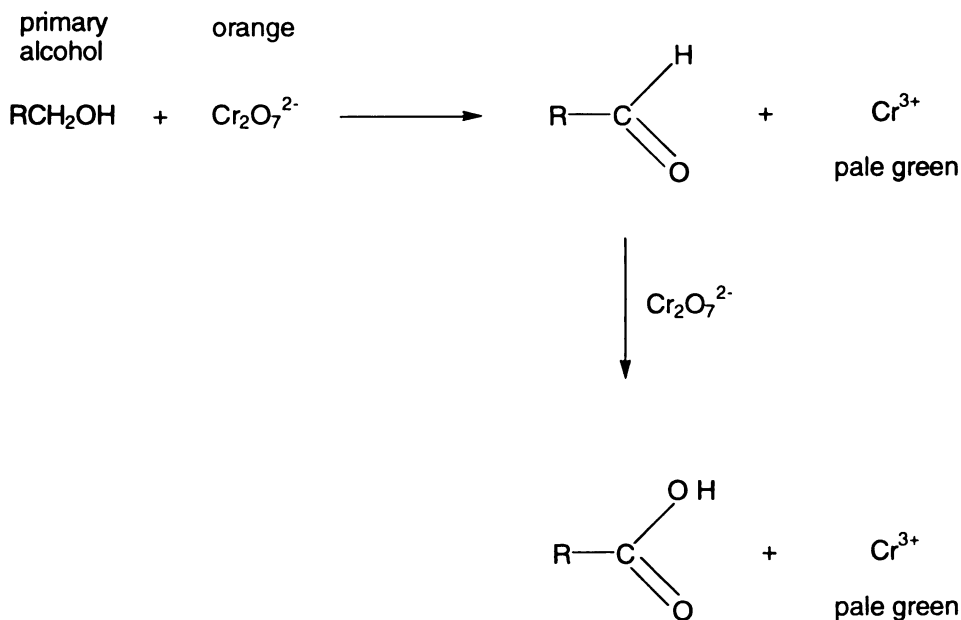
Blood alcohol level concentrations can be measured from 0 to 0.40 % weight by volume by measuring the absorbance difference between the test sample and a reference solution of potassium dichromate. A catalyst must be added to ensure the complete oxidation of ethanol to acetic acid. Due to the poor reliability of the test, new modern methods have been developed for testing blood alcohol levels. Infrared spectroscopy (IR) has been the primary test of ethanol since the 1980s [74]. One advantage of IR spectroscopy is the real-time measurement of ethanol concentrations compared to the Breathalyzer, which requires a reaction time of 1.5 minutes. Although there are advantages to IR detection, the disadvantages are the high cost of achieving specificity, inaccuracy at low alcohol concentrations and the nonlinear output of the detector. A third alternative for blood alcohol sensors are fuel cells, where a breath sample passes through a layer of platinum black into an acidic electrolyte solution. An electrochemical signal heralds the presence of ethanol, which is converted to acetic acid. Fuel cell technology, in contrast to IR spectroscopy is very specific to ethanol [75].

Other optical tests for atmospheric ethanol based on absorption spectroscopy are based on films of a vanadium-oxinate-polymer [76]. Vanadium oxinate is insoluble and non-reactive in water and has been used to determine levels of ethanol in beer, wine, blood and other solvents [77,78]. Ethanol concentrations are determined by UV-VIS spectrometry, where a change in color from the gray-green vanadium oxinate complex to a red color, the complex with alcohol, is observed. Two obvious disadvantages of this method is that the detection is based on absorption (and thus a reference I_0 is needed), and the active compound chemically reacts with the analyte, making the sensor irreversible.

grey-green   red
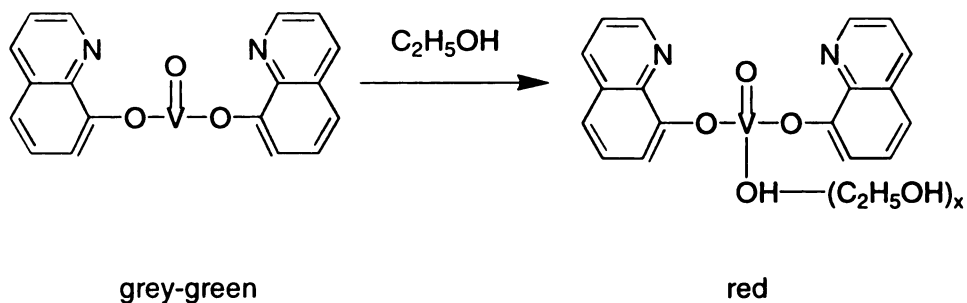
Alcohol sensors based in fluorescence have recently appeared. An optode (optical electrode) used to monitor the content of ethanol in alcoholic beverages [79] has been developed with an active material composed of n-acetyl-N-dodecyl-4-trifluoroacetylaniline (TFAn) coated onto polyvinylchloride (PVC) polymer. A change in absorption spectrum is transduced upon contact of ethanol with TFAn from the formation of hydrates and hemi-acetals. The mechanism of sensing occurs because of the highly electrophilic nature of the carbonyl carbon atom of TFAn, which is magnified further by the highly electron withdrawing trifluoromethyl group.
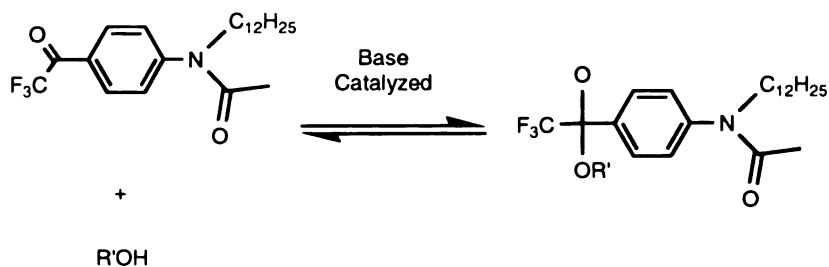
Interaction with ethanol results in a loss of electron delocalization and a hypsochromic shift of the absorption band. Selectivity towards primary alcohols such as methanol, ethanol, 1-propanol, 1-n-butanol is imparted by the nucleophilic character of the analyte,

and secondary alcohols such as tert-butanol and isopropanol are rejected by a factor of 10. A dynamic range of ethanol concentrations from 0.5 to 35 % (v/v) can be determined by this optical method based on absorption.

A similar optical sensor is also available for use in determining ethanol concentrations in alcoholic beverages [80]. This optode is fabricated with a chitosan and poly(vinyl alcohol) cladding. The chitosan membrane separates ethanol from water as swelling and shrinking of the cladding induces a change in refractive index and consequently the intensity of transmitted light. This sensor operates in the ethanol concentration range of 0-60 % (v/v).

In addition to optical sensors based on absorption and refractive index changes, there are also optodes that rely on changes in fluorescence to herald the presence of alcohol. The active receptor site of the two sensors are 1,3-oxazole or thiazole [81] and fluorescein octadecyl ester (FODE) [82]. The oxazole/thiazole fiber optic sensor is based on the effect of twisted intramolecular charge transfer (TICT), which causes a decrease and a red shift of the fluorescence of the dye molecule upon exposure of these dye molecules to polar ethanol or methanol. Since the most common application of optical sensing of simple alcohols is for measuring their levels in fuel blends, the fiber optics can be immersed in non-polar octane solutions. Concentrations of polar alcohols between 0.5 and 6% will trigger a change in the fluorescence of the dye emission. The fluorescence spectrum of fluorescein, also a dye molecule, is sensitive to hydrogen bonding interactions with alcohols, resulting in an increase in the relative fluorescence intensity upon addition of alcohol. This sensor also triggers fluorescence in the presence of carboxylic acids such as formic, acetic, propionic and benzoic acid. Both of these sensors

use visible light to excite the laser dyes and measure increases or decreases in fluorescence intensity. However, the selectivity of the sensors is compromised by the variety of polar and hydrogen bonding substrates that can also trigger a luminescent signal.

Thus there is a diverse scope of ethanol sensors, based mainly on optical (infrared, UV-VIS absorption and refractive index) and electrical techniques (fuel cells). However, they posses several disadvantages. For an automobile application, electrical transduction techniques (fuel cells) are undesirable in an environment already crowded with electrical signals. The optode sensors are based on absorption signals, which involve measuring small changes in *transmitted* light. Finally, many of the devices and mechanisms described are not specific to ethanol and methanol.

Optodes based on luminescence spectroscopy have the advantages of low cost, real-time measurements, simple design and ease of miniaturization. They do not require a reference signal and are not subject to electrical interferences, [83]. The challenge of sensing ethanol and other alcohols by luminescence spectroscopy is that the analytes are neutral molecules that do not absorb or emit light. Although ethanol can effect a change in absorption of vanadium oxinate and trifluoroacetylaniline, perturbations in phosphorescence and fluorescence are more difficult to achieve and many times non-specific.

How can substrates such as alcohols be detected? They do not coordinate to metal ions, absorb light or have any characteristics that would easily lend themselves toward optical detection by triggered luminescence. Our interest in elaborating a method for alcohol detection by a luminescence response led us to become interested in the

properties of lumophores included in cyclodextrin cups. It is well-known that the nonradiative decay processes of lumophores are significantly attenuated, and hence luminescence intensity increased, in the protected microenvironment of a CD cup [84-87]. Many investigations have focused on the fluorescence of CD-included polyaromatic hydrocarbons or azo dyes, and the effect of alcohol on fluorescence [88]. The perturbation by the alcohol on the fluorescence properties has been attributed to the alcohol increasing the association of the fluorophore within the CD cup [89-91], modifying CD-fluorophore interactions [88,92,93], and/or physically shielding fluorophore from quenchers present in bulk solution [94]. We became interested in integrating the concepts of room-temperature phosphorescence of lumophores in CD cups [95-98] with that of ternary complex formation among aromatic hydrocarbons, CDs, and alcohols to design a scheme for the luminescent detection of alcohols. Specifically, we were intrigued by Turro's investigation of host-guest inclusion complexes between CDs and bromonapthalene appended to detergent chains [96b,99]. Although the cationic surfactant phosphorescent probes are quenched efficiently by $Co(NH_3)_6^{3+}$ in aqueous solution, their inclusion within the CD cup preserves their intense phoshorescence. The bromonaphthyl moiety is protected from quencher by the coiled hydrocarbon chain within the CD cavity. We wondered if the protective function of the long detergent chain could be assumed by alcohols in the formation of a complex among bromonaphthalene, β-CD, and alcohol. In this case, the possibility exists for alcohols to trigger the intense, green, room-temperature phosphorescence of bromonaphthalene, which is otherwise efficiently quenched by oxygen.

We have shown that simple alcohols can assume the role of long detergent chains in ternary complexes [100]. The alcohol acts as a lid for the CD cup, shielding 1-BrNp from oxygen and thereby preserving 1-BrNp's intense green phosphorescence. Phosphorescence enhancements can be very large, depending on the fit of the alcohol lid on top of the CD cup. We investigate here the topological features of the alcohol that lead to the best shielding. In addition, the recognition of other hydrogen bonding substrates by the CD•1-BrNp is defined and the relationship between the structure of the CD•1-BrNp•S (S = substrate) and its photophysical properties leading to a triggered luminescence response is described.

Experimental

Materials

Mono glucosyl-β-cyclodextrin (G-β-CD) was purchased from CTD, Inc. and used without further purification. *Tert*-butanol (t-BuOH), pivalic acid (PA), and neopentylamine (NpNH$_2$) were purchased from Fisher, MCD and ICN Biomedical, respectively and used as received. All other substrates, neopentanol (NpOH), 3,3-dimethyl-1-butanol (DMB), cyclohexanol (CycOH), cyclohexylmethanol, (CycMeOH), 2-cyclohexylethanol (CycEtOH), *cis*-1,2-cyclohexanediol (1,2-Cyc-diOH), 1,3-cycloheanediol (1,3-Cyc-diOH), 1,4-cyclohexandiol (1,4-Cyc-diOH) *tert*-butylacetic acid (t-BuAA), *tert*-butylamine (t-BuNH$_2$), trimethylacetaldehyde (TMA) and methyl trimethylacetate (MTMA) were purchased from Aldrich and used without purification. The diols 1,3-Cyc-diOH and 1,4-Cyc-diOH were used as mixtures of cis and trans isomers. 1-Bromonaphthalene (1-BrNp) was purchased from Aldrich and vacuum distilled before use.

Electronic Absorption Spectroscopy and Binding Constants

All experiments were performed using room temperature aerated aqueous solutions unless otherwise noted, where the concentration of oxygen in water is 2.4×10^{-4} M. Absorption Spectra were collected on double beam Hitachi U2001 or OLIS retrofitted Cary 17 spectrophotometers. Changes in the absorption spectra upon binding were used to determine association constants. In all cases the hydrophobic guest molecules were insoluble in water. We therefore devised a novel way to measure the binding of cyclodextrins in saturated aqueous solutions with a large excess concentration of the aromatic hydrocarbon of interest [100-101].

Before the association constant can be measured, two parameters must be accounted for: the solubility concentration of aromatic hydrocarbon in water and the changes in index of refraction. The first quantity is gleaned by collecting an absorption spectrum of aromatic hydrocarbon saturated in water versus a water reference. Using Beer's Law we obtain the concentration as $[Ar] = A_0/\varepsilon b$, where $[Ar]$ is the concentration of aromatic in water, A_0 is the absorption of the solution, ε is the molar absorptivity of the aromatic at the maximum and b is the path length. In all subsequent equations the path length will be set to 1 cm and therefore appears to be excluded. Secondly, the refractive index must be corrected for, as addition of cyclodextrin creates a new equilibrium between the aromatic solute and water solvent, which results in solubilization of the aromatic hydrocarbon. Therefore, a baseline is scanned prior to titration, with a saturated solution of aromatic in both the sample and reference chambers.

As concentrated cyclodextrin solution (25 mM CD) is added to the sample compartment, the absorption increase results from the complex of cyclodextrin with

aromatic hydrocarbon, [CD•Ar], where CD = cyclodextrin and Ar = aromatic hydrocarbon. A plot of $[A-A_0]/A_0$ versus $[CD]_{tot}-[CD•Ar]$ yields K, the binding constant as the slope. The derivation of the equation is given below, where [CD] is the concentration of unbound cyclodextrin, CD_0 is the initial concentration of titrated CD (before complexation with Ar), [CD•Ar] is the amount of complexed CD, A_0 is the absorbance of an aromatic saturated in water, A_{CD} is the absorbance of an aromatic hydrocarbon with added CD in water, ε is the molar absorptivity at the wavelength where the A_0 and A_{CD} is collected (in this case λ = 284 nm),

$$[Ar] + [CD] \xrightleftharpoons{K} [Ar•CD] \tag{7}$$

$$[CD] = CD_0-[CD•Ar] \text{ and } [CD•Ar] = \left[\frac{A_{CD} - A_0}{\varepsilon}\right] \tag{8}$$

$$K = \frac{[CD•Ar]}{[CD][Ar]} \tag{9}$$

$$[CD•Ar] = K[CD][Ar] \tag{10}$$

$$\left[\frac{A_{CD} - A_0}{\varepsilon}\right] = K\left[CD_0 - \frac{A_{CD} - A_0}{\varepsilon}\right]\left[\frac{A_0}{\varepsilon}\right] \tag{11}$$

$$\left[\frac{A_{CD} - A_0}{A_0}\right] = K\left[CD_0 - \frac{A_{CD} - A_0}{\varepsilon}\right] \tag{12}$$

After separating the independent ($[CD_0]$) and dependent (A) variables, the equation is,

$$A_{CD} = \frac{KA_0\varepsilon}{KA_0 + \varepsilon}[CD_0] + A_0 \tag{13}$$

Therefore the binding constant is obtained from the slope, molar absorptivity and the absorption of saturated aromatic in water and the y-intercept is related to the concentration of aromatic in water.

The following assumptions are made for this experiment. First, extinction coefficient of 1-bromonapthalene does not change significantly upon complexation in the cyclodextrin cavity. Secondly, we do not see a shift in the absorption maximum of 1-BrNp upon complexation. Lastly, the solution remains saturated with aromatic hydrocarbon throughout the titration and never reaches the asymptotic limit that is typical for most binding curves. This linear equation applies because the titration occurs in the linear regime of binding, where $[CD_0] << [1\text{-}BrNp]$.

Steady State Luminescence Spectroscopy, Quantum Yield and Titrations

Quantum yields were determined on a high resolution emission instrument built at Michigan State University [102] that employed an R943 or R1104 Hamamatsu PMT as the detector. The instrument was modified from its original lock-in amplifier configuration (EG&G) to photon counting detection (SRS 400 Photon Counter) [103]. LABVIEW is used to computer control the photon counter, lock-in amplifier and two SPEX monochromators, a 0.22 M double 168 and 0.5 M single 1870B, for selecting excitation and emission wavelengths respectively. The 313 nm line of a XeHg lamp was used to excite 1-BrNp Light and dark counts are collected when a 13 or 338 Hz chopper is open and closed, and the signal is calculated as the difference between light counts and dark counts. Two chopper frequencies allow us to control the time interval for collecting fluorescence or phosphorescence quantum yields. A single blade chopper (Terahertz

Technologies) with speeds ranging from 3-4000 Hz was added to allow for more consistent positioning, more flexibility in the optical path and also for computer control by LABVIEW.

The phosphorescence intensity of 1-BrNp (saturated) in Gβ-CD (2.5 mM) was observed to increase to an asymptotic limit with increasing amounts of alcohol or hydrogen-bonding substrates. Substrate additions were between 0 and 300 μl, so that the total volume change for the solution (10 ml) was not significant. All measurements were performed at 22 ± 2°C in aerated aqueous solutions. The stoichiometry of the ternary complex was determined from a Job plot by the method of continuous variation [104]. The concentrations of Gβ-CD and *tert*-butanol were varied so that their total concentration was equal to 2.5×10^{-3} M as the concentration of 1-BrNp was held constant at 1×10^{-5} M, the solubility limit in water. The phosphorescence intensity was measured at 530 nm. Quantum yields were measured using solutions saturated in 1-BrNp, 2.5 mM Gβ-CD and in the asymptotic limit of added substrate. Absorbances measured at 313 nm were ~ 0.1. Quantum yields were derived by integrating the phosphorescence of 1-BrNp from 450 to 700 nm and correcting for the refractive index differences between hexane and water. The quantum yield was evaluated relative to 2,3-butanedione (biacetyl; ϕ_{phos} = 0.05 in hexane at room temperature) [105]. Biacetyl was freeze-pump-thawed 3-5 times before the phosphorescence was observed, and contributions due to fluorescence were subtracted by measuring fluorescence from aerated solutions. The phosphorescence quantum yields of all bromonapthalene compounds in chapters 3 and 4 are measured relative to biacetyl.

Stern-Volmer Quenching

The extent of static and dynamic quenching can be determined from the Stern-Volmer method of luminescence lifetimes [106]. If quenching is purely dynamical then plots of intensity and lifetime as a function of quencher concentration will be linear and the slope proportional to the Stern-Volmer quenching rate constant, which is the product of the lifetime in the absence of quencher and the bimolecular quenching rate constant.

$$\frac{I_0}{I} = \frac{\tau_0}{\tau} = 1 + K_{sv}[Q]\mathrm{I} \tag{14}$$

$$K_{sv} = k_Q \tau_0 \tag{15}$$

If static quenching is also present, then there is binding in the excited state as well, and the intensity plot has a positive deviation from the lifetime plot, which is given by the following equation.

$$\frac{I_0}{I} = \left(1 + K_{sv}[Q]\right)\left(1 + K_{eq}[Q]\right) \tag{16}$$

Therefore if the Stern-Volmer quenching rate constant is known from the lifetime plot, the equilibrium constant can be found by the quadratic equation.

Stern-Volmer quenching was used to establish the extent of dynamic and static quenching [107]. In the case of 1-BrNp phosphorescence in a ternary complex, the dynamic quenching of triplet oxygen was obtained by measuring the lifetime for three oxygen concentrations in degassed solutions, aerated solutions at atmospheric pressure and in saturated oxygen solutions (0 M, 2 x 10^{-4} M, 12 x 10^{-4} M, respectively) on a nanosecond-time resolved laser instrument. Oxygen concentrations were determined

according to Henry's law with methods that we have previously discussed [100]. For the covalent compounds of 1-BrNp and cyclodextrin, a cobalt hexammine chloride complex, $[Co(NH_3)_6]Cl_3$,was used as a quencher to define the dynamic quenching kinetics, since for the case of compound **2** (bromonaphthalene on the secondary side) oxygen was not an efficient quencher. Monoexponential decays of 1-bromonapthalene were fit using Kaleidagraph or Origin Software packages.

Nanosecond Time-Resolved Spectroscopy

All laser systems used were in the *LASER* laboratory shared facility in the Department of Chemistry at Michigan State University. To determine the lifetimes and risetimes of phosphorescence, nanosecond pulsed lasers were used. Lifetimes longer than the pulsewidth of a 10 ns can be measured on the nanosecond Quanta Ray DCR2 Nd:YAG systems. In the normal timing mode, the laser pulse directly or the laser pulse scattered onto a photodiode acts as the trigger signal for data collection. A TEK DSA 602A fast oscilloscope was employed to collect time-resolved luminescence and lifetimes of 1-BrNp phosphorescence. Phosphorescence of 1-BrNp at 530 nm was collected at right angles to the excitation beam and measured by a R928 Hamamatsu PMT (700-800 V) after being selected by a SPEX 1681 single monochromator. The entrance slit was kept as small as possible for stray light rejection purposes. As phosphorescence is typically long lived (milliseconds), it was necessary to open the exit slit to an average of 4 mm.

The 532 nm output of a nanosecond Quanta Ray DCR2 Nd:YAG laser was used to pump a variety of laser dyes (rhodamine, DCM, kiton red) in a side pumped

configuration. The wavelengths selected by the dye were doubled by a WEX, where the angle of the doubling crystal could be tuned if the laser was scanned or a fixed wavelength could be selected by a Pellin-Broca prism. The power of ultraviolet light emanating from the WEX was typically 10-40 mW (10 -15 % conversion efficiency). Alternatively, a nanosecond Quanta Ray DCR2 Nd:YAG laser could be used as a source when it is configured with a H_2 Raman shifter (10-20 psi) to obtain 309 nm anti-Stokes shifted 355 nm light. This wavelength (309 nm) was used to measure phosphorescence decay of 1-BrNp.

Molecular Modeling

Energy minimized conformations of the 1-BrNp•Gβ-CD•substrate ternary complex were determined from an energy minimization run on a Silicon Graphics IRIS Elan χ^2 computer using Biosym Insight Discover with the assistance of Mike H.B. Gray. The method of steepest descent and conjugate gradient algorithms of a consistent valence force field (CVFF) were employed. The Gβ-CD was minimized first, and then successive minimizations were performed as the 1-BrNp and substrate molecules were added.

Results

Quantum Yields and Binding Constants

When excited with ultraviolet light, an aerated aqueous binary system of 1-BrNp•CD emits only blue fluorescence at 320 nm typical of aromatic hydrocarbons, although inclusion of 1-BrNp does cause slight changes in the vibrational fine structures (Figure 6)[108]. Green phosphorescence of 1-BrNp at 530 nm appears only when
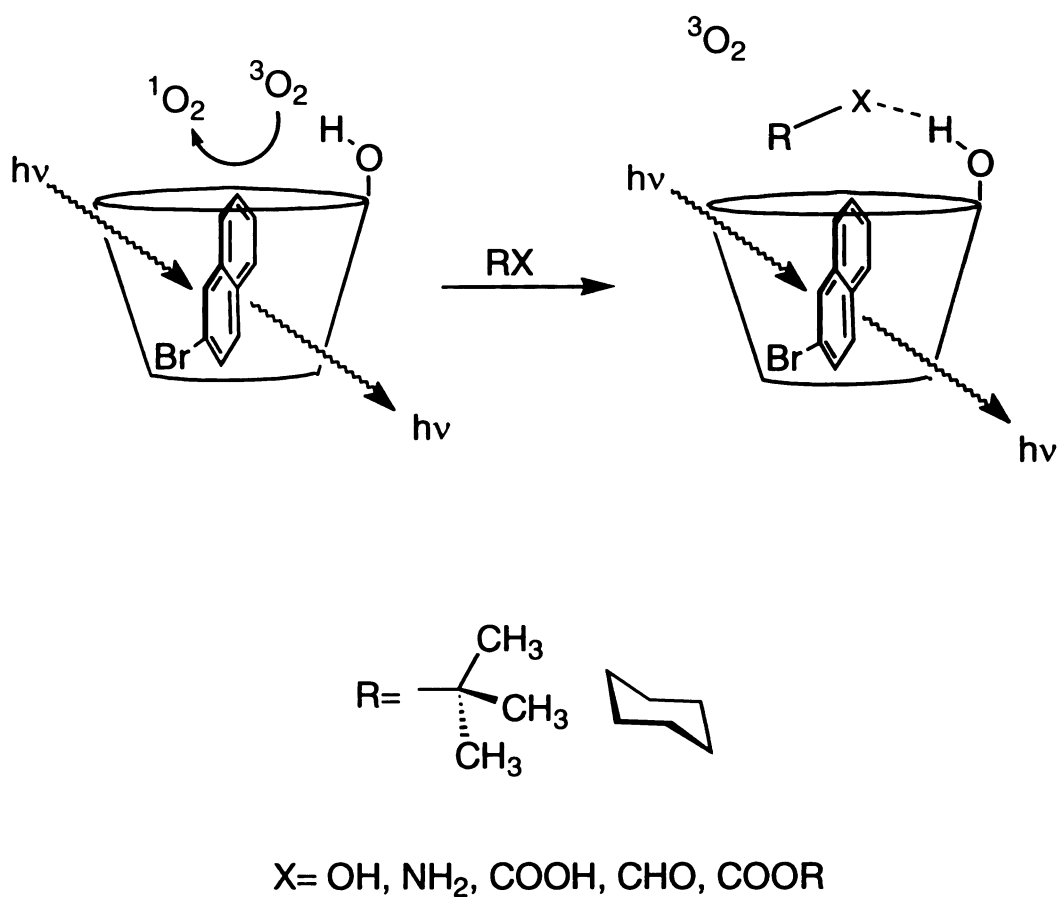
Figure 6. Ternary complex of 1-bromonaphthalene, glucosyl-β-CD and hydrogen bonding substrate. The alkyl group (R) is a bulky t-butyl or cyclohexyl and the hydrogen bonding group (X) is a hydroxyl, carboxylic acid, amine, aldehyde or ester.

alcohols are added to the binary system of 1-BrNp•CD to form a ternary complex. Figure 7 shows the similar phosphorescence profiles for 1-BrNp in β-CD in ternary complexes with *tert*-butyl and cyclohexyl alcohols. Although the shape of the phosphorescence profile is unchanged, the intensity varies markedly as a function of the nature and concentration of the alcohol.

Titration profiles of 1-BrNp at λ_{em} = 530 nm (λ_{ex} = 313 nm) as a function of substrate concentration are shown in Figure 8. For all substrates shown, the emission intensity increases monotonically with increasing alcohol concentration to a different asymptotic limit for each substrate. Within the *tert*-butyl and cyclohexyl series the greatest response is observed for neopentanol (NpOH) and cyclohexylmethanol (CycMeOH), respectively, where the bulky groups are removed from the alcohol group by one methylene spacer.

The quantification of the phosphorescence response is achieved by measurement of the quantum yields. Table 1 provides a list of the phosphorescence quantum yields of 1-BrNp in β-CD in the presence of various *tert*-butyl and cyclohexyl alcohols at concentrations range near the asymptotic limit provided by the titration profiles. The largest quantum yields are observed for alcohols in which the aliphatic bulky group is separated from the hydrogen-bonding hydroxyl group by one methylene spacer, followed by alcohols with no spacer. The quantum yields decrease when -$(CH_2)_n$- reaches n > 2. The method of continuous variation (Job plot) was used to determine the stoichiometry of the 1-BrNp•Gβ-CD•substrate complex for t-BuOH [109]. The concentration of 1-BrNp was held constant while the molar ratio of Gβ-CD and t-BuOH were varied, keeping the total concentration ([Gβ-CD] + [t-BuOH] = 2.5 x 10^{-3} M) the same throughout the course
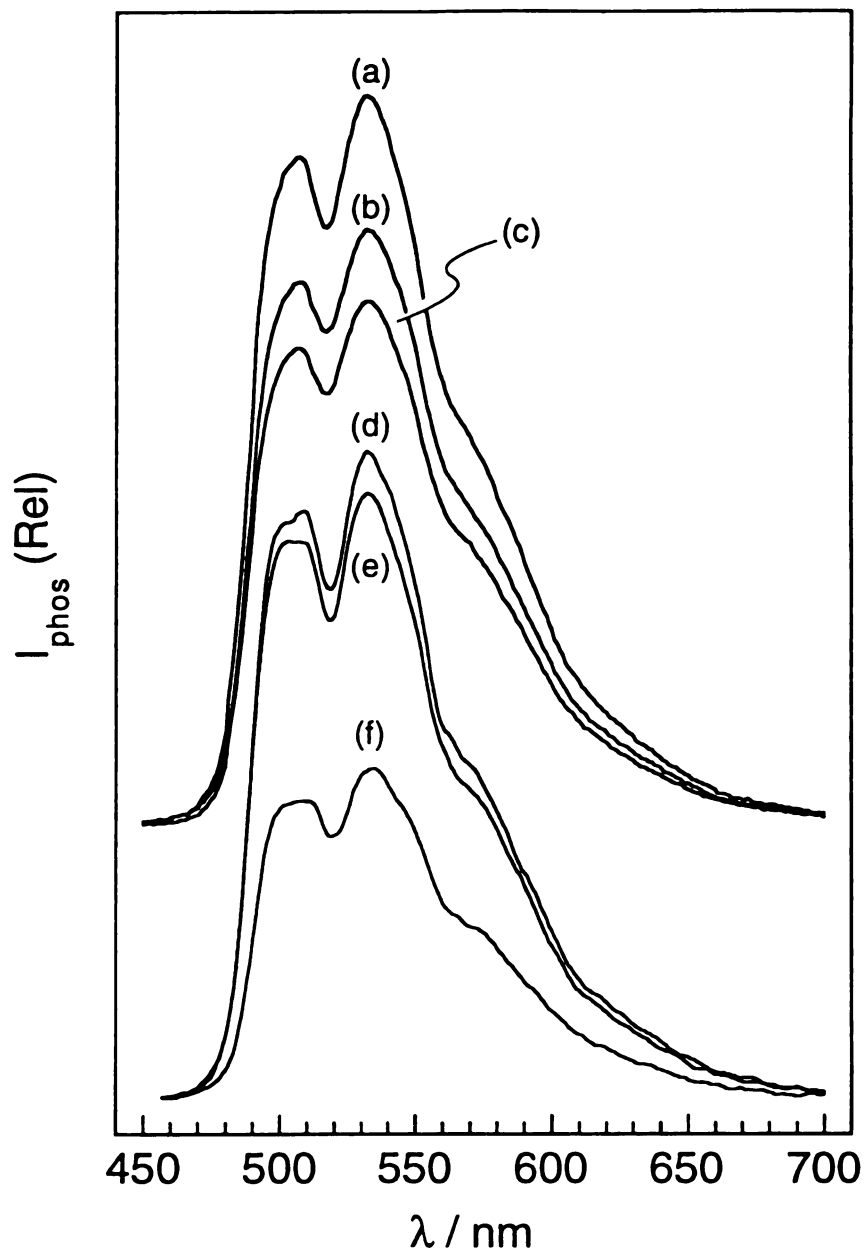
Figure 7. Luminescence spectra of 1-BrNp from aerated aqueous solution of Gβ-CD (10^{-3} M) in the presence of ~ 3% v/v of (a) NpOH (b) t-BuOH (c) DBM (d) CycMeOH (e) CycOH (f) CycEtOH. Spectra were normalized for 1-BrNp absorbance and were collected in the asymptotic limit of the titration profiles shown in Figure 8.
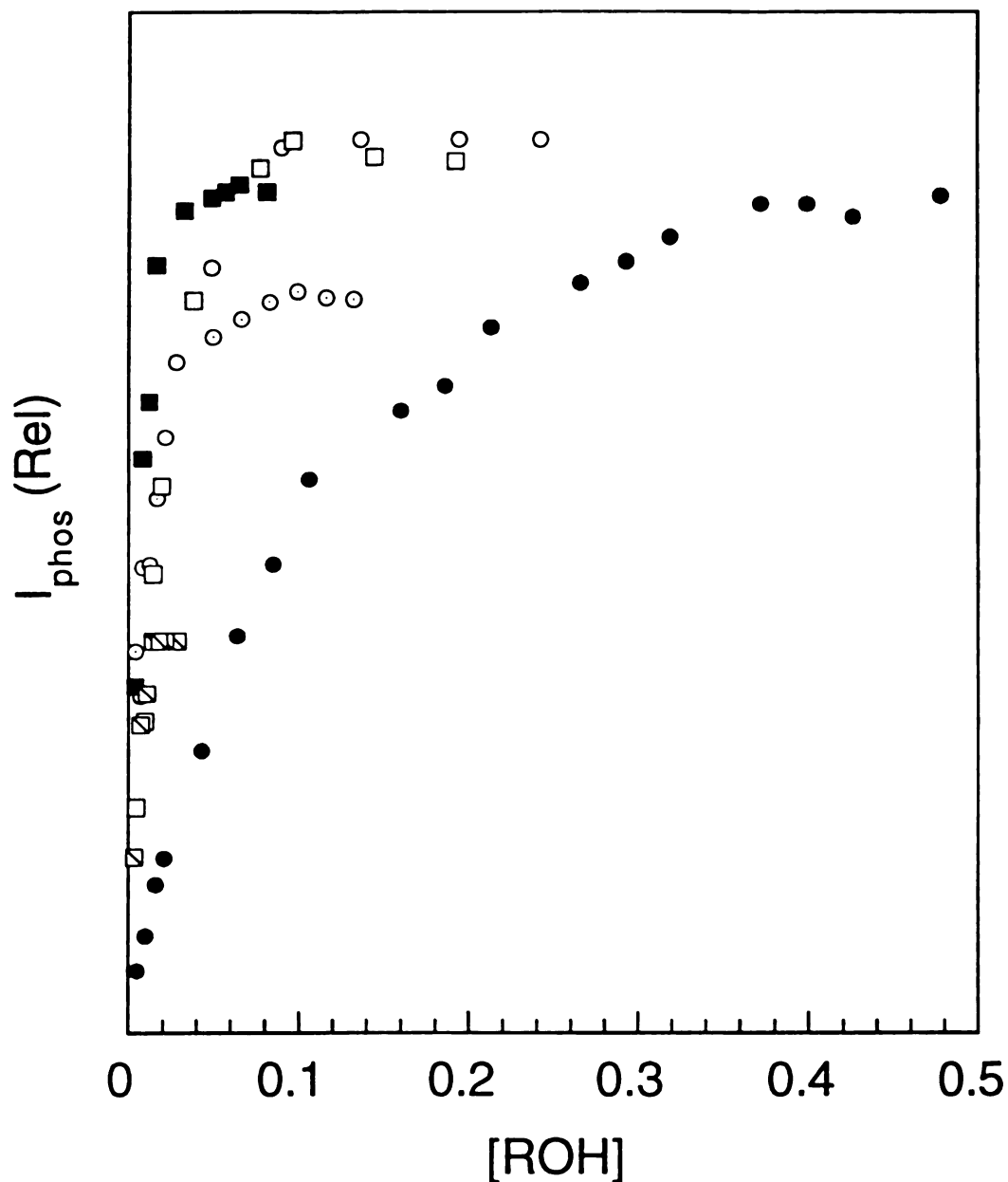
Figure 8. Dependence of relative phosphorescence intensity of 1-BrNp at 530 nm from aerated solutions containing Gβ-CD (10^{-3} M) concentration of t-BuOH (●) NpOH (O) and DBM (⊙), and CycOH (□), CycMeOH (■), and CycEtOH (⊠). As a reference, the plateau region for NpOH is 2.1 x 10^5 times greater than the phosphorescence intensity in absence of alcohol.

Table 1. Quantum yields, equilibrium constants and oxygen quenching rate constants for alcohol substrates.

Substrate	Symbol	$\phi_{phos}/10^{-4}$	K_4/M^{-1}	$k_q/10^5\,M^{-1}s^{-1}$
tert-Butanol	t-BuOH	340	1344	8.9
Neopentanol	NpOH	1149	1264	0.3
3,3-Dimethyl-1-butanol	DMB	789	2162	1.6
Cyclohexanol	CycOH	350	1972	1.2
Cyclohexylmethanol	CycMeOH	771	1107	0.2
Cyclohexylethanol	CycEtOH	364	1022	0.8
cis-1,2-Cyclohexanediol	1,2-Cyc-diOH	883	763	2.0
1,3-Cyclohexanediol	1,3-Cyc-diOH	51	653	32
1,4-Cyclohexanediol	1,4-Cyc-diOH	$<10^{-2}$	<10	$>10^4$

of the experiment. Figure 9 shows the Job plot for 1-BrNp•Gβ-CD•*tert*-butanol as the molar ratio of *tert*-butanol and Gβ-CD is varied. As the binary complex of 1-BrNp•Gβ-CD does not phosphoresce, the phosphorescence intensity at 530 nm directly reflects the stoichiometry of the ternary complex. A maximum value of the intensity occurs between 0.4 and 0.5, thus providing evidence for a nearly equimolar ratio of CD and alcohol. Since naphthalene and its derivatives have been proven to form 1:1 complexes with cyclodextrins [110-112], we can conclude with confidence that the data are consistent with the formation of a 1:1:1 ternary complex of 1-BrNp:Gβ-CD:t-BuOH.

Many equilibria can be expressed for the 1-BrNp•Gβ-CD•substrate system. Either 1-BrNp or substrate will bind to CD to form binary complexes (K_1, K_3 respectively). The ternary complex 1-BrNp•Gβ-CD•substrate can be formed by either binary complex (1-BrNp•Gβ-CD or Gβ-CD•substrate) associating with the third molecule (substrate and alcohol respectively) given by K_2 and K_4. The equilibria are described as follows, where S equals the substrate,

$$1\text{-BrNp} + G\beta\text{-CD} \xrightleftharpoons{K_1} BrNp\bullet G\beta\text{-CD}$$

$$1\text{-BrNp}\bullet G\beta\text{-CD} + S \xrightleftharpoons{K_2} 1\text{-BrNp}\bullet G\beta\text{-CD}\bullet S$$

$$G\beta\text{-CD} + S \xrightleftharpoons{K_3} G\beta\text{-CD}\bullet S$$

$$G\beta\text{-CD}\bullet S + 1\text{-BrNp} \xrightleftharpoons{K_4} 1\text{-BrNp}\bullet G\beta\text{-CD}\bullet S$$
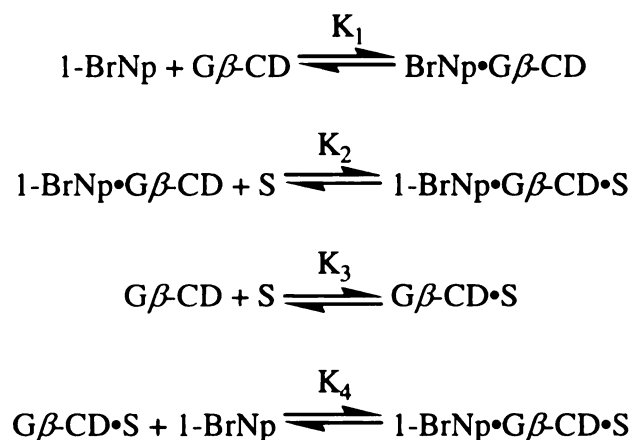
The equilibrium constants are related by $K_1 K_2 = K_3 K_4$, as verified by previous measurements [100]. K_4 was shown to be the dominant equilibrium by those studies. The
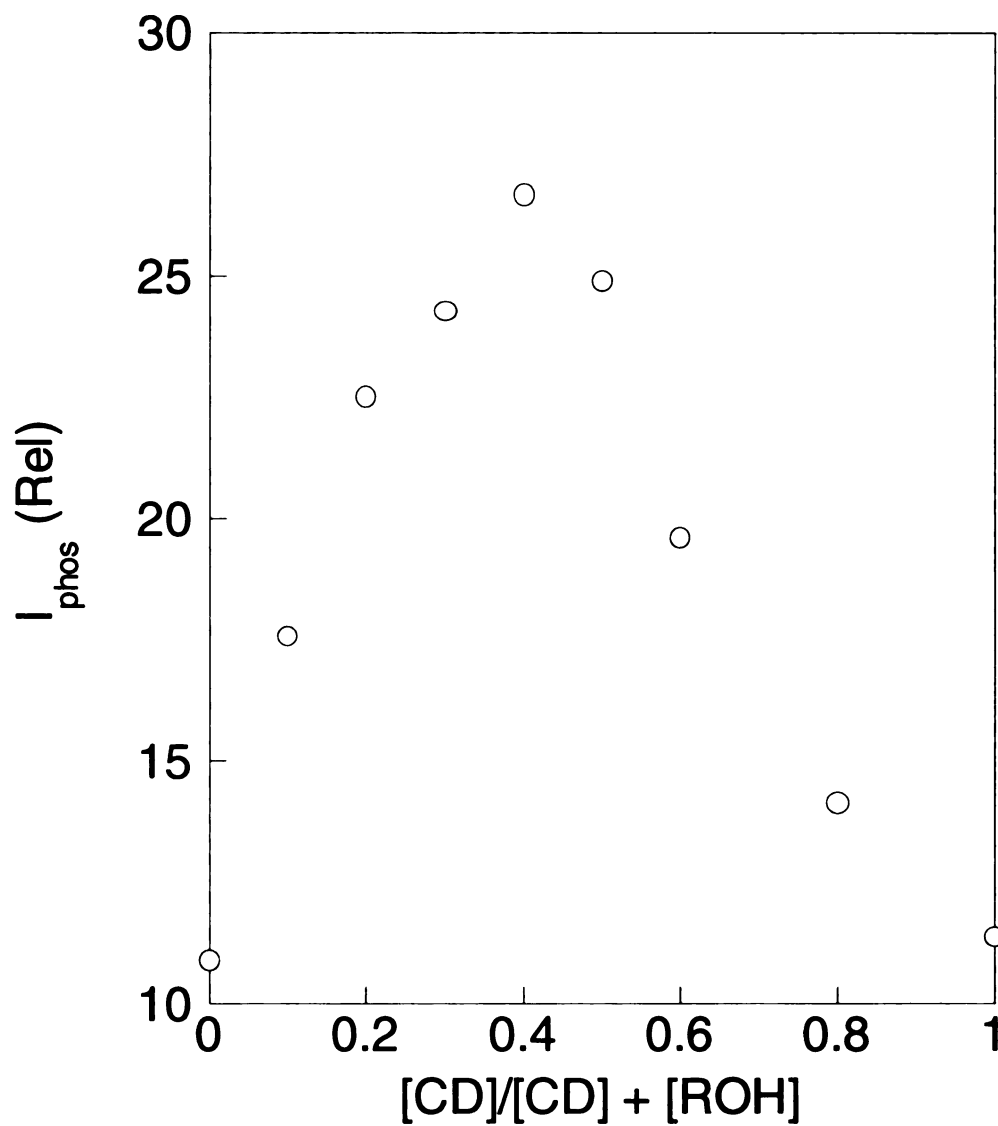
Figure 9. Job plot of the relative phosphorescence intensity from a 1-BrNp•Gβ-CD•t-BuOH complex monitored at 530 nm. The 1-BrNp concentration was 1 x 10^{-5} M, and [Gβ-CD] + [t-BuOH] = 2.5 x 10^{-3} M.

concentrations of free Gβ-CD and 1-BrNp•Gβ-CD are negligible in the limit of large excess concentrations of alcohol with respect to Gβ-CD. Consequently, measurement of the binding constant of 1-BrNp to Gβ-CD in an alcohol/water mixture is an effective measure of K_4. The binding is determined experimentally as described previously by measuring an optical change in the absorbance of 1-BrNp at 284 nm upon the addition of Gβ-CD alcohol/water solutions. K_4 for each ternary complex was determined from the slope of the linear plot of absorbance vs. [Gβ-CD]; the values are summarized in Table 1. The association constants were generally large (> 1000 M^{-1}), but did not correlate well with the quantum yield. For example, NpOH has the highest quantum yield of phosphorescence of 1-BrNp, whereas the binding to CD is smaller than t-BuOH or DBM. In the cyclohexyl series, the quantum yield of CycMeOH is the largest, but the magnitude of the value for K_4 is intermediate. Accordingly, a comparison of the binding and photophysical data (quantum yield) reveal that factors other than the association of the ternary complex govern the radiative processes of the triplet state of 1-bromonaphtalene from a 1-BrNp•Gβ-CD•alcohol complex.

The photophysics of 1-BrNp phosphorescence included in Gβ-CD dissolved in water/alcohol mixtures is described by the following scheme:

$$^*\text{1-BrNp} + \text{G}\beta\text{-CD·S} \underset{}{\overset{K_4}{\rightleftharpoons}} {}^*\text{1-BrNp·G}\beta\text{-CD·S}$$

$$\swarrow {}^{k_0} \quad {}^{3}\text{O}_2 \quad {}^{k_{q0}} \searrow \qquad\qquad \swarrow {}^{k_1} \quad {}^{3}\text{O}_2 \quad {}^{k_{q1}} \searrow$$

1-BrNp 1-BrNp 1-BrNp·Gβ-CD·S 1-BrNp·Gβ-CD·S

$$+ \qquad\qquad\qquad\qquad\qquad +$$

$$^1\text{O}_2 \qquad\qquad\qquad\qquad\qquad {}^1\text{O}_2$$
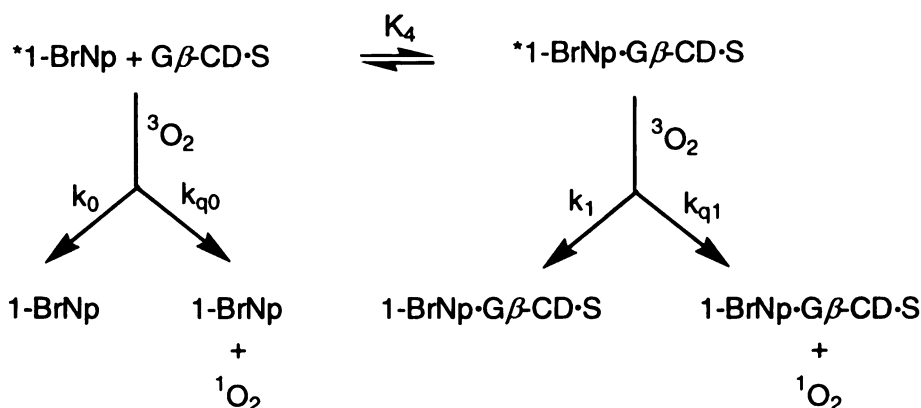
where k_0 and k_1 are the excited state decay rate constants of the phosphorescence of 1-BrNp in water and within the Gβ-CD and k_{q0} and k_{q1} are the bimolecular oxygen quenching rate constants of 1-BrNp in water and within the Gβ-CD, respectively. Gβ-CD and 1-BrNp•Gβ-CD were excluded since their concentrations are negligible as mentioned previously. The above scheme is based on the dominance of the K_4 equilibrium and on the assumption that the binding constant of the ground and excited states of 1-BrNp to Gβ-CD are comparable. Ground and excited state binding differ when excitation produces a large dipole change in the excited state, as is the case for molecules that may contain ketone groups [113]. A dipole moment change that causes the exit rate from the CD to increase in the excited state relative to the ground state will result in a smaller excited state formation constant. In the case of 1-BrNp, a significant change in charge redistribution is not expected. Further, dipole moments can be predicted by changes in the Stokes shift in solvents of varying dielectric constants [114]. Solutions of 1-BrNp in acetonitrile, toluene, ethanol and ethyl acetate did not show an appreciable Stokes shift. Consequently, similar K_4s are expected for 1-BrNp and 1-BrNp*.

Stern-Volmer Quenching

The long-lived green phosphorescence of 1-BrNp (τ_0 = 0.64 ms) is quenched efficiently by oxygen in aerated solutions of methanol and water (1/1). The quenching rate constant of 1-BrNp determined by linear Stern-Volmer plots of the lifetime as a function of oxygen concentration is 5.0 x 10^8 $M^{-1}s^{-1}$ [100]. Addition of alcohols diminishes the rate of oxygen quenching dramatically in solutions with Gβ-CD to 10^3 - 10^4 $M^{-1}s^{-1}$. In fact, the quenching rate constants and quantum yields directly correlate

with one another, as shown in Figure 10, which plots $k_q(O_2)$ and the quantum yield of phosphorescence of 1-BrNp, ϕ_{phos} for all the ternary complexes in Tables 1 and 2. The quantum yield increases with decreasing quenching rate constant and generally follows equation 1 in Chapter 1.

Addition of a second hydroxyl group also significantly alters the phosphorescence of 1-BrNp in the ternary complex. Table 1 lists the quantum yields, binding constants and quenching rate constants for cyclohexyldiol substrates. The quantum yield of 1-BrNp phosphorescence with a 1,2-Cyc-diOH is greater than that observed for CycOH capping 1-BrNp•Gβ-CD. However as the two hydroxyl groups are spaced further apart around the cyclohexyl ring, an attenuation of 1-BrNp emission is observed. Although the formation constants of 1,2-Cyc-diOH and 1,3-Cyc-diOH are similar, 1,3-Cyc-diOH has a smaller quantum yield and larger quenching rate constants by a factor of 15. When the two hydroxyl groups occupy the 1,4- position of the cyclohexyl ring the phosphorescence is barely detectable and the oxygen quenching rate constants are at the detection limit. Hence, it appears the 1,4-Cyc-diOH is very weakly associated with 1-BrNp•G-β-CD and inefficiently protects the triplet state of 1-BrNp.

Other Hydrogen-Bonded Substrates

Alcohols are not the only substrates that are recognized by the 1-BrNp•Gβ-CD complex. Table 2 presents the data collected for a variety of other hydrogen-bonding substrates that trigger 1-BrNp phosphorescence from a ternary complex at room temperature. The t-butyl moiety is maintained across the amine, aldehyde, carboxylic acid, ester series for purposes of comparison. The overall quantum yield of 1-BrNp
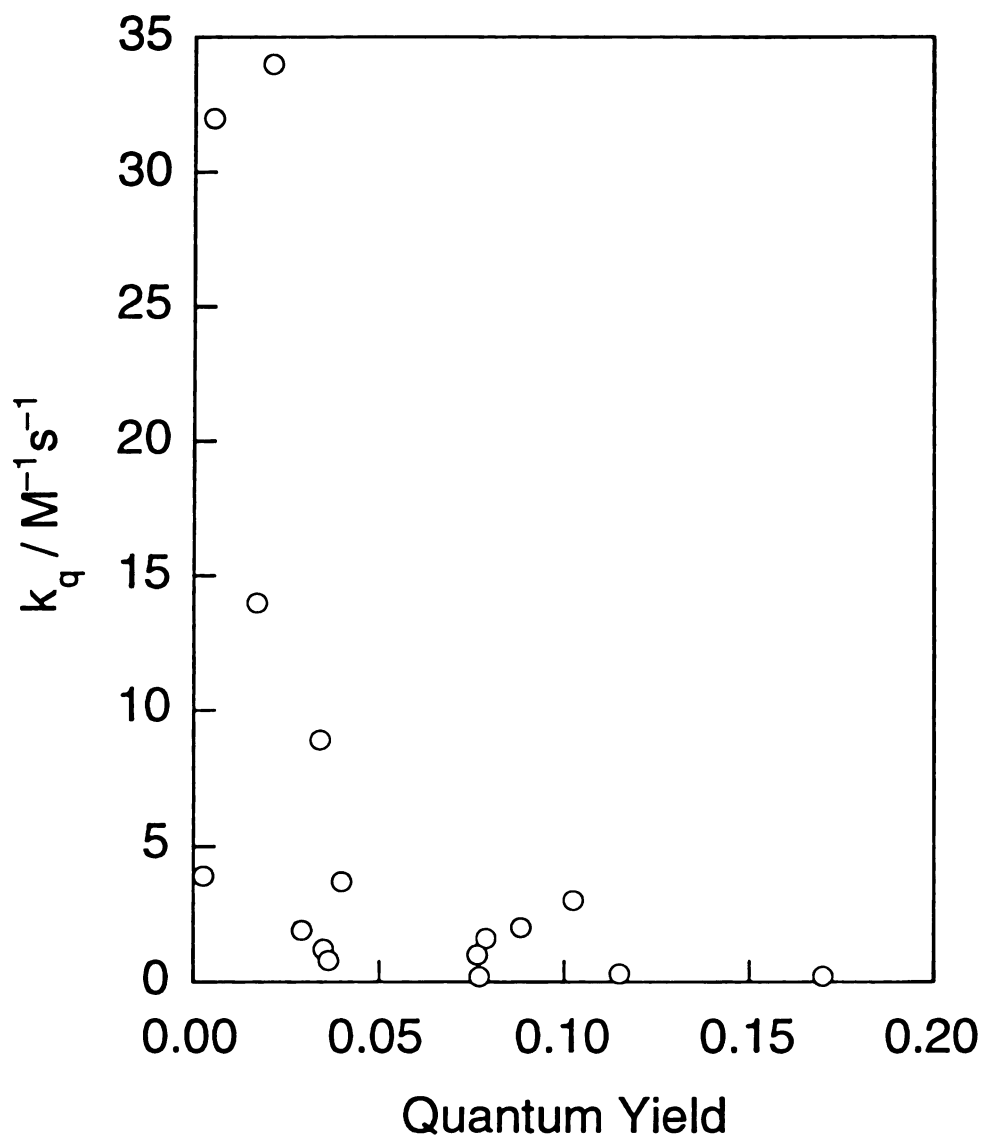
Figure 10. Oxygen quenching rate constant as a function of quantum yield for the 1-BrNp•Gβ-CD•substrate complexes listed in Tables 1 and 2.

Table 2. Quantum yields, equilibrium constants and oxygen quenching rate constants for other hydrogen bonding substrates.

Substrate	Symbol	$\phi_{phos}/10^{-4}$	K_A/M^{-1}	$k_q/10^5\ M^{-1}s^{-1}$
Pivalic acid	PA			
pH 2.9		1697	2340	0.21
pH 9.0		27	3771	3.9
tert-Butylacetic acid	t-BuAA			
pH 2.9		765	1881	0.99
pH 9.0		292	3934	1.9
tert-Butylamine	t-BuNH$_2$	210	1330	34
Neopentylamine	NpNH$_2$	1024	359	3.0
trimethylacetaldehyde	TMA	299	330	3.7
Methyl trimethylacetate	MTMA	171	1817	14

phosphorescence increases along the series ester (MTMA) < aldehyde (TMA) < amine (t-BuNH$_2$) < alcohol (t-BuOH) < acid (PA). In the case of the amines, t-BuNH$_2$ and NpNH$_2$, additional quenching pathways involving charge transfer quenching of the excited state are possible. Secondary and tertiary amines are known to quench triplet states of aromatic hydrocarbons by single electron transfer, owing to their low ionization potentials [115]. In deaerated methanol, t-BuNH$_2$ does quench 1-BrNp phosphorescence, with a Stern-Volmer quenching rate constant of 0.84 x 10^5 M^{-1}s^{-1}. Notwithstanding, 1-BrNp included in a cyclodextrin cup is not quenched. An invariant phosphorescence lifetime for 1-BrNp in Gβ-CD provides evidence that addition of the amines, t-BuNH$_2$ and NpNH$_2$, have little effect on the triplet state radiative decay. On that account, the rate constants listed in Table 2 reflect exclusively the quenching of 1-BrNp triplet by oxygen.

Similar trends appear for amine substrates as were observed for alcohol substrates. In particular, the most intense phosphorescence was noted when the t-butyl group was separated from the hydrogen-bonding group by one methylene spacer. Although the overall quantum yields are smaller than the t-butyl alcohols, the quantum yield measured for NpNH$_2$ was substantially larger (5 times) than t-BuNH$_2$. Consistent with the data for alcohols, the quenching rate constant for the amines also decreased by an order of magnitude upon addition of the methylene spacer. A comparison to carboxylic acids, PA and t-BuAA, also yields similar results, except the carbon spacer that was previously a methylene is replaced with a carbonyl group.

The carboxylic acid complexes, PA and t-BuAA, also have a significant dependence on pH, as is shown by the quantum yield at 2.9 and 9.0. The phosphorescence of 1-BrNp decreases with increasing pH and shows the largest changes

at the pK_a of PA (5.24) and t-BuAA (5.05). The association constant of PA and t-BuAA is larger for the carboxylate form than for the acid form; however, the oxygen quenching rate constant is larger as well. Oddly enough, although the carboxylate forms have larger binding, their ability to shield photoexcited 1-BrNp is decreased. The increase in the formation constant is most likely due to the fact that an ionic species has a stronger interaction with the hydroxyl rim of the cyclodextrin than does a neutral molecule.

Molecular Modeling

Energy minimizations on the Biosym program Discover have given us some insight on the topology of the ternary complexes and allowed us to visualize their geometrical arrangements as a result of changes to the substrate. In many instances the visualizations helped make sense of the experimental results and gave us explanations for the unpredictable binding behavior.

The minimizations were performed by successive additions of each of the three molecules in the ternary complex. The binary inclusion complex of 1-BrNp and Gβ-CD was first minimized. The results demonstrated that the bromine of bromonaphthalene has a preferred orientation on the secondary (wider) side of the cyclodextrin, most likely due to the fact that the glucose moiety is located on the primary side. It was thought that bitopic recognition of bulky hydrogen-bonding substrates occurred as the hydrogen-bonding group associated with the hydroxyl rim of the CD and the bulky portion protected the hydrophobic interior. We then added substrates to the primary side of the cyclodextrin (narrower side); however, it is possible that substrates could interact with the secondary side as well. The secondary side provides 14 hydroxyls that a substrate

could interact with, whereas the primary side has 7 (3 more when a glucosyl is attached). It remains to be seen which side of the cyclodextrin and therefore which part of the 1-BrNp is most susceptible to attack by oxygen; the next section will describe results for covalent systems that may explain the mechanism of oxygen quenching.

Molecular models of t-BuOH, NpOH and DBM complexes reveal that the methylene spacer better positions the t-butyl group over the unprotected 1-BrNp, as compared to no spacer (t-BuOH) and an ethylene spacer (DBM) (Figure 11). In the case of t-BuOH, it is pulled slightly inside the cyclodextrin, pushing the bromonaphthalene out of the secondary side. The addition of a methylene spacer, however, acts as a hinge, and this substrate sits snugly atop the cyclodextrin. When the ethylene spacer of DBM is added however, it appears that the aliphatic group has an affinity for the cup and pushes 1-BrNp even further outside than t-BuOH.

The disparate properties of carboxylate and carboxylic acids are also explained very well when one looks at the molecular modeling minimizations. The models show that ion-dipole interactions of the carboxylate at the hydroxyl rim lead to a pronounced distortion of the cup. Since there is a negative charge present, more hydroxyl groups must surround the carboxylate than in the case of a neutral carboxylic acid, resulting in the distortion. The ability of the substrate to shield 1-BrNp is compromised, as the cyclodextrin conformation is drastically changed and as a result 1-BrNp is exposed to oxygen.
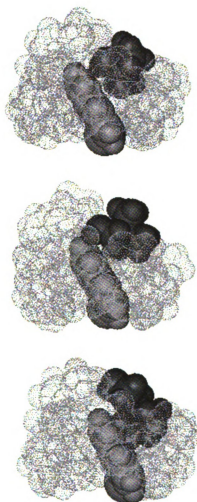
Figure 11. Molecular model of ternary complexes of 1-BrNp (light gray), β-cyclodextrin (shaded) and alcohol substrates (black): t-BuOH (top), NpOH (middle) and DBM (bottom).

Conclusions

The first study illustrated that substrates such as alcohols trigger phosphorescence from 1-bromonapthalene included in the cavity of β-CD. The substrate is bitopically recognized by the hydroxyl rim and hydrophobic interactions with the cyclodextrin. The bulky tert-butyl groups and cyclohexyl groups were maintained across the series of substrates because the steric bulk of the aliphatic groups does not permit them to coinclude with guests in the β-CD. The position of the t-butyl or cyclohexyl group over the CD cup is one important factor in shielding 1-BrNp from oxygen. For all the series investigated, the presence of a single carbon spacer produces the highest emission quantum yields. Molecular models shed some qualitative insight into the role of the spacer (Figure 11). Of the three alcohols in the t-butyl series, the methylene spacer of NpOH better positions the t-butyl group over the CD as compared to t-BuOH with no spacer and DMB, which has an ethylene spacer between the t-butyl and hydroxyl groups. The positioning of the alcohol over the primary side of the cyclodextrin causes the 1-BrNp to protrude from the secondary side. Interestingly, NpOH sits on top of the CD, while minimially perturbing the orientation of the 1-BrNp within the cup. Conversely, both the t-BuOH and DMB tend to get pulled inside the cavity as the hydrogen bond develops, pushing the 1-BrNp slightly outside the CD cup on the secondary side. For t-BuOH, the hydrogen bond directs the t-butyl group into the CD cup. With the addition of a flexible methylene spacer, the t-butyl group is better able to sit on top of the cup. However, as the spacer increases in length, the t-butyl group tends to show a higher affinity for the CD cup and therefore sterically crowds the 1-BrNp, pushing deeper into the CD. The cyclohexyl alcohol series shows similar results with the cyclohexyl group

crowding its way into the CD cavity to partially expel the 1-BrNp; this steric crowding is minimized for CycMeOH.

The strength of the hydrogen bond appears to be an additional contributing factor to determining the photophysics of the complex. The luminescence intensity increases along the series ester < aldehyde < amine < alcohol < acid and generally follows the propensity of the substrates to hydrogen bond to the rim of the CD cup. The better hydrogen bonding ability of the substrate is reflected in smaller oxygen quenching rate constants of 1-BrNp phosphorescence, presumably resulting from the substrates ability to be a more effective cap of the 1-BrNp•Gβ-CD complex.

Because hydrogen-bonding is important, we suspected that the introduction of additional hydroxyl groups on cyclohexanol might significantly enhance the intensity of the observed phosphorescence of the complex. This appears to be the case but only if the hydroxyl are judiciously placed about the cyclohexyl ring. For hydroxyls at the 1,2 positions of the ring, the diol appears to be a particularly excellent cap of the 1-BrNp•Gβ-CD complex and we observe the smallest quenching rate constant for any substrate. Examination of molecular models of the diol and CD cup shows the possibility for two-point hydrogen bonding, which is the situation for 1,3- and 1,4-diols. However, the 1,3-diol exhibits only intermediate behavior for oxygen inhibition and the 1,4-diol shows negligible inhibition of the oxygen quenching reactivity. While racemic mixtures of the cis and trans diols were employed, as opposed to the cis form of the 1,2-diol, the excess concentration of diols was large enough to ensure that the trans and cis conformers were each in the concentration independent regime of the luminescence response. As the hydrogen bonding groups move around the ring, the dispersion interaction between the

aliphatic cyclohexyl group and the hydrophobic interior of the CD is reduced, leading to a decrease in the stability of the complex owing to stronger dipolar interactions of the diol with water. Consequently, the substrate is less able to shield the 1-BrNp from oxygen. Decreased stability of CD complexes in aqueous solution upon increases in substrate polarity are well documented and also occurs when the basicity of the substrate increases [116]. Better hydrogen bonding interactions available in the more acidic environment of water are preferred to those offered by the CD hydroxyls.

CHAPTER 3

REGIOISOMERIC EFFECTS ON THE EXCITED STATE PROCESSES OF A CYCLODEXTRIN MODIFIED WITH A LUMOPHORE

Introduction

Supramolecular topologies based on cyclodextrin molecules may be exploited to engender novel physical and chemical processes. The hydroxyl rims, as shown in the last chapter, can be used as points of intermolecular attachment in a ternary supramolecular complex. In this chapter, the covalent attachment of lumophore to the primary and secondary rims of CDs will be discussed as receptor sites for bulky alcohol chemosensors. A covalent lumophore-CD complex is advantageous for marrying to optical fibers. Typically, the primary hydroxyls provide the most convenient points of attachment to the CD, because the reactivity of the secondary hydroxyl groups is diminished. However, when CDs are derivatized on the primary and secondary OH groups with the same functional group [117-119], substantial differences in thermal reactivity have been observed.

In recent years, the use of CDs to control molecular processes has been extended to reaction pathways proceeding through excited states. As a complement to the macromolecular fluorescent schemes designed for ion sensing [120], lumophores have

been appended [20,121] onto CDs to afford supramolecules that produce a luminescent signal upon association of neutral substrates. An important and outstanding issue in the design of photoactive CD supramolecules is whether regioisomeric effects on reactivity, so prominent in ground state processes, are manifested in excited state processes as well. The synthesis of photoactive CD regioisomers is rare [122], and to date no significant differences have been observed in the photophysics or photochemistry of these congeners. We now report an unusual example of differences in the excited state properties of regioisomers and in the chemistry of a bromonaphthalene lumophore appended to the primary (**1**) and secondary (**2**) OH groups of β-cyclodextrin.

Experimental

The reaction of dry β-CD with NaH in dry DMF, followed by addition of 1-bromo-2-bromomethylnaphthalene, yielded two regioisomers of the covalently bound phosphor-CD (Figure 12). The 1-bromonaphthalene is covalently tethered either to the primary or the secondary side of β-CD. These syntheses were developed by Dr. Mark Mortellaro and have been described in detail previously [101]. The compounds will be referred to as 1-BrNp-β-CD1 or **1** and as 1-BrNp-β-CD2 or **2**, for the primary and secondary side complexes, respectively. Emission spectra were collected on a Hitachi F4500 and lifetimes were collected as described in Chapter 2.

Results

The emission spectra of the two compounds showed dramatic differences in the photophysical properties of the triplet state (Figure 13). Whereas both molecules
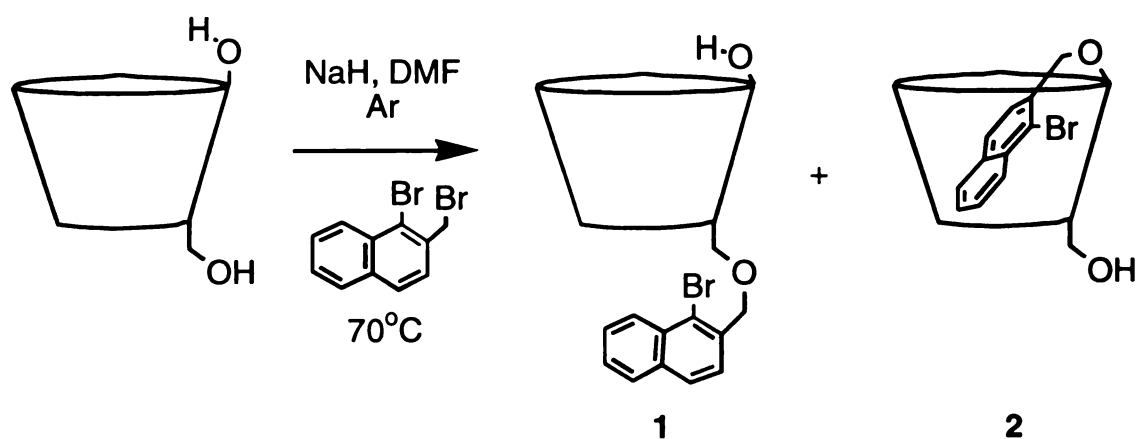
Figure 12. Synthesis of regioisomers of 1-bromonaphthalene covalently tethered to the primary (1) and secondary (2) hydroxyl rims of β-CD [101].
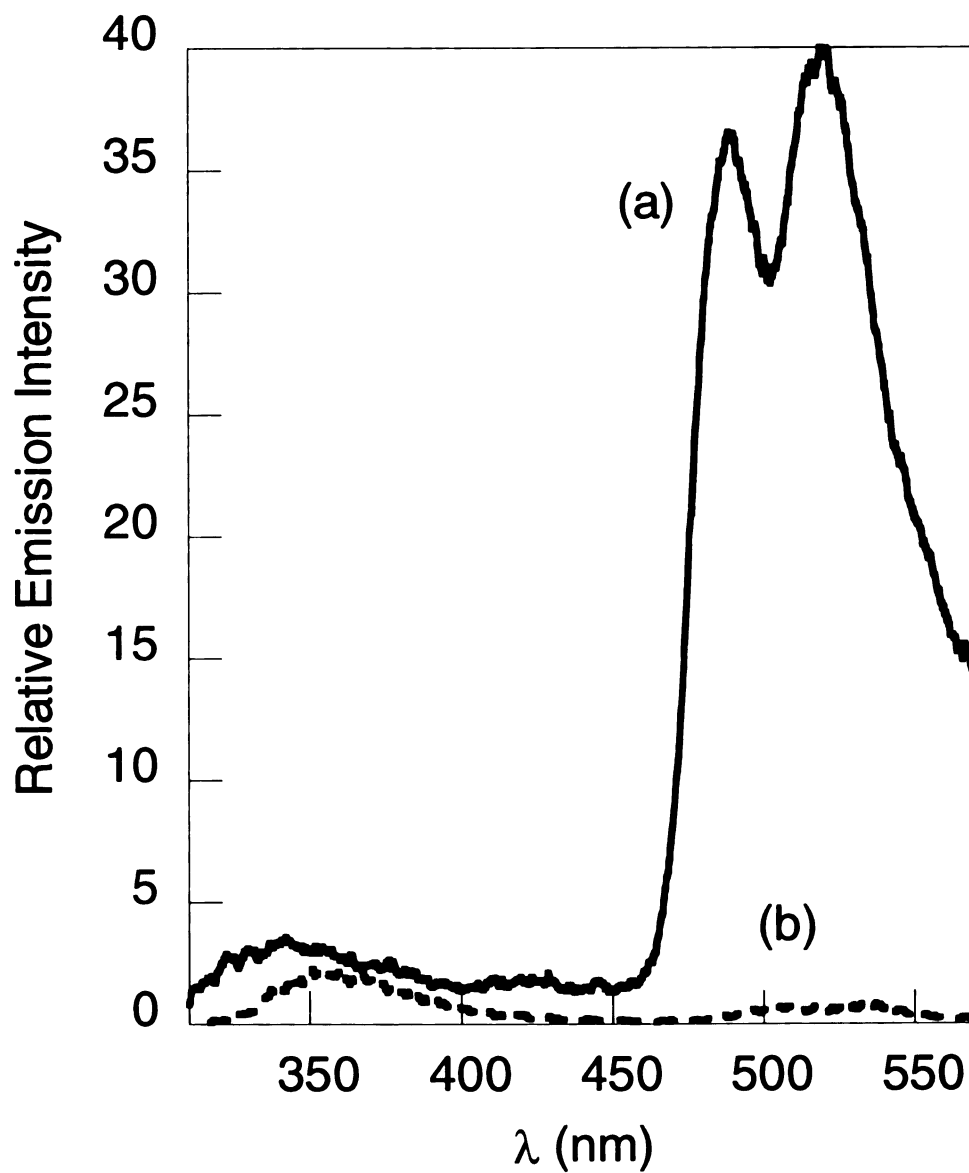
Figure 13. Relative emission intensity of (a) **2** and (b) **1** (each 1.0×10^{-4} M) in air-saturated aqueous solution (excitation wavelength $\lambda_{ex} = 290$ nm).

fluoresce at 350 nm, with nearly equivalent quantum yields, the phosphorescence quantum yield of 1-BrNp-β-CD2 at 530 nm is more than 10^2 times more intense than that observed for equimolar solutions of 1-BrNp-β-CD1 (ϕ_e^{530}(1) $\leq 10^{-4}$; ϕ_e^{530}(2) = 0.05 in aerated H$_2$O; ϕ_e^{530}(1 and 2) $\approx$ 0.06 in the absence of oxygen). Deoxygenation by freeze pump thaw or nitrogen purging results in a dramatic increase in the phosphorescence intensity of 1-BrNp-β-CD1, but only a slight increase for 1-BrNp-β-CD2, suggesting that the bromonaphthalene moiety of 1 is unprotected, whereas 2 is not. The fluorescence intensity is not affected significantly by deaeration.

The dissimilar properties of 1 and 2 may be attributed to the latter compound forming an intramolecular complex in which the bromonaphthalene moiety is included in the CD cavity. To prove this hypothesis, we looked for competitive binders that would displace the bromonaphthalene moiety of the cavity, thereby quenching the phosphorescence. Dodecyltrimethylammonium bromide (DTAB), a water soluble surfactant, was chosen as it is known to form inclusion complexes with β-CD [123]. Titration of 2 with DTAB results in a decrease of phosphorescence intensity of the bromonaphthyl moiety at 520 (Figure 14). The phosphorescence intensity approaches zero as DTAB concentration increases (to below the critical micelle concentration 5-15 mM). A fit of the data to a least squares routine [124], yields a K$_a$ of 1600 $\pm$ 160 M^{-1} for the binding of the bromonaphthyl moiety of 2 with the β-CD cavity, which is larger than the association of DTAB to β-CD [123]. Other cyclodextrins modified on the secondary face show a greater tendency to bind aromatic residues owing to increased hydrophobic interactions and solvent shielding [125]. Therefore the increased stability of 2 leads to an
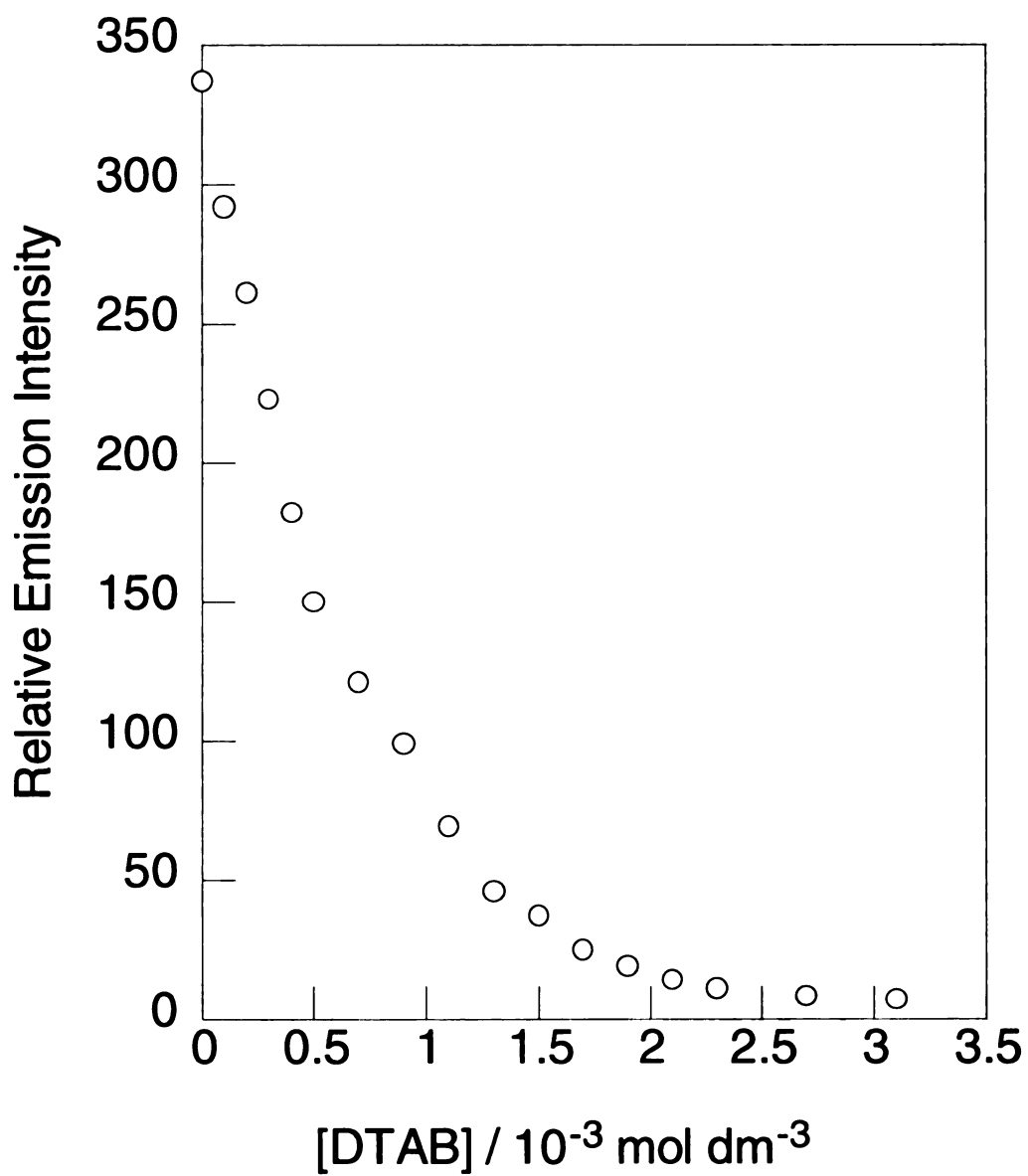
Figure 14. Phosphorescence intensity at 520 nm from **2** in aerated aqueous solution titrated with DTAB.

attenuation in the binding of DTAB. The results of the titration of DTAB can be ascribed to the quenching of 1-BrNp phosphorescence when the phosphor is excluded from the CD cup by a competitive guest.

To better define the quenching kinetics of the bromonaphthalene moiety of **1** and **2**, a water-soluble inorganic complex, $Co(NH_3)_6^{3+}$, was procured as a quencher of the excited state in deoxygenated solutions [126]. A list of the phosphorescence quenching rate constants in the absence of oxygen for **1, 2, 2** with DTAB, the binary complex of 1-BrNp•G-β-CD and free 1-BrNp in a methanol/water solution is given in Table 3. Stern-Volmer plots of the phosphorescence lifetime of 1-BrNp (τ_0/τ) versus concentration of Co^{3+} were linear with a y-intercept of unity. Several conclusions can be drawn from the data in Table 3. First, the large quenching rate constants of **1** and free 1-BrNp are similar in magnitude, indicating that the bromonaphthalene moiety of **1** is exposed to bulk solvent. Since 1-bromonaphthalene included in Gβ-CD shows nearly two orders of magnitude lower quenching, the data are consistent with in inability of **1** to form an intramolecular inclusion complex at a low concentration (intermolecular complexation is not observed). Table 3 shows that the quenching rate of 1-BrNp-β-CD2 is more than 10^4 slower than **1**. However, when **2** is saturated with DTAB, the bromonaphthalene moiety is quenched by Co^{3+} at a high rate, 1.7×10^8 $M^{-1}s^{-1}$, coinciding with the rates for **1** and free 1-BrNp. We can therefore conclude with certainty that compound **2** contains an intramolecularly included bromonaphthalene and that addition of DTAB displaces BrNp, thus exposing the excited state to quenching in solution by Co^{3+}. CPK modeling provided a more accurate description of the topology of the covalent complexes of BrNp and β-CD, **1** and **2**. The secondary side of β-CD is wide enough for inclusion of BrNp;

Table 3. Rate constants (k_q) for the phosphorescence quenching by $Co(NH_3)_6^{3+}$ in systems containing 1-bromonaphthalene and/or β-cyclodextrin, in deaerated aqueous solutions at 25 °C. Emission lifetimes were measured at 520 nm; excitation wavelength 309 nm.

Compound	$k_q/M^{-1}s^{-1}$
1-BrNp-β-CD2	1.5×10^3
1-BrNp•G-β-CD[a]	1.9×10^6
1-BrNp-β-CD1	8.2×10^7
1-BrNp-β-CD2•DTAB	1.7×10^8
1-BrNp[b]	1.8×10^8

[a] binary complex formed from G-β-CD and 1-BrNp [Ref. 100-101]

[b] 1-BrNp in methanol/water (1/1).

however, conversely, the primary side is too narrow for the unobstructed intramolecular binding of BrNp. We hope to use these novel results for future design of CD-based supramolecular assemblies and in determining how energy flows, based on the topology of a phosphor appended CD. The next section discusses model ternary systems for designing linkages that will maximize the geometry restraints of bromonaphthalene in a β-cyclodextrin cavity.

Conclusions

Electronic structure and conformational geometry both contribute to the overall phosphorescence response of bromonaphthalene emission in regioisomeric covalent complexes of cyclodextrin and bromonaphthalene and in ternary complexes of CDs, alcohols and bromonaphthalene derivatives. From the study of regioisomeric compounds, only the derivative **2** formed an intramolecular complex in which the appended bromonaphthalene is inside the cyclodextrin cavity, giving rise to novel room temperature phosphorescence in an oxygenated and aqueous environment. These results show that regioisomeric effects can control reactions of the excited state of photoactive CDs. Such issues will play an especially prominent role in the design of CD-based supramolecules for optical sensing, especially those that derive their function from equilibria of appended lumophores inside and outside the CD cup.

CHAPTER 4

ELECTRONIC STRUCTURE EFFECTS OF BROMONAPHTHALENE-CD COVALENT AND TERNARY COMPLEXES

Introduction

The synthesis of regioisomeric compounds of 1-BrNp and β-CD, **1** and **2**, revealed that the structure of an intramolecular inclusion complex can significantly affect the photophysical properites. Covalent attachment of 1-BrNp to β-CD at the 2-position of the naphthyl ring with one methyl spacer did not provide us with a phosphorescence triggered optical signal in the presence of bulky alcohols. We presumed that the close proximity of the bromine to the CD linking position was not the optimal topology for the intramolecular complex. Therefore, an investigation of substituted bromonaphthalenes in ternary complexes with G-βCD and t-BuOH was initiated in an attempt to predict the photophysical properties of a covalent lumophore-CD complex. Our efforts to study various substituted 1- and 2-BrNp and to predict the behavior of bromonaphthalene appended cyclodextrin complexes prior to synthesis are now described.

Experimental

The synthesis of 2-bromo-6-alkoxynaphthyl-β-CD was achieved by Jude Rademacher [127] using methods similar to the synthesis of the regioisomeric cyclodextrins prepared in Chapter 3. Mono glucosyl-β-cyclodextrin (Gβ-CD) was purchased from CTD, Inc. and used without further purification. *Tert*-butanol (t-BuOH) was purchased from Fisher and used as received. The following substituted naphthalenes were obtained from Aldrich: 5-bromoacenaphthalene (5-BrAcNp), 1-bromo-2-methylnaphthalene (1-Br-2-MeNp), 1-bromo-4-methylnaphthalene (1-Br-4-MeNp), 1-bromo-2-naphoic acid (1-Br-2-NpA), 2-bromo-6-naphoic acid (2-Br-6-NpOH), 2-bromo-6-methoxynaphthalene (2-Br-6-MeONp). Other compounds employed in this study were 1-bromo-2-naphthoic acid (1-Br-2-NpA, Sigma) and 1-bromo-2-methoxynaphthalene (1-Br-2-MeONp, Crescent Chemicals). Absorption spectra were collected on the OLIS Cary 17, and emission spectra and quantum yields were collected on the high-resolution research instrument as described in Chapter 2.

Results

The absorption spectra of bromonaphthalene derivatives, 1-BrNp, 1-Br-2-NpA, 1-Br-2-MeNp, 1-Br-4-MeNp, 1-Br-2-NpOH, 2-Br-6-NpOH, 1-Br-2-MeONp and 2-Br-6-MeONp have different absorption maxima (Figure 15 and Figure 16). The maxima for 1-BrNp, 1-Br-2-NpA and 1-Br-2-MeNp coincide at 285 nm, whereas 1-Br-4-MeNp is red-shifted (λ_{max} = 290 nm) and all other derivatives are blue shifted, 1-Br-2-MeONp (λ_{max} = 283 nm), 1-Br-2-NpOH (λ_{max} = 279nm), 2-Br-6-NpOH (λ_{max} = 276nm) and 2-Br-6-MeONp (λ_{max} = 272nm). Additionally, the hydroxyl and methoxy substituted
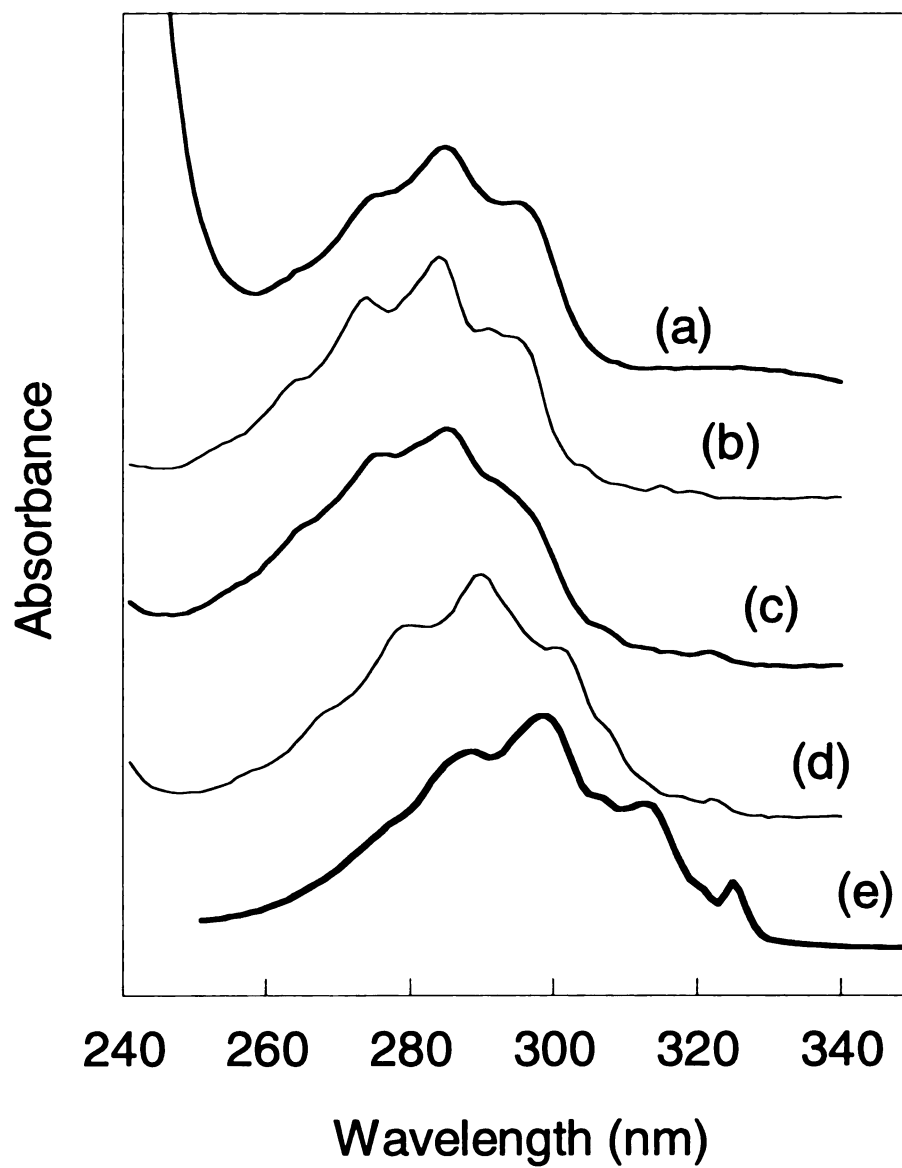
Figure 15. Absorption spectra of (a) 1-Br-2-NpA, (b) 1-BrNp, (c) 1-Br-2-MeNp (d) 1-Br-4-MeNp, (e) 5-BrAcNp in methanol.
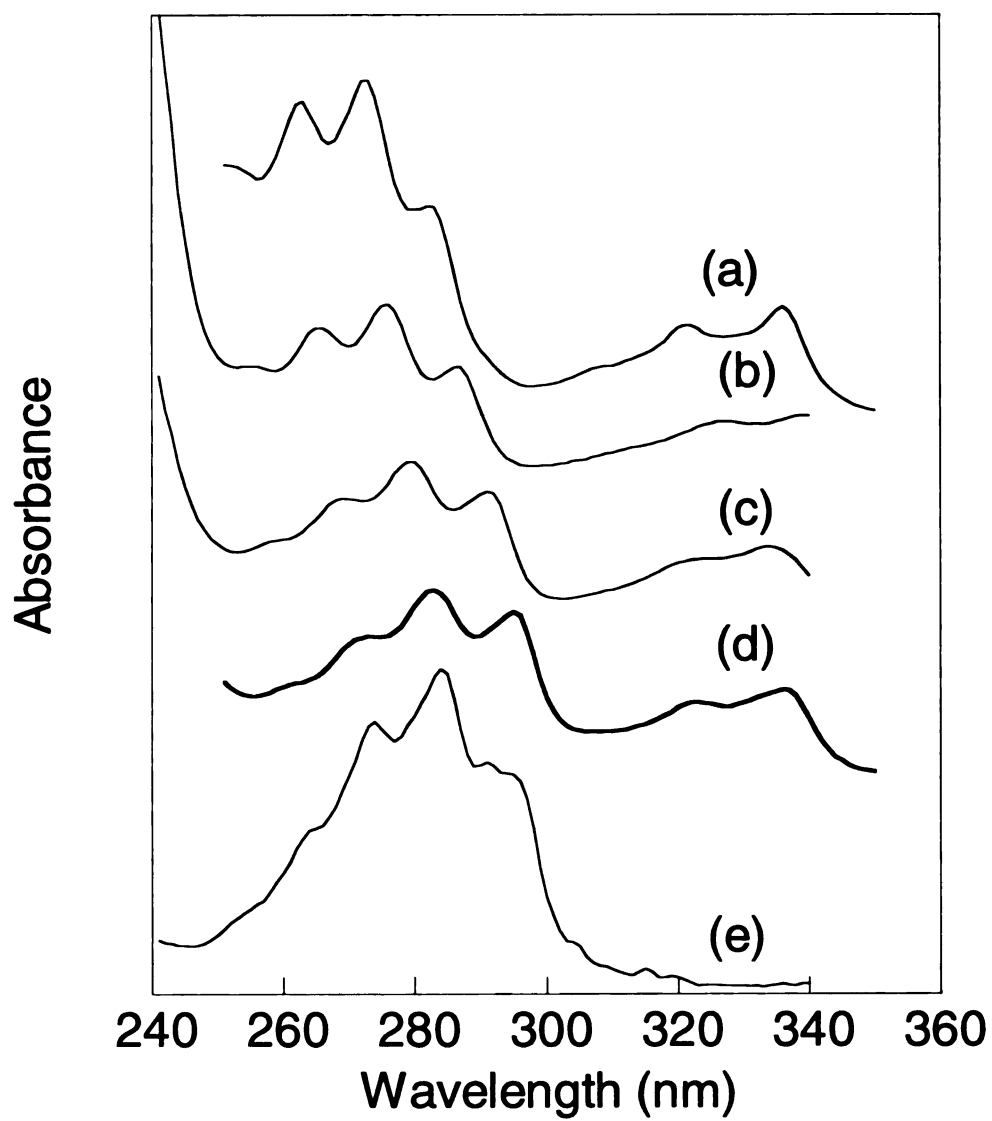
Figure 16. Absorption spectra of (a) 2-Br-6-MeONp, (b) 2-Br-6-NpOH, (c) 1-Br-2-NpOH (d) 1-Br-2-MeONp, (e) 1-BrNp in methanol.

bromonaphthalenes show the appearance of a second absorption band in the 320-430 nm range. Therefore, the excited state energy is unchanged when substitutents in the 2-position are methyl or carboxylic acids, is stabilized upon substitution in the 4- position and is destabilized when hydroxyl or methoxy groups are substituents. Table 4 lists the absorption maxima and the molar absorptivities measured in methanol solutions. The molar absorbtivites were derived from Beer's law with a dilute solution (1×10^{-4} M). The molar absorptivies of 1-BrNp, 1-Br-2-MeNp, 1-Br-4-MeNp and 5-BrAcNp are all around 8000 $M^{-1}cm^{-1}$, whereas the compounds containing hydroxyl or carbonyl groups have significantly smaller molar absorptivies around 5000-6000 $M^{-1}cm^{-1}$.

The titration profiles of *tert*-butanol with 1-BrNp, 1-Br-4-MeNp, 1-Br-2-MeNp, 1-Br-2-NpOH and 2-Br-6-MeONp and 2.5 mM Gβ-CD are shown in Figure 17. The methyl substituted bromonaphthalenes show the largest phosphorescence response with added alcohol, followed by the bromonaphthols. 2-Br-6-MeONp shows no increase in bromonaphthalene phosphorescence. The phosphorescence emission spectra of bromonaphthalene derivatives are shown in Figure 18. With the exception of 2-Br-6-MeONp the phosphorescence profiles for 1-Br-4-MeNp, 1-Br-2-MeNp, 1-Br-2-NpOH and 5-BrAcNp have identical phosphorescence profiles. The maxima of 1-Br-4-MeNp is noticeably red shifted relative to 1-BrNp and to the other derivatives.

The results for the bromonaphthalene derivatives are summarized in Table 4.The quantum yields show that bromonaphthalenes with only methyl substituents have a larger quantum yields than 1-Br-2-NpOH, 2-Br-6-NpOH, 1-Br-2-NpA, 1-Br-2-MeONp and 2-Br-6-MeONp. The oxygen quenching rate constant follows the trend of the quantum yields; roughly, the quenching rate constant decreases with increasing quantum yield.

Table 4. Quantum yields, equilibrium constants and oxygen quenching rate constants for bromonaphthalene phosphor derivatives with Gβ-CD (10^{-3} M) and t-BuOH (in the asymptotic limit).

Phosphor	λ_{max} /nm abs	$\phi_{phos}/10^{-4}$	$\varepsilon/M^{-1} cm^{-1}$	$k_q/10^5 M^{-1}s^{-1}$
1-BrNp	285	340	8670	8.87
1-Br-2-NpA	285	0	5162	$>10^3$
1-Br-2-MeNp	285	124	8006	5.89
1-Br-4-MeNp	290	269	7837	4.28
1-Br-2-NpOH	279	37	5027	33.0
5-BrAcNp	299	134	8315	11.0
2-Br-6-NpOH	276	0	5054	$>10^3$
1-Br-2-MeONp	283	0	6210	$>10^3$
2-Br-6-MeONp	272	0	5787	$>10^3$
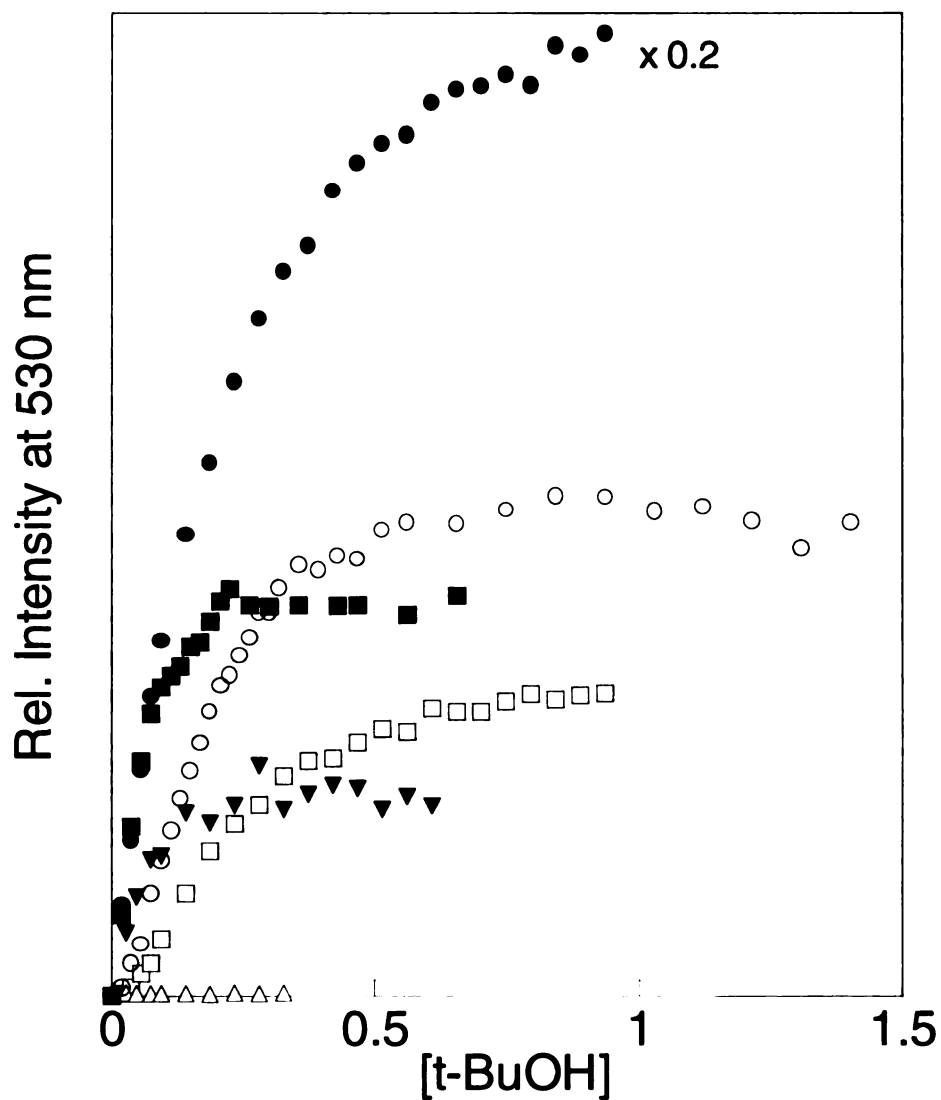
Figure 17. Dependence of relative phosphorescence intensity of 1-BrNp (●) 1-Br-4-MeNp (O) 1-Br-2-MeNp (■), 5-BrAcNp (□), 1-Br-2-NpOH (▼) and 2-Br-6-MeONp (△) at 530 nm from aerated solutions containing Gβ-CD (10⁻³ M) concentration and increasing concentration of t-BuOH.
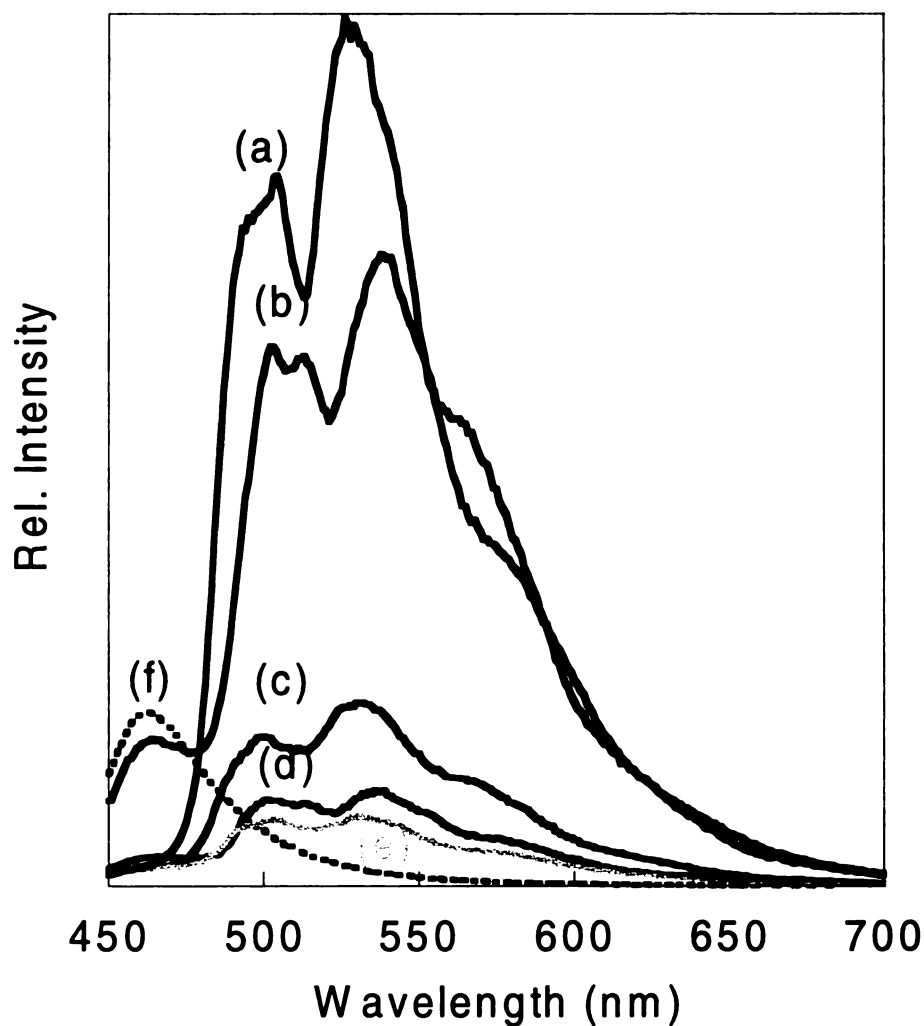
Figure 18. Luminescence spectra of (a) 1-BrNp (b) 1-Br-4-MeNp (c) 1-Br-2-MeNp (d) 5-BrAcNp (e) 1-Br-2-NpOH (gray) (f) 2-Br-6-NpOH (dotted line) from aerated aqueous solution of Gβ-CD (10^{-3} M) in the presence of ~ 3% v/v of t-BuOH. Spectra were collected in the asymptotic limit of the titration profiles shown in Figure 17.

We were interested in studying the photophysical properties of 2-Br-6-MeONp covalently linked to β-CD because of its lack of phosphorescence in the presence of added alcohol. Figure 19 shows the fluorescence and phosphorescence of the covalent lumophore-CD complex, 2-bromo-6-alkoxy-naphthyl-β-CD (2-Br-6-NpCD), in aerated and degassed solutions. Addition of t-butanol and cyclohexanol to 2-Br-6-NpCD did not result in triggered phosphorescence. The explanation for this behavior may be related to the conformational and electronic differences between 1- and 2-substituted bromonaphthalenes in a cyclodextrin cavity. It has been shown by circular dichroism that 1- and 2-substituted naphthalenes have different orientations in a β-cyclodextrin [128]. The two modes of inclusion of naphthyl-moities in a CD cavity are axial and equatorial, as shown in Figure 20. Naphthalenes substituted in the 1 position on the ring can orient in either axial or equatorial positions, whereas 2-substituted naphthalenes prefer an axial conformation. Since 2-BrNp and its derivatives are axially oriented in the cyclodextrin cavity, this topology could result in a triplet excited state that is readily quenched by oxygen. The equatorial conformation that 1-BrNp can assume in a CD cavity appears to be optimal for shielding the triplet state. Therefore complexes that favor the equatorial conformation are ideal for the design of covalent BrNp-CD complexes.

Molecular Modeling

Energy minimizations on Discover were used for visualizing the geometrical constraints of covalent and binary complexes of 1-bromo-X-methyl naphthalene (where X is the position on the naphthyl ring) and Gβ-CD. The results are shown in Figure 21.
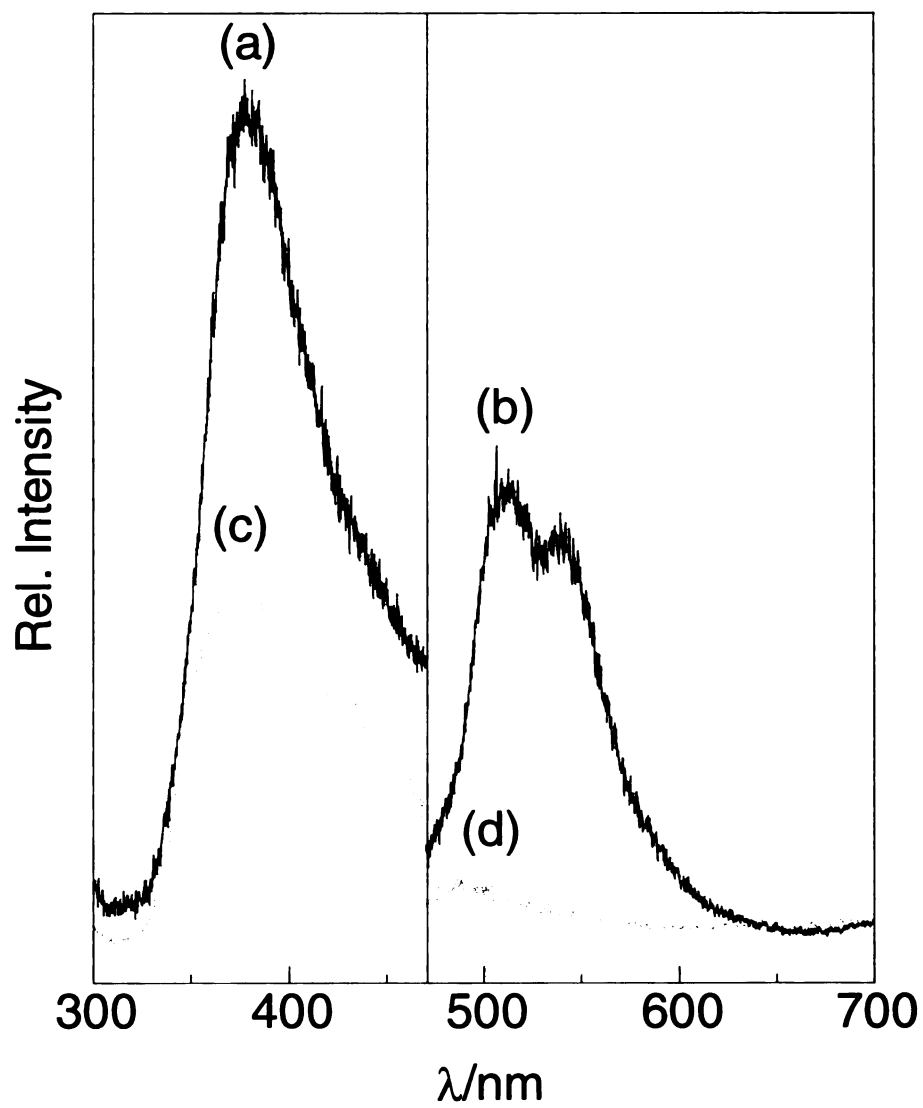
Figure 19. Fluorescence (a,c) and phosphorescence (b,d) of 2-bromo-6-alkoxy-*β*-cyclodextrin in water for degassed (a,b) and aerated (c,d) solutions.
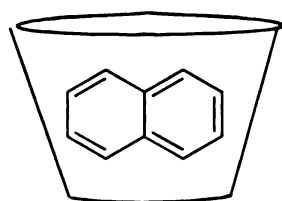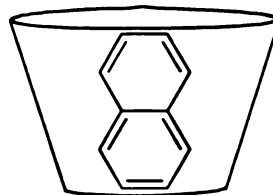
Equatorial   Axial

Figure 20. Equatorial and axial conformations of naphthalene in a β-cyclodextrin cavity.

(a)
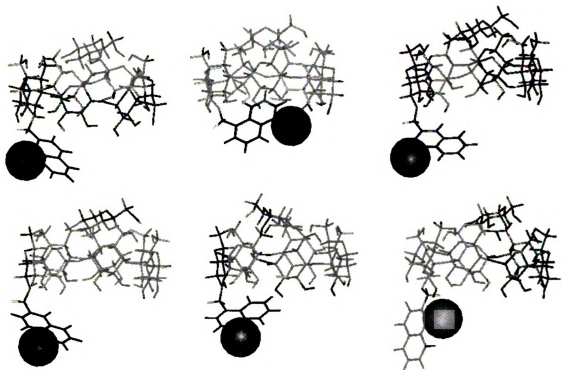
(b)
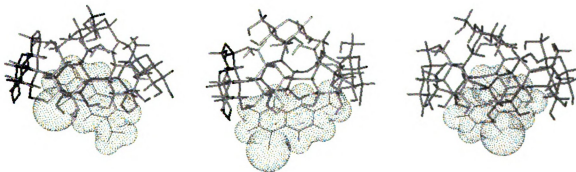
Figure 21. (a) Energy minimizations of bromonaphthalene derivatives covalently bound to Gβ-CD. From left to right the molecules are: (first row) 1-bromo-7-methyl-Gβ-CD, 1-bromo-5-methyl-Gβ-CD, 1-bromo-3-methyl-Gβ-CD, (second row) 1-bromo-6-methyl-Gβ-CD, 1-bromo-4-methyl-Gβ-CD, 1-bromo-2-methyl-Gβ-CD. (b) Energy minimizations of binary complexes of bromonaphthalene derivatives. 1-bromo-7-methylnaphthalenewith Gβ-CD (left), 1-bromo-6-methylnaphthalenewith Gβ-CD (middle) and 1-bromo-5-methylnaphthalenewith Gβ-CD (right).

The covalent complexes of 1-bromo-5-methylnaphthalene and 1-bromo-4-methyl naphthalene have geometries where the naphthyl ring is close to the hydrophobic cavity. The naphthalene moieties are attached to the secondary side and the glucosyl group is on the primary side. The bromonaphthyl substituted covalent cyclodextrins (X = 2, 3, 6, and 7) give conformations where the phosphor moiety is far away from the hydrophobic pocket. In all cases of the covalent complexes it appears that the bromonaphthalene is unprotected.

The lower half of the figure shows minimizations for binary complexes of 1-bromo-7-methylnaphthalene, 1-bromo-6-methylnapthalene and 1-bromo-5-methylnapthalene with Gβ-CD. In all cases the included molecule prefers an orientation where the bromine atom extends away from the secondary side of the cyclodextrin. A comparison of the binary complexes of 1-Br-7-MeNp, 1-Br-6-MeNp, 1-Br-5-MeNp and Gβ-CD with the covalent complexes shows that none of these complexes have similar conformations once they are covalently linked to the cyclodextrin. This indicates that a covalent bond significantly hinders the movement of the bromonaphthyl moiety.

Figure 22 and Figure 23 reveal the conformations for binary complexes of 1-BrNp, 2-BrNp, 1-Br-2-MeNp, 1-Br-2-MeNp and 1-bromo-2-naphthoate with Gβ-CD. The structures on the left are minimized with the bromine portion of bromonaphthalene away from the cavity and the right side shows minimizations for binary complexes where bromine was pointed towards the cyclodextrin cavity. From these models we observe that bromine protrudes from the either primary and secondary side of the cyclodextrin for both isomers depending on the orientation prior to minimization. Another observation is that 1-bromonapthalene orients itself at a 45° angle between an axial and equatorial

(a)
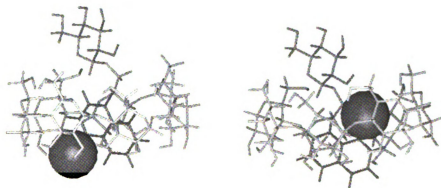
(b)
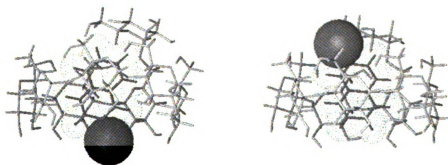
Figure 22. Energy minimization of (a) 1-bromonaphthalene with Gβ-CD (b) 2-bromonaphthalene with G-β-CD. The cyclodextrin is shown as a gray stick, bromonaphthalene is a black stick and bromine is a solid ball.

(a)

(b)
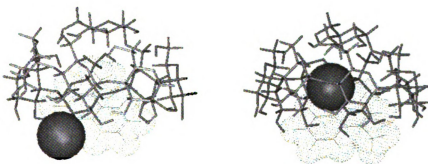
(c)
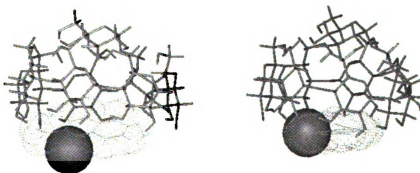
Figure 23. Energy minimization of (a) 1-bromo-2-methylnaphthalene with Gβ-CD (b) 1-bromo-4-methylnaphthalene with Gβ-CD (c) 1-bromo-2-naphthoate with Gβ-CD.

orientation, whereas 2-bromonapthalene prefers an axial position. These molecular models are consistent with the circular dichroism data. Additionally, they may explain why we do not see phosphorescence for 2-bromonapthyl derivatives. Turro et al. have also observed weaker emission from 2-bromonaphthalene in comparision with 1-bromonaphthalene [96a]. The dipole moment of bromonapthalene is also related to the orientation in the cyclodextrin cavity [128]. However, although there is a slight difference in the ground state dipole moment between 1-BrNp and 2-BrNp, orientations of 1-BrNp and 2-BrNp in the cyclodextrin cavity is dramatic.

The orientation of binary complexes of 1-Br-2-MeNp and 1-Br-4-MeNp in Gβ-CD is shown in Figure 23. The similarity between the orientation of the two methyl substituted naphthalenes and the 1-bromonapthalene is striking. In contrast, the minimization of 1-bromo-2-naphthoate, reveals that the bulkiness of the group hinders the molecule from entering the hydrophobic cavity.

Conclusions

Synthesis of another appended bromonaphthalene-β-CD, 2-bromo-6-alkoxy-β-cyclodextrin, also reveals that the orientation of bromonaphthalene in the cyclodextrin has profound effects on the photophysical properties of the excited state. Although bromonaphthalene was attached at the secondary face of the cyclodextrin, room temperature phosphorescence was not observed under aerated conditions, and only appeared when the solutions were degassed. Addition of tert-butanol and cyclohexanol also failed to trigger a luminescent response. It appears that 2-Br-6-alkoxy-β-CD does not form an intramolecular complex with the cavity.

As a result of the unpredictable results of covalent complexes of Gβ-CD and bromonaphthalene, investigations of the photophysics of other bromonaphthalene compounds were performed. In general, bromonaphthalene derivatives containing methyl groups only slightly perturb bromonaphthalene phosphorescence from ternary complexes of 1-bromo-X-naphthalene•Gβ-CD•t-BuOH, whereas hydroxy and methoxy groups greatly decrease the phosphorescence intensity. It has been proven that the orientation of the bromonaphthalene in cyclodextrin cavities is related to the dipole moment of the guest [128]. Therefore a measurement of the dipole moment may allow us to predict the orientation of bromonaphthalene in a CD cavity. Circular dichroism studies may assist in determining the orientation and therefore allow us to determine which orientations lead to bromonaphthalene phosphorescence. It appears that an equatorial conformation of BrNp in the cyclodextrin cavity is necessary for phosphorescence. Molecular modeling, through the use of Biosym Insight Discover, has proven insightful in explaining many of the properties of binary and tertiary cyclodextrin complexes with bromonaphthalene guests and alcohol substrates. However, it does not provide an accurate description of the topology of the covalent compounds of bromonaphthalene attached at the primary and secondary rims (**1** and **2**). The difficulty in visualizing these structures by computer modeling is that the structures shown are only one of many possible local minima. CPK modeling is more accurate in predicting the structure and orientational restrictions of covalent complexes, as the models are more rigid.

In conclusion, we have demonstrated that we can synthesize supramolecular architectures with a phosphor and host structure that trigger very bright luminescence. The enhancements in phosphorescence approached 10^5. From the study in this chapter it

appears that the next logical choice of bromonaphthalene starting material for the synthesis of covalent phosphor materials is 1-Br-4-MeNp with β-CD. Secondly, lengthening the linking group between the bromonaphthlalene and cyclodextrin may also allow for more flexibility. Lastly, studies of other water soluble methylated β-cyclodextrins may be another alternative to Gβ-CDs for synthesizing photoactive sites for optical chemosensing of alcohols. The challenge that remains is balancing the structure of the complex to compliment the desired photophysics. We are in the final steps of incorporating optical transductions schemes into a prototype sensing device.

CHAPTER 5

ENERGY TRANSFER THROUGH COVALENT BONDS:
LANTHANIDE CHELATES

Introduction

Energy transfer processes for the design of BTX and PAH optical sensors will be developed with (1) an understanding of simple model complexes where energy transfer donors and acceptors are held at fixed distances; and (2) authentic systems where the PAH or BTX analyte is juxtaposed to the lanthanide ion and energy transfer does not occur through covalent bonds. Electronic energy transfer is the transfer of energy from an excited state donor molecule to a ground state acceptor. The functional form of the distance dependence is determined by the type of interaction between the donor and acceptor. Dipole-dipole interactions (Förster) engender a transfer rate proportional to $1/R^6$ (Figure 24a) [17]. For this mechanism, energy transfer may occur over distances as long as 80-100 angstroms (Å), as is the case for photosynthetic reaction centers [129]. Conversely, exchange (Dexter) (Figure 24) interactions vary as a function of e^{-R}

**Förster
(Coulombic)**

**Dexter
(Exchange)**

$$k_{en} = \frac{1}{\tau_D} \left(\frac{R_o}{R_{DA}}\right)^6$$

$$k_{en} = \frac{2\pi}{h} KJ \cdot exp\left(\frac{-2R_{DA}}{L}\right)$$

$$R_o^6 = \frac{9000(\ln 10)\kappa^2 \Phi_D J}{128\pi^5 n^4 N_{AV}}$$
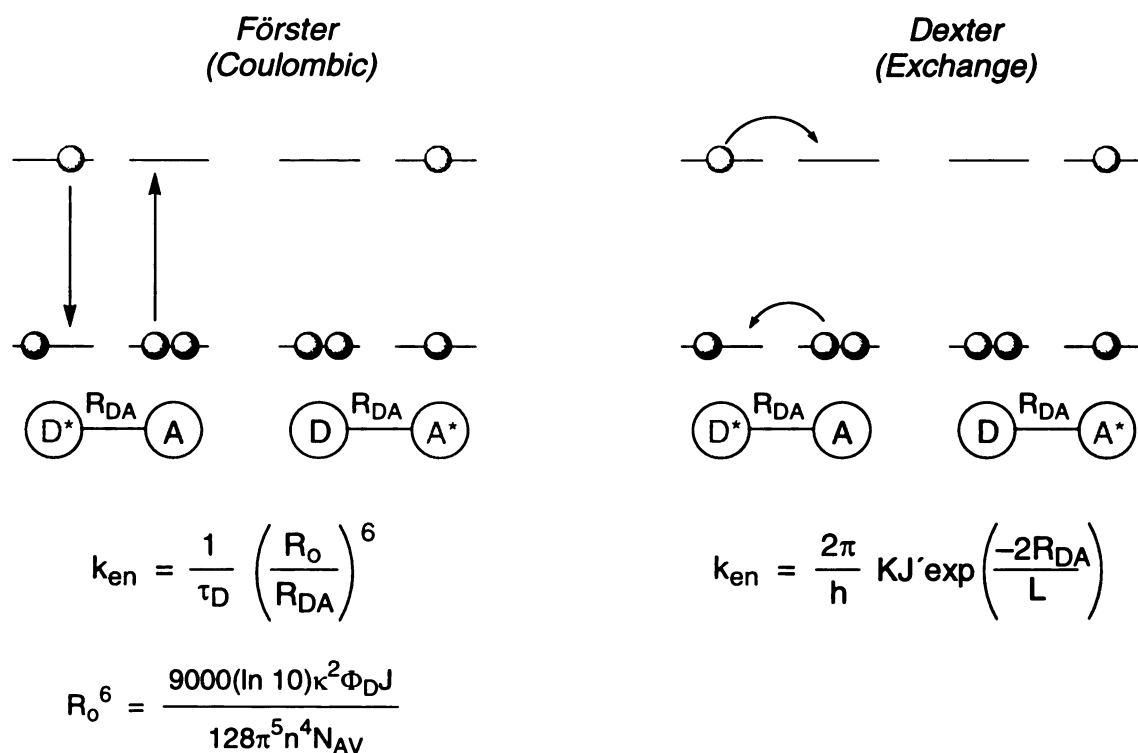
Figure 24. Two possible mechanisms of energy transfer and the rate expressions [17] D^* and A^* are the excited electronic states of the donor and acceptor. D and A are the ground states. R_{DA} is the intermolecular distance. Other variables are described in the text.

and require that the donor and acceptor orbitals overlap at van der Waals contact. Consequently, this type of energy transfer dominates at short distances.

Förster Coulombic Theory

Förster described the theory of dipole-dipole (coulombic, resonance) interactions where a fluorescent molecule loses its excitation energy non-radiatively and noncollisionally [130]. Since light, a beam of photons, is an electromagnetic wave propagating through space, there are electric and magnetic vectors both oriented perpendicular to the direction of propagation. The probability that light is absorbed is dependent on the angle between the electric field vector of the incident light and the absorption axis of the molecule. When a donor molecule is excited by this electromagnetic wave there is a transition dipole moment created for the absorption and emission of the light [131]. The transition moments are related to the absorption and emission spectra of the molecule. For dipole-dipole energy transfer, only the emission dipole of the donor and absorption dipole of the acceptor are involved. When these two dipoles interact across a distance of $1/R^6$, the donor transition dipole induces a dipole oscillation in the acceptor and causes non-radiative energy transfer. The equation that describes dipole-dipole energy transfer is,

$$k = \frac{1}{\tau_D}\left(\frac{R_0}{R}\right)^6 \tag{17}$$

where τ_D is the donor lifetime, R_0 is the critical energy transfer distance or Förster distance and R is the actual distance between the donor and acceptor. The equation for R_0

measured in angstroms (Å) is

$$R_0 = 9.78 \times 10^3 \left\{ Q_D \kappa^2 n^{-4} J \right\}^{1/6}$$ (18)

where J, the overlap integral, is measured in units of $M^{-1} cm^3$ units. Q_D is the donor quantum yield, κ is the orientation factor (2/3 for an isotropic distribution), and n is the index of refraction, which appears because of the two point dipole interaction in an isotropic medium.

The overlap integral is measured by taking the emission spectrum of the donor, the absorption spectrum of the acceptor, and evaluating the following integral over wavenumber, $\tilde{\nu}$.

$$J = \int_0^\infty \frac{f_D(\tilde{\nu}) \varepsilon_A(\tilde{\nu})}{\tilde{\nu}^4} d\tilde{\nu}$$ (19)

It is important to note that this overlap integral includes the normalized donor emission spectrum, $f_D(\tilde{\nu})$, and the molar absorptivity, $\varepsilon_A(\tilde{\nu})$, which is not normalized to unity. The factor of $(\tilde{\nu})^4$ originates from the classical harmonic oscillator approximation and oscillator strengths. The overlap integral, J, is directly related to the critical distance, R_0, and can vary from 10^{-14} to 10^{-20} M^{-1} cm^3.

If one can experimentally determine the rate of the energy transfer and therefore determine the distance R, it is possible to determine the efficiency of energy transfer by inspection of the calculated values of R_0 derived from J. When $R_0 = R$ the efficiency of energy transfer is 50%. Half of the energy goes to the acceptor, and the other half is dissipated by heat and other processes. The smaller R becomes relative to R_0, the more efficient the process; the larger R becomes relative to R_0, the less efficient the process.

From R_0 and R, we can evaluate the efficiency of the process by the following equation:

$$E = \frac{R_0^6}{R_0^6 + R^6} \qquad (20)$$

There are numerous examples of dipole-dipole energy transfer in the literature, among the most prominent are photosynthetic chlorophyll [129] and artificial light-harvesting centers [132]. Resonance energy transfer (another term for the dipole-dipole mechanism) is invoked in many biological systems to obtain donor-acceptor distances [131]. One additional example of Förster energy transfer where a solid state photon antenna device with efficiencies approaching unity is being developed is the work of Daschak and Mallouk [133].

Dexter Exchange Theory

Energy transfer events occur at van der Waals distances if exchange interactions dominate. The theory of exchange energy transfer was derived by D.L. Dexter [134]. The rate constant for this type of interaction is,

$$k = KJ \, exp\left(\frac{-2R}{L}\right) \qquad (21)$$

where K is a constant related to specific orbital interactions, J is the spectral overlap integral of the normalized emission of the donor and normalized absorption of the acceptor, R is the distance from the donor to the acceptor relative to L, the sum of the van der Waals radii [17].

There are several differences between Förster and Dexter energy transfer. Electron exchange interactions are purely quantum mechanical and, unlike Förster dipole-dipole interactions, have no classical description. The efficiency cannot be related

to an experimental quantity. Exchange interactions are strongest at shorter distances and dipole-dipole interactions dominate at longer distances, depending on the oscillator strengths of the acceptor and the overlap integral. Photosynthetic systems, where the oscillator strengths of chlorophyll are large, have efficient transfers at 80-100 Å because the values for the overlap integral J are larger (1 x 10^{-14} M^{-1} cm^3). The rate of dipole-dipole energy transfer depends on the oscillator strength, whereas for exchange interactions there is no dependence on oscillator strength as the acceptor's molar absorptivity is normalized.

Closs and coworkers, have defined the most renowned study of triplet-triplet energy transfer, an exchange interaction involving an electron transfer and a hole transfer [135]. As shown in Figure 24 the rate for triplet-triplet energy transfer can actually be derived from the rates for electron transfer (k_{ET}) and hole transfer (k_{HT}):

$$k_{TT}(St, N) = C k_{ET}(St, N) k_{HT}(St, N) \qquad (22)$$

where St represents the steric factor, N is the number of σ bonds between the donor and acceptor, and C is a constant containing the ratio of the electronic coupling matrix element and the Frank Condon weighted density of states. Distance and driving force were varied in the Closs triplet-triplet energy transfer systems.

Another example of a triplet-triplet exchange energy transfer is the non-covalent system of biacetyl donor and hemicarcerand-aromatic acceptor complexes examined by Farran and Deshayes [136]. Bimolecular energy transfer between biacetyl and aromatic hydrocarbons has a diffusion controlled energy transfer rate. However when trapped inside a hemicarcerand cage, the rate of the energy transfer from biacetyl to various aromatic acceptors follows a Marcus curve and is well below the diffusion limited value,

so that energy transfer rates in the Marcus inverted region are observed. In this case, the hemicarcerand walls prevent direct contact between donor and acceptor and retard the rates of energy transfer. Structural models revealed that the distance between the biacetyl donor and the acceptor on the outside of the hemicarcerand complex is 7 Å. The decrease in rate when the hemicarcerand is used as a spacer is concomitant with a decrease in electronic coupling. Another equation for exchange energy transfer relates the rate to the driving force (ΔG) of the reaction. The driving force is proportional to the energy gap between the donor and acceptor excited states:

$$k = A \, exp \left[-\frac{\left(\lambda_s + \Delta G + \lambda_v\right)^2}{4\lambda_s k_B T} \right] \tag{23}$$

where A is the preexponential factor, λ_s is the solvent reorganization energy, λ_v is the vibrational reorganization energy and ΔG is the thermodynamic driving force. The theoretical curve was fit with values of 0.20 eV for both λ_s and λ_v.

A third example of a Dexter mechanism that has been studied extensively in the literature is energy transfer in photosynthetic systems where the donors are carotenoids (polyenes) and the acceptors are chlorophyll [129]. Originally it was thought that energy transfer was due to a dipole-dipole interaction; however upon closer inspection some groups are beginning to find evidence that both singlet-singlet and triplet-triplet mechanisms actually follow Dexter exchange theory more closely [129, 137]. The reason given for a Dexter mechanism was a small spectral overlap between carotenoid emission and Q_y transition of chlorophyll, a small transition dipole moment and forbidden optical and spin transitions.

Lanthanide Spectroscopy and Electronic Structure

Lanthanide ions are ideal for optical chemosensing of BTXs and PAHs. When directly excited very weak emission is observed, owing to the low molar absorptivites of lanthanide ions. However, once excited indirectly these ions luminesce efficiently in the visible region of the electromagnetic spectrum with long radiative lifetimes.

The electronic structure of lanthanide ions is unique as a result of the properties of f-orbitals and spin-orbit coupling (Figure 25). Because the f-orbitals are buried in the atom core, their bonding involves a much weaker overlap when compared to d-orbitals. The spectroscopy of d-block elements is therefore dominated by the coordination environment of the metal ion. The crystal field splittings due to the presence of the ligands is large in d-block elements, whereas the spin-orbit coupling is small. However, lanthanide spectroscopy is dominated by spin-orbit coupling; therefore transitions between "spin forbidden" states is no longer an issue. The spherical symmetry of a lanthanide ion is destroyed when it is surrounded by ligands in a crystal, glass or solution [138]. Figure 25 shows the splitting into terms due to interelectronic repulsions (~ 20000 from spin-orbit coupling, and into sublevels from ligand crystal field splittings.

The selection rules for lanthanide electronic transitions are derived from Judd-Ofelt theory of forced electronic dipole transitions, since transitions within the f-orbital manifold are electronically and spin forbidden [139]. The forced electronic dipole selection rules for lanthanides state that neither the $\Delta S = 0$ nor the $\Delta L = 0$ rules are obeyed. A description of the lanthanide selection rules can be found in Bünzli's chapter in *Lanthanide Probes in Life, Chemical and Earth Sciences* [138]. As a result of the
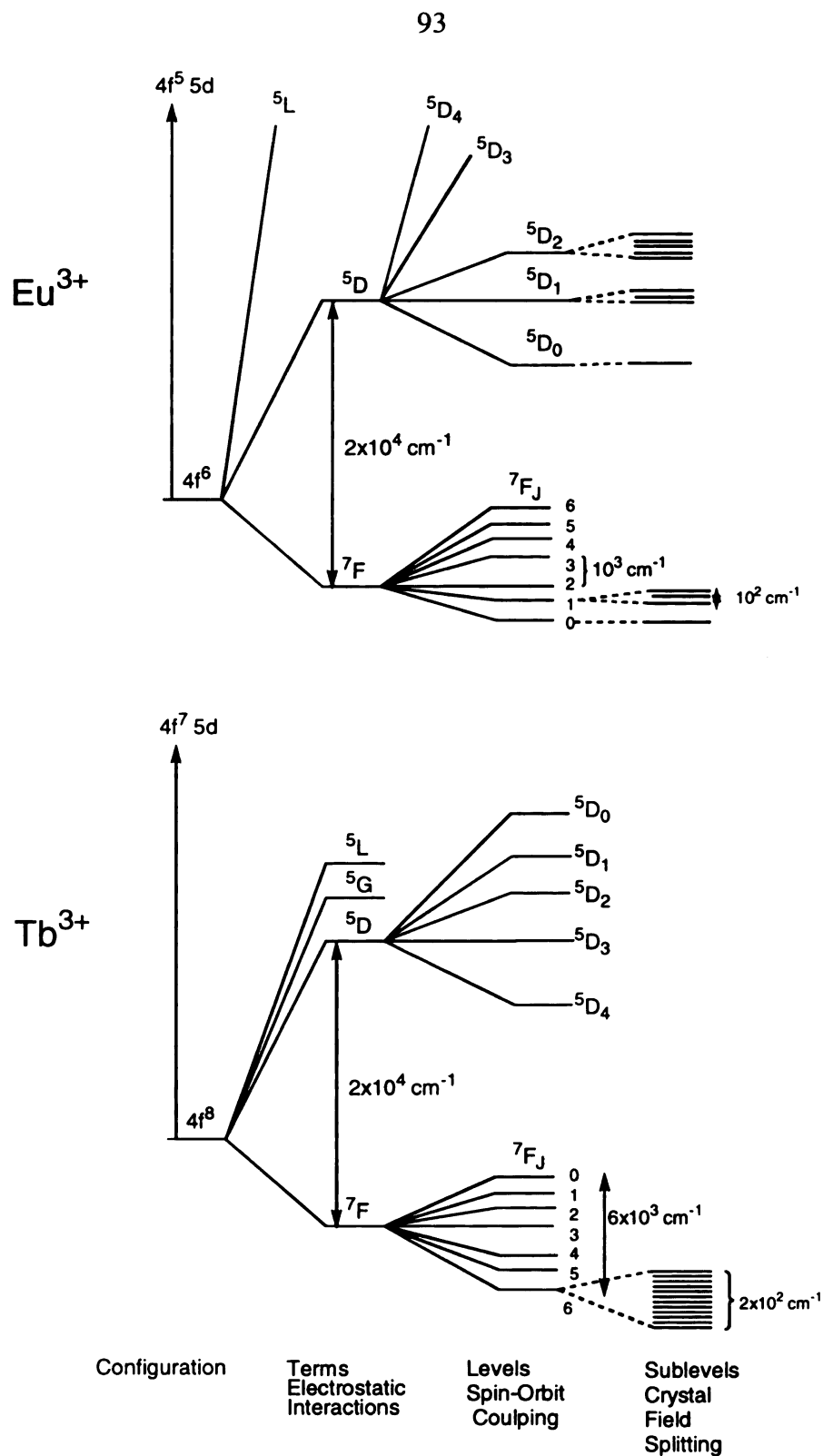
Figure 25. Energy level diagram for Eu^{3+} and Tb^{3+} in the free ion and crystal field limit of the chemical environment. The configuration is split into terms by electrostatic interactions, levels by spin-orbit coupling and sublevels by crystal field splittings [138].

forbidden nature of the intra f-electronic transitions, the oscillator strengths and consequently the molar absorptivites are small (<1 $M^{-1}cm^{-1}$).

Non-Radiative Transitions

Lanthanide ions can be easily deactivated by vibrational oscillations in the surrounding environment. Multiphonon (vibrational) deactivation leads to energy loss from electronically excited lanthanide ions. Non-radiative deactivation is dependent on the energy gap between manifolds, the photon energy and the photon-electron Hamiltonian overlap integral [140]. The larger the energy gap between the two lanthanide states, the slower the rate. The non-radiative deactivation has been measured in some cases [141]. Our aim is to try to avoid populating the higher excited state levels of the lanthanide ion by judiciously choosing the donor molecules.

One potential quencher of lanthanide luminescence is water, whose O-H vibrations non-radiatively deactivate the excited states of lanthanides. To avoid quenching by water, the nine coordination sites need to be occupied by ligands that will cage the lanthanide. Typical ligands that have been employed for this purpose are cryptands, which have seven nitrogen and oxygen coordination sites. The remaining two sites are occupied by water molecules. However, shielding by the macrocycle is still effective. Horrocks et al. developed the following equation for determining the number of molecules of water located in the coordination sphere of a lanthanide [142] by measuring the lifetimes of various lanthanide complexes in water and deuterium oxide solutions.

$$n_{H_2O} = c\left(\frac{1}{\tau_{H_2O}} - \frac{1}{\tau_{D_2O}}\right) \tag{24}$$

where c is a constant (c = 4.2 for Tb^{3+} and 1.05 for Eu^{3+}) and τ_{H_2O} and τ_{D_2O} are the lifetimes in solutions of water and deuterium oxide, respectively.

To shield the deleterious effect of O-H oscillators, lanthanide ions can be encapsulated in molecular cages such as cryptands. Two nitrogens and five oxygens comprising the three straps of 2.2.1 cryptand ligand occupy seven of the nine coordination sites of the Ln^{3+} ion. The two remaining coordination sites of the Ln^{3+} cryptand provides the opportunity for light-harvesting substrates to enter the coordination sphere of the lanthanide and be detected by the energy transfer process. In this manner the optical excitation is efficiently pumped to the Ln^{3+} excited state via the light-harvester. We have been able to increase the emission efficiency of Tb^{3+} and $Eu^{3+} \subset 2.2.1$ complexes by upwards of three orders of magnitude upon coordination of light-harvesting substrates such as β-diketonates. Compelling evidence that the increase in emission intensity is due to energy transfer comes from the excitation spectrum, which is not that of the native $Eu^{3+} \subset 2.2.1$ as is the case when no light harvester is present, but rather corresponds to the absorption spectrum of the light harvester.

In our laboratories, we have studied the energy transfer rates of acetylacetonate (acac) ligands to a cryptand-encapsulated lanthanide ion ($Tb^{3+} \subset 2.2.1$) in real-time at room temperature [143]. The luminescence decay of acac at 435 nm is monoexponential with a lifetime of 1.7 ± 0.4 ns. This shortened acac emission is attributable to oxygen quenching of the $^3\pi\pi^*$ radiative decay at room temperature [144]. A monoexponential decay of 1.4 ± 0.2 ns is also observed for Gd(acac)$_3$ at 435 nm. As the lowest energy level of Gd^{3+} (32000 cm^{-1}) is energetically far removed for energy transfer relative to the

acac triplet (25600 cm^{-1}). The shorter triplet lifetimes for the chelate Gd(acac)$_3$ is consistent with the presence of a heavy atom enduced intersystem crossing rate.

In the presence of Tb^{3+} $\subset$ 2.2.1, a biexponential lifetime is observed, indicative of more complicated kinetics. The two components of the decay are 103 ± 23 ps and 1.73 ± 0.07 ns; the short component arises from triplet decay of acac associated with Tb^{3+} $\subset$ 2.2.1 and the long component originates from unbound acac. The relative weights of the short and long component are 11% and 89% respectively, and the short component increases with increasing concentration of Tb^{3+} $\subset$ 2.2.1. Associated with the biexponential decay is the appearance of Tb^{3+} luminescence at 546 nm ($^5D_4 \rightarrow {}^7F_5$). The risetime of the Tb^{3+} luminescence is 85 ± 40 ps, consistent with the timescale of decay of acac emission (103 ps). The lifetime of the $^5D_4$ state Tb^{3+} state (546 nm) in the acac•Tb^{3+} $\subset$ 2.2.1 complex is 1.7 ms. The length of the decay is typical of a lanthanide excited state. The correspondence of acac phosphorescence decay and Tb^{3+} luminescence rise components supports the hypothesis of direct energy transfer from the acac triplet (25600 cm^{-1}) to the metal luminescent excited state (20500 cm^{-1}). Fast energy transfer with a rate of 9.7 x 10^9 s^{-1} is observed with this system of acac bound to Tb^{3+} $\subset$ 2.2.1. Excluding studies done in our laboratory there have been no real-time measurements of the rates of through bond energy transfer in lanthanide chelate systems.

The acac•Tb^{3+} $\subset$ 2.2.1 adduct represents energy transfer in a system under dynamic equilibrium. ^1H NMR spectra reveal that acac undergoes an equilibrium with Tb^{3+} $\subset$ 2.2.1 (15 % for 1:1 binding). It is therefore difficult to determine the distance of the energy transfer between the acac and Tb^{3+}. Energy transfer rates and mechanisms of few aromatic systems to lanthanide acceptors have been investigated. Lanthanide chelates

[145] and triphenylene doped into lanthanides in rigid glasses at 77K [146] exhibit energy transfer by a Dexter mechanism. The energy transfer mechanisms to two other well studied systems, aromatics (naphthalene and Bph) in micelles with Tb^{3+} and Eu^{3+} [147] and lanthanide calixarenes [148] have not yet been determined. We therefore decided to investigate the energy transfer process lanthanide acetylacetonate chelate complexes where the acac is directly coordinated to the lanthanide ion.

Three mechanisms have been proposed for through-bond energy transfer of lanthanide chelates: (1) fast intersystem crossing (S_1 to T_1) and transfer from the ligand triplet to the lower levels of the lanthanide excited state; (2) transfer from the ligand singlet state to the rare earth excited state; and lastly (3) a cascading of energy back and forth from the ligand to the metal to the lowest emissive state of the lanthanide (Figure 26) [149]. Energy transfer from the triplet requires a fast intersystem crossing rate that is competitive with singlet radiative emission. Intersystem crossing rates of chelates were examined by Tanaka [150] and El Sayed [151]. The rates were estimated to be $10^{11}\,s^{-1}$ by Bhaumik and El Sayed and measured by Tanaka and coworkers at $7.5 \times 10^8\,s^{-1}$ for lanthanide ions complexed with methyl salicylate. This chapter describes measurements in our laboratory of the emission, excitation and time-resolved luminescence for lanthanide chelates and evidence of a triplet state mechanism (Mechanism I).

First, gadolinium acac chelate complexes are used to determine the ligand phosphorescence. Phosphorescence of the ligand from $Gd(acac)_3$ is observed for two reasons, spin-orbit coupling of the donor molecule is enhanced by the heavy atom effect, and the first excited state of gadolinium is energetically indisposed relative to the donor

Mechanism I

Mechanism II
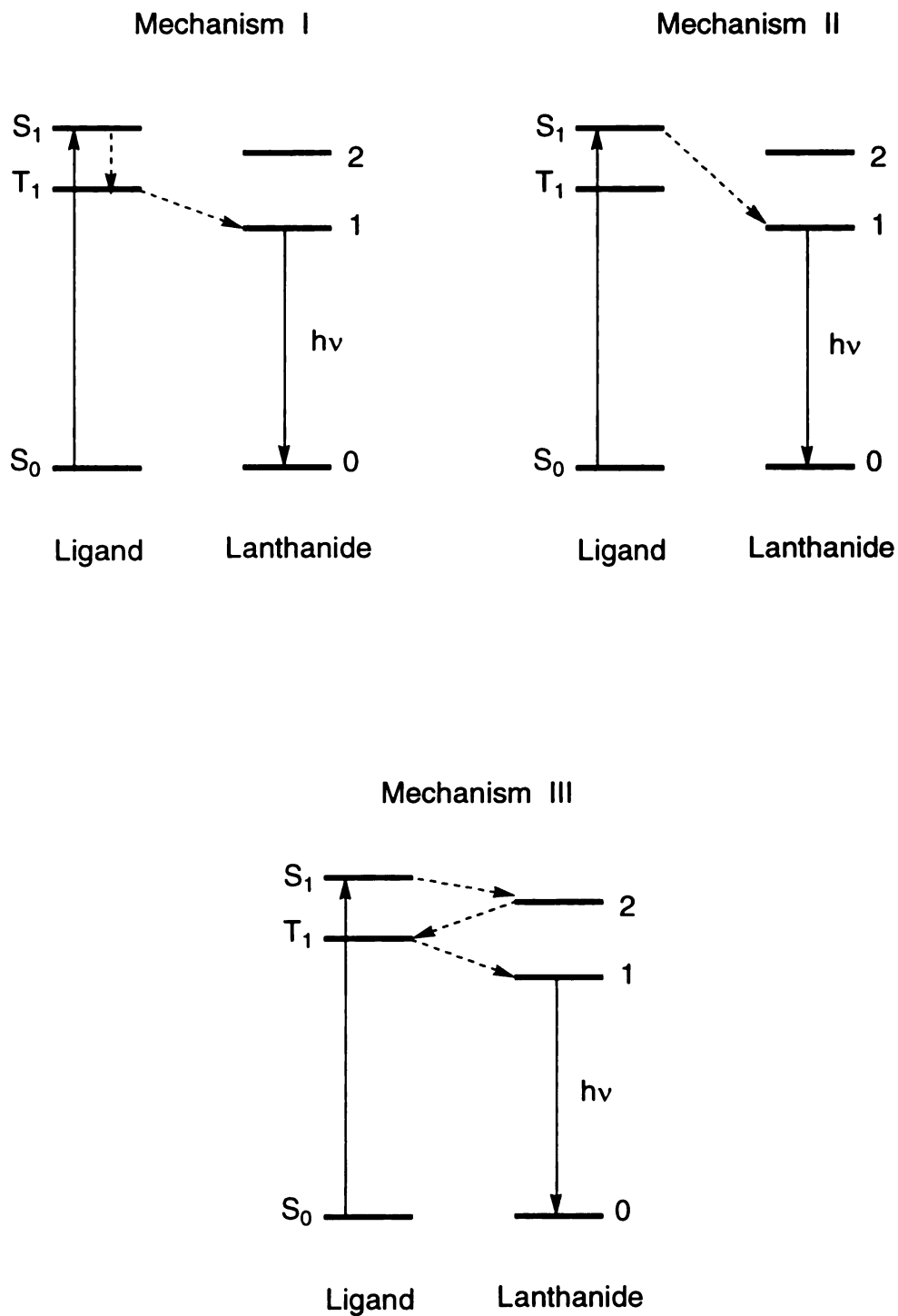
Mechanism III

Figure 26. Three mechanisms for intramolecular energy transfer in lanthanide chelates: energy transfer through the triplet, singlet and multiple levels [149].

excited state (Figure 27). Secondly, europium and terbium are substituted for gadolinium order to select a specific lanthanide excited state. Europium(III) has low lying excited states at 17000 and 19000 cm^{-1}, whereas terbium (III) has states at 20000 and 26000 (Figure 27). The two acac based ligands that have been chosen are dibenzoylmethide (DBM) and dinitrodibenzoylmethide(dNDBM). The triplet state of DBM is located at an energy that will populate both excited states of Eu^{3+} but only the lowest level emissive excited state of Tb^{3+}. Located lower in energy than DBM, dNDBM populates only the emissive state of Eu^{3+} and no energy transfer occurs to Tb^{3+}.

We have chosen lanthanide chelate systems for many reasons, the most prominent being the precedence in the literature [149]. Lanthanide chelates were examined in the 60s and 70s as potential candidates for lasing materials. In a 1966 review of rare earth complexes, Crosby [145] gives an estimate of the energy transfer rate of 10^9 to 10^{13} s^{-1} for β-diketonate complexes and an exchange mechanism is postulated, implying that the lanthanide and diketonate orbitals are physically overlapped. Tanaka [150] and Crosby [145] performed experiments on lanthanide β–diketonate complexes, indicating that a short distance and a paramagnetic lanthanide are important for enhancement of spin-orbit coupling. The heavy atom effect must therefore operate over the distance of a bond in order to have a pronounced effect on the intersystem crossing rates of aromatics. Covalent bonds in lanthanide β-diketonate complexes impose a short energy transfer distance, and therefore it is reasonable that the energy transfer rates are fast.

Energy transfer has been examined for a non-covalent system comprised of an aromatic (Bph and naphthalene) imbedded in the core of a micelle with lanthanide ions on the polar surface. Energy transfer involves diffusion of the aromatic donor to the
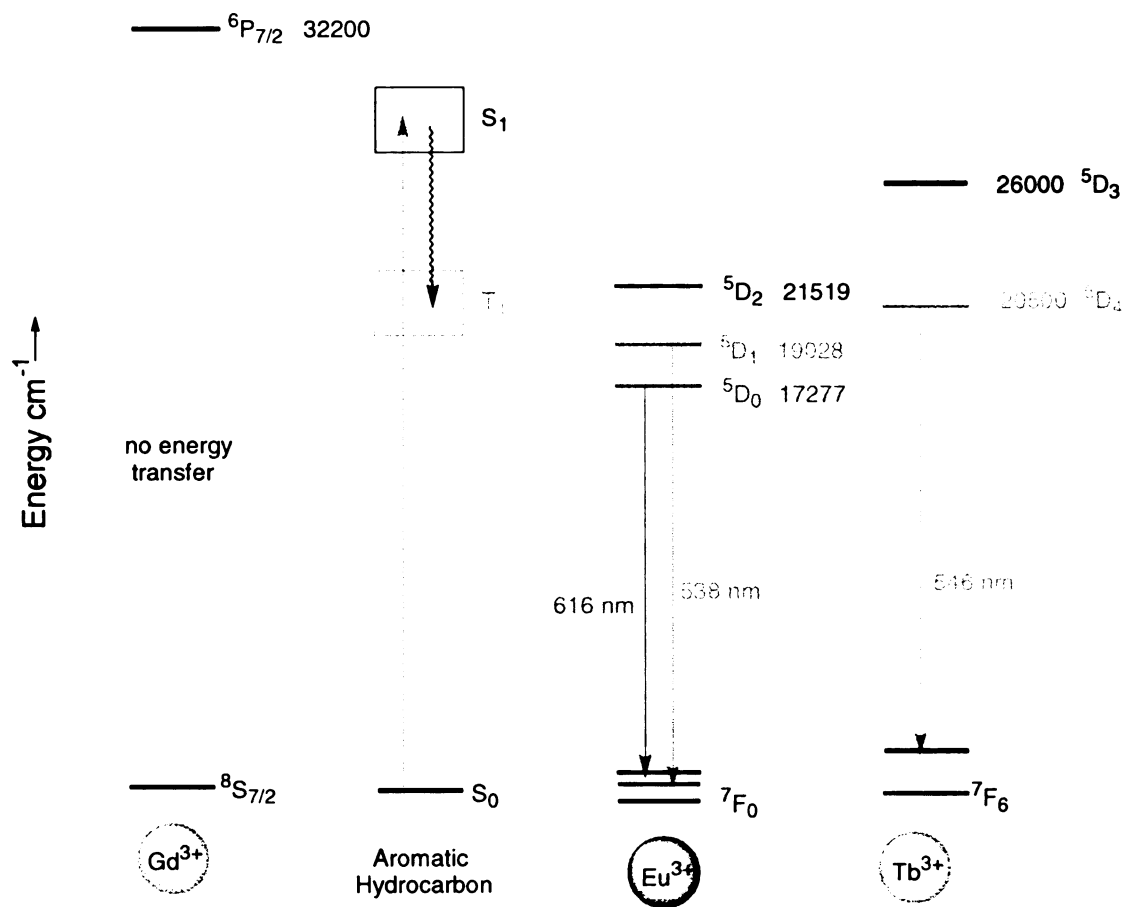
Figure 27. Energy level diagram of Gd^{3+}, Eu^{3+} and Tb^{3+} with a typical aromatic hydrocarbon, showing the range of energy of the triplet and singlet states. The emissive transitions of europium and terbium are shown.

lanthanide acceptor. Almgren and Thomas [147] and Wagner and Schott [152] have independently shown that the second order rates are slow, 10^5 M^{-1} s^{-1}. From a measure of the binding (K = 500), they were able to determine that the rate due to bound complexes is 6.2 x 10^2 s^{-1} and 1.4 x 10^3 s^{-1} for 1-bromonapthalene and Bph respectively.

Experimental

Dibenzoylmethide (DBM) ligand, $GdCl_3 \cdot 6H_2O$, $EuCl_3 \cdot 6H_2O$ and $TbCl_3 \cdot 6H_2O$ were obtained from Aldrich and used without further purification. Tris chelate $(Ln(DBM)_3)$ complexes were synthesized by refluxing a mixture of 1.3 g (6 mmol) of dibenzoylmethide ligand, 48 ml of acetone and 12 ml of 0.5 M KOH to which a 2 mmol of solution of $LnCl_3 \cdot 6H_2O$ (Ln = Gd, Eu, Tb) in 10 ml of water was added. The solution was filtered hot to remove all impurities and upon cooling yielded yellow needles in 60 % yield. Characterization was done by infrared spectroscopy and melting point analysis.

Dinitrodibenzoylmethide (dNDBM) ligand was synthesized by Adrian Ponce by reacting 54 g of anhydrous $AlCl_3$ and 70 g of p-nitrobenzoylchloride in 100 g of tetrachloroethane with 17g of vinyl acetate. The product of this reaction was worked up with HCl and followed by distillation to remove tetrachloroethane. dNDBM was recrystallized in glacial acetic acid in 30% yield. Characterization of dNDBM was done by NMR, IR and GC mass spectrometry. The chelate complexes $Ln(dNDBM)_3$ were synthesized by the same method as $Ln(DBM)_3$.

Emission spectra from 1×10^{-5} M or 1×10^{-6} M lanthanide chelates in EPA glasses (ethanol/diethyl ether/isopentane 2:5:5) were collected on the high resolution emission instrument at Michigan State University. A 13 Hz chopper was used to collect long-lived

luminescence and phosphorescence. Emission spectra were collected by exciting DBM chelates at 365.7 nm, and scanning the emission from 400 nm to 600 nm. dNDBM chelates were excited at 435 nm and the emission monitored from 450-650 nm. Nanosecond lifetimes and risetimes of Gd, Eu and Tb complexes of $Ln(DBM)_3$ and $Ln(dNDBM)_3$ were collected with a TEK 602a oscilloscope, following excitation of the ligand at λ_{ex} = 355 nm, one of the harmonics of the Nd:YAG DCR 2 nanosecond laser. The ligand phosphorescence lifetimes were measured for $Gd(DBM)_3$ at 494 nm and for $Gd(dNDBM)_3$ at 550 nm. Europium and terbium luminescence lifetimes were collected at 616 and 546 nm, respectively.

Results

Energy transfer does not occur in gadolinium chelate complexes because the lanthanide ion excited state is too high in energy (32200 cm^{-1}); therefore ligand luminescence, is only observed. Figure 28 and Figure 29 show the luminescence spectra of $Gd(DBM)_3$ and $Gd(dNDBM)_3$. Ligand fluorescence (400-460 nm) and phosphorescence (470-600 nm) is observed from $Gd(DBM)_3$ upon excitation at 365.7 nm. The phosphorescence band shows a vibrational progression at 488, 518, 552 nm, which gives an energy spacing of 1186 and 1189 cm^{-1}. This progression can be attributed to the vibrational modes of the phenyl ring. The lifetime of $Gd(DBM)_3$ is 1.8 µs at 494 nm and < 10 ns between 400-460 nm.

The emission of $Gd(dNDBM)_3$ shows four bands at 492, 550, 590 and 640 nm. The first band at 492 nm corresponds to fluorescence of the ligand and has a lifetime of <10 ns. The other three peaks correspond to vibrational structure in the phosphorescence.
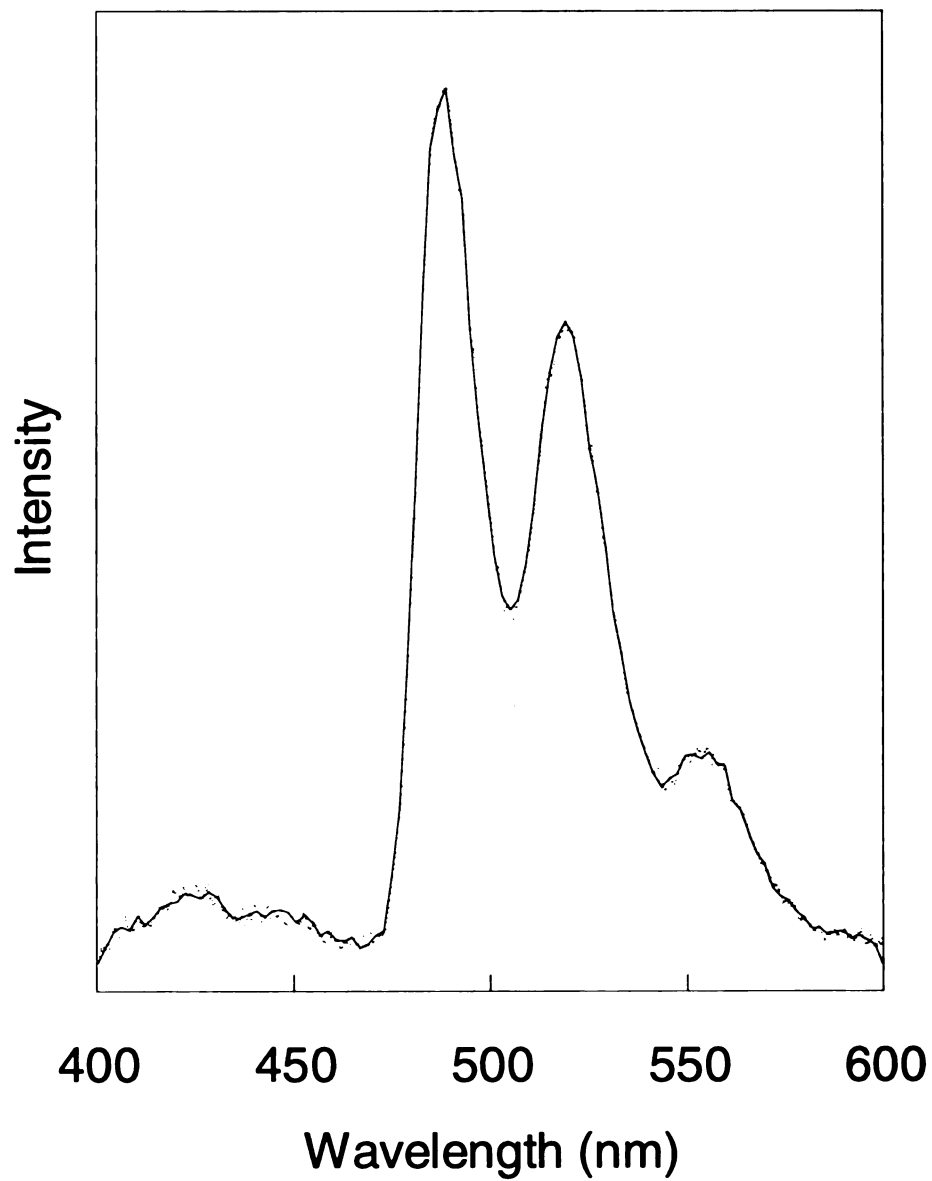
Figure 28. Luminescence Spectrum of Gd(DBM)$_3$ λ_{ex} = 365.7 nm.
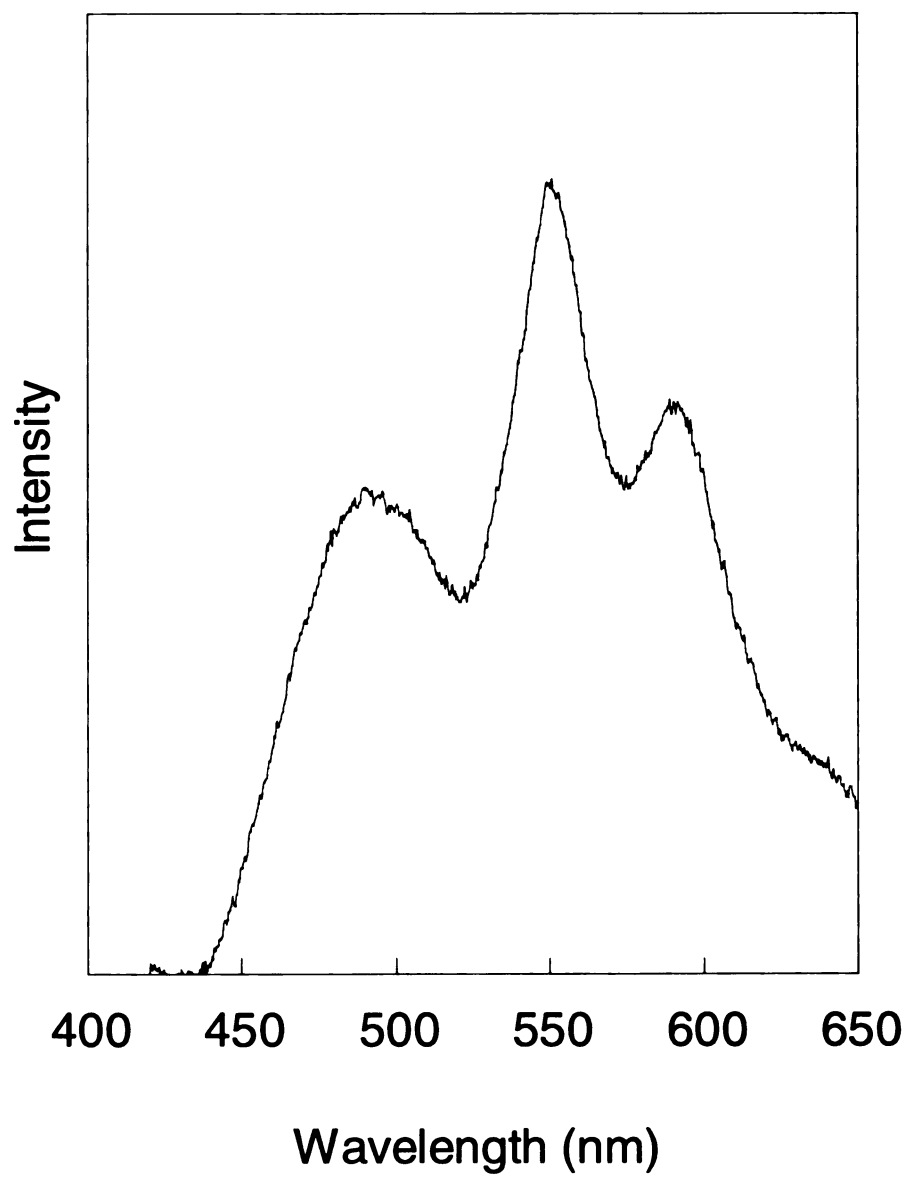
Figure 29. Luminescence Spectrum of Gd(dNDBM)₃ λ_{ex} = 435 nm.

(separations of 1266 and 1324 cm^{-1}). The progression is lower in energy due to the electron withdrawing nitro groups on the phenyl ring. The lifetime of phosphorescence at 550 is 1.2 μs.

The excitation and emission spectra of $Eu(DBM)_3$ are shown in Figure 30. The excitation spectrum shows a broad band with a maximum at 375 nm (26666 cm^{-1}) and vibrational structure, which is assigned to the first excited singlet state of the DBM ligand. The emission spectrum shows two narrow emission lines at 548 nm (magnified 100 times) and 616 nm that are assigned to the $^5D_1 \rightarrow {}^7F_1$ and $^5D_0 \rightarrow {}^7F_2$ electronic transitions, respectively. The former transition is very weak whereas the latter transition is intense; the intensities are related to the symmetry of the coordination environment of the lanthanide ion. The $^5D_0 \rightarrow {}^7F_2$ is a hypersensitive transition; if the ion lies on a center of inversion this transition is absent from the spectrum. The tris chelates (C_3 point group) do not have a center of inversion and therefore the 616 nm line is very intense. The excitation spectrum for $Tb(DBM)_3$ (Figure 31) shows a similar excitation profile to that of $Eu(DBM)_3$. The emission spectrum, however, shows narrow emission lines that are typical for Tb^{3+} at 488 ($^5D_4 \rightarrow {}^7F_6$) and 546 nm ($^5D_4 \rightarrow {}^7F_5$). Therefore we observe ligand absorption in the excitation spectrum and lanthanide emission in the emission spectrum, providing evidence of an absorption-energy transfer-emission process.

The excitation spectrum of $Eu(dNDBM)_3$ shows a broad band centered at 425 nm, 23529 cm^{-1} (Figure 32). The emission spectrum shows some residual singlet emission from the dNDBM ligand and, in contrast to $Eu(DBM)_3$, there is only one narrow Eu^{3+} emission line at 616 nm. The presence of only one luminescence transition, $^5D_0 \rightarrow {}^7F_2$, is
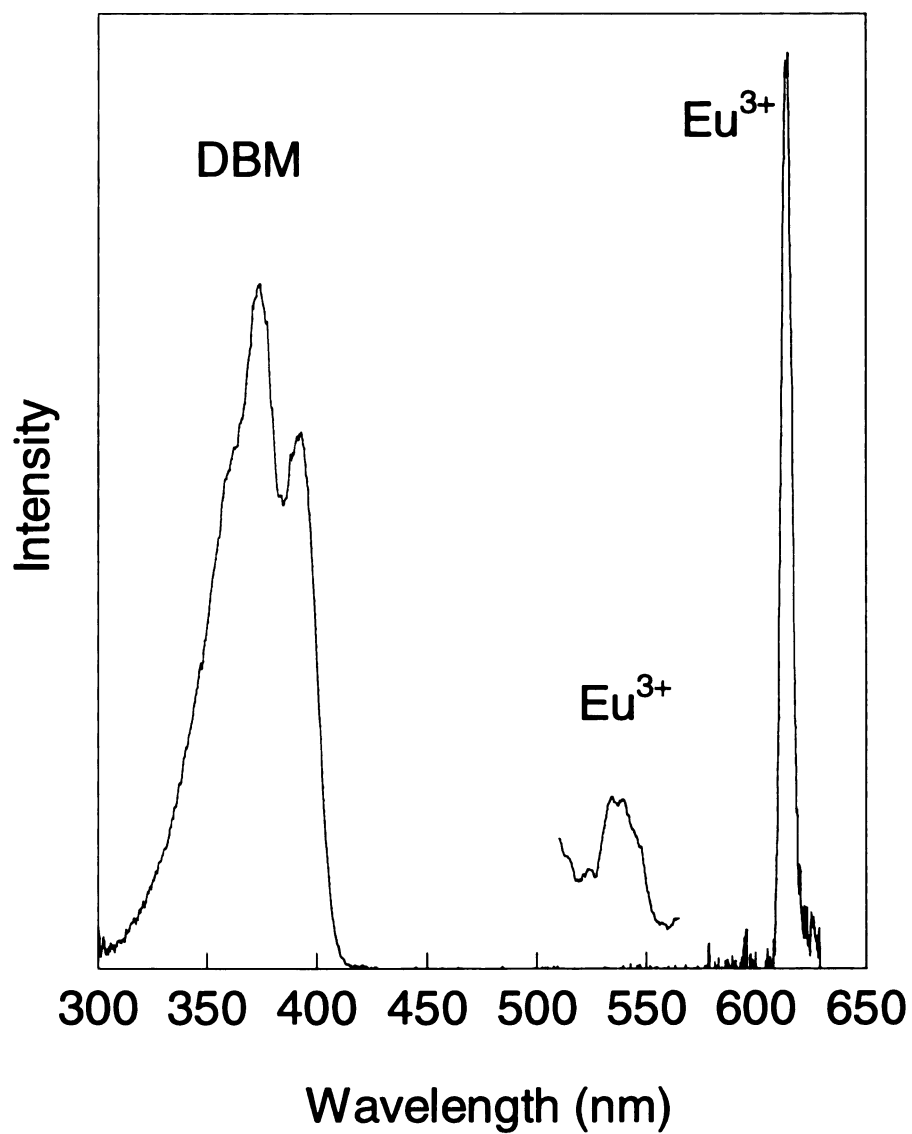
Figure 30. Excitation (300-410 nm) and emission spectra (500-650 nm) of Eu(DBM)$_3$, showing excitation of the dibenzoyl ligand and emission from Eu^{3+} at 548 and 616 nm.
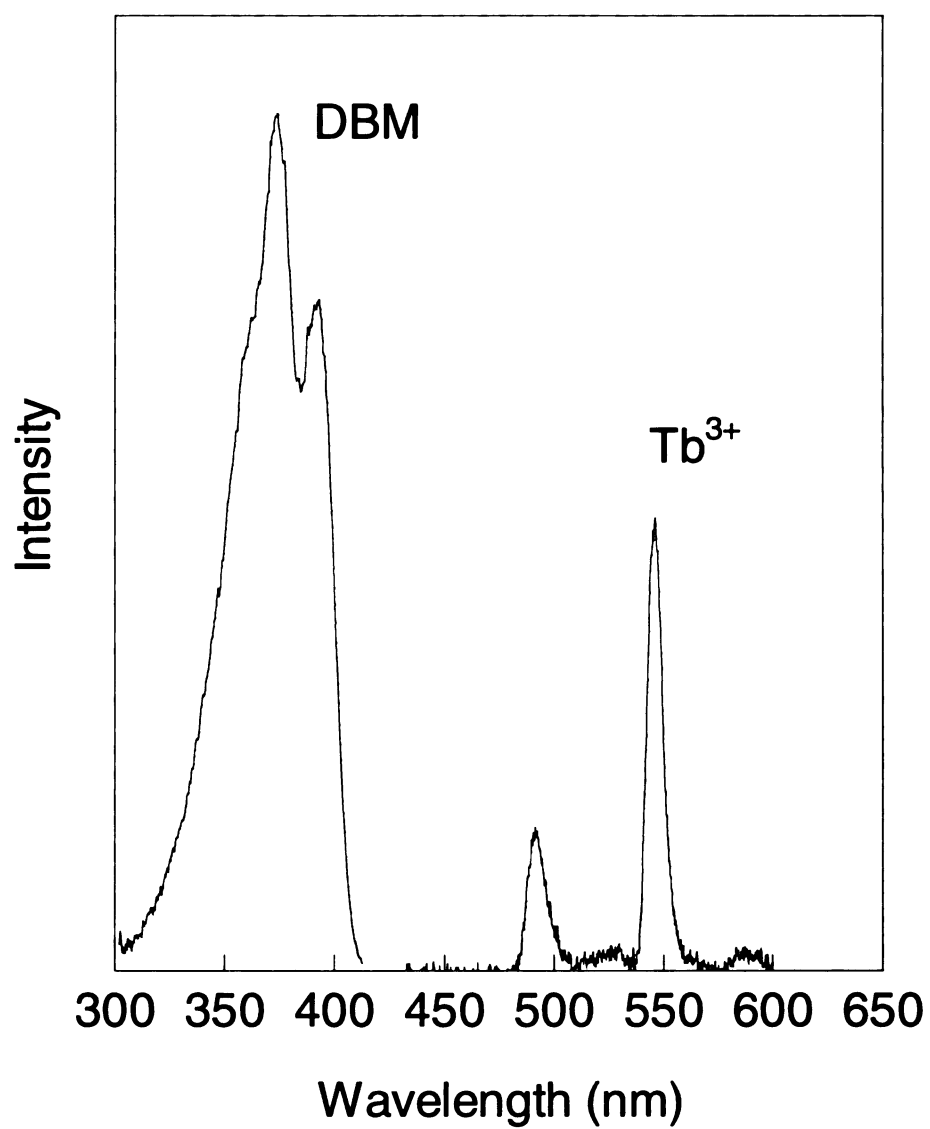
Figure 31. Excitation (300-410 nm) and emission spectra (425-600 nm) of Tb(DBM)$_3$, showing excitation of the dibenzoyl ligand and emission from Tb^{3+} at 488 and 546 nm.
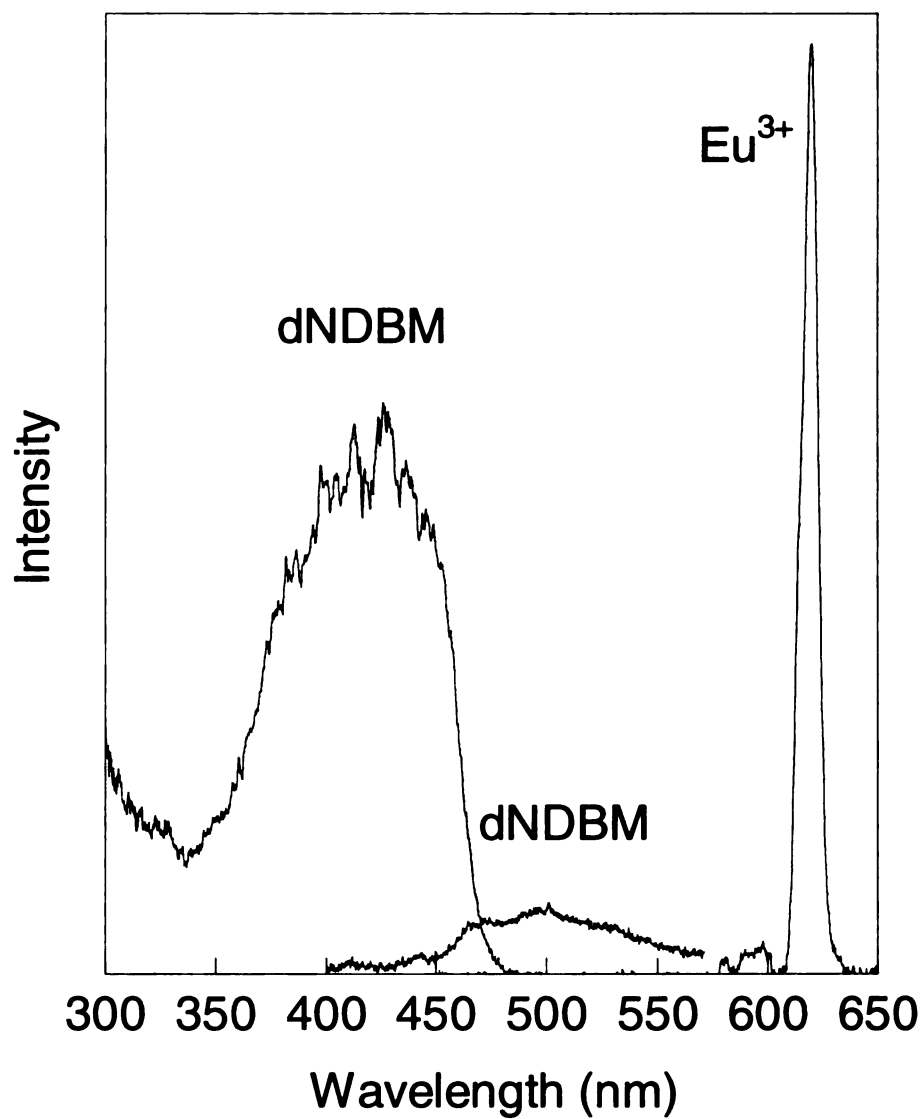
Figure 32. Excitation (300-475 nm) and emission spectra (400-650 nm) of Eu(dNDBM)$_3$ showing excitation of the dinitrodibenzoyl ligand and emission from dNDBM at 500 nm and from Eu^{3+} at 616 nm.

consistent with the lower energy singlet and triplet states of the dNDBM ligand. Apparently, the higher energy $^5D_1$ state is not populated by energy transfer and no emission from that state is observed. These data sustain the hypothesis that light absorbed by dNDBM is transferred only to the lower state of Eu^{3+}, affirming the mechanism I (Figure 26), energy transfer from the ligand triplet state to the lanthanide manifold of states.

The luminescence and phosphorescence lifetimes of all complexes of DBM and dNDBM are listed in Table 5. The lifetimes of lanthanide luminescence of the $^5D_0 \rightarrow {}^7F_2$ and $^5D_4 \rightarrow {}^7F_5$ states of Eu(DBM)$_3$, Eu(dNDBM)$_3$ Tb(DBM)$_3$ respectively are very similar at 400, 338 and 555 μs. The risetimes of the lanthanide states, $^5D_0$ for Eu(dNDBM)$_3$ and $^5D_4$ for Tb(DBM)$_3$, are both too fast to be measured by a nanosecond laser pulse (< 10 ns). However the risetime of the $^5D_0$ state of Eu(DBM)$_3$ is slow (1.8 μs). This measurement of the buildup of the $^5D_0$ state includes three processes: intersystem crossing of the ligand, energy transfer from the ligand to the metal and internal conversion (metal) from $^5D_1 \rightarrow {}^5D_0$. The non-radiative transition from $^5D_1 \rightarrow {}^5D_0$ has been measured previously to be 1.8 μs and is slower than expected upon comparison to organic systems [141]. This slow intersystem crossing is typical for non-radiative transitions between states in lanthanide ions. Inspection of the energy diagram in Figure 33 shows the timescale for non-radiative transitions. The 1.8 μs process that is measured for the risetime of the $^5D_0$ of Eu^{3+} is the sum of three processes: singlet to triplet intersystem crossing, energy transfer and internal conversion between the lanthanide states. As intersystem crossing for ketones is inherently fast ($\sim$1 x 10^8 s^{-1}) we can assume that for our case this value is the lower bound of k_{isc} and that the presence of the heavy atom will

Table 5. Lifetimes and Risetimes for Eu(DBM)$_3$, Eu(dNDBM)$_3$, Tb(DBM)$_3$, Gd(DBM)$_3$, and Gd(dNDBM)$_3$.

Chelate	Electronic Transition	Lifetime	Risetime	Wavelength/nm
Eu(DBM)$_3$	$^5D_0 \rightarrow {}^7F_2$	400 μs	1.8 μs	616
	$^5D_1 \rightarrow {}^7F_1$	1.8 μs	<10ns	548
Eu(dNDBM)$_3$	$^5D_0 \rightarrow {}^7F_2$	338 μs	<10 ns	616
Tb(DBM)$_3$	$^5D_4 \rightarrow {}^7F_5$	555 μs	<10 ns	546
Gd(DBM)$_3$	$T_1 \rightarrow S_0$	1.8 μs	-	494
Gd(dNDBM)$_3$	$S_1 \rightarrow S_0$	< 8 ns	-	490
	$T_1 \rightarrow S_0$	1.2 μs	-	550

S^1 27248 ————

a + b = 1.8 ms
b = 1.8 ms *
therefore a is fast

k_{isc}

S_1 22946 ————

T_1 20242 ————   a $^5D_1$ 19028 ———— k_{isc}

< 10 ns   b   < 10 ns T_1 18181 ————

$^5D_0$ 17277

Eu^{3+}

O_2N ⌬ — — ⌬ NO_2
O⁻ O

S^1 27248 ———— $^5D_3$ 26000 ————

k_{isc}

S_1 22946 ————

T_1 20242 ————   < 10ns k_{isc}

$^5D_4$ 20500 T_1 18181 ————

Tb^{3+}

O_2N ⌬ — — ⌬ NO_2
O⁻ O
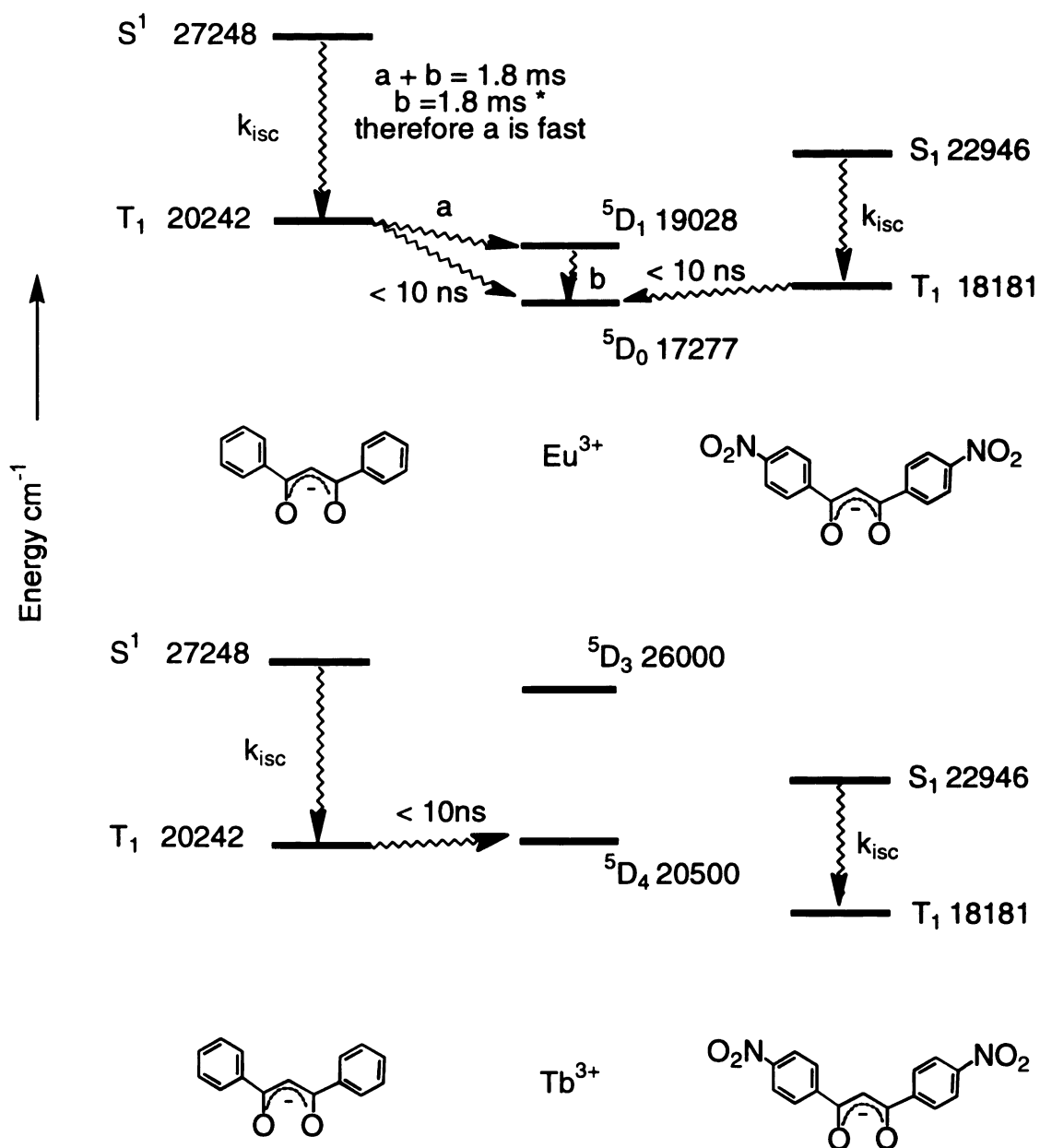
Figure 33. Energy flow from DBM (left) and dNDBM (right) triplet excited state to Eu^{3+} and Tb^{3+} excited states. The arrow from the singlet to triplet excited state of the ligands shows the intersystem crossing. The rates labeled (a) and (b) were measured in our laboratory and by Speiser and coworkers, respectively [141].

Energy cm^{-1}

increase the rate by an order of magnitude [150]. The internal conversion of the lanthanide, as mentioned previously, is slow (1.8 μs) and by deduction we can approximate the rate of energy transfer to be very fast! The fast rate is consistent with the risetime of Tb^{3+}, which occurs on a timescale within the pulsewidth of the nanosecond laser (< 10 ns).

Conclusions

Data from steady state and time-resolved luminescence of chelate complexes of $Ln(DBM)_3$ and $Ln(dNDBM)_3$ where $Ln = Gd^{3+}$, Eu^{3+} and Tb^{3+} point to one conclusion: there is absorption by antennae acac ligands, rapid intersystem crossing, rapid energy transfer, and long lived lanthanide luminescence. The timescale of energy transfer is faster than diffusion, with a lower limit of 1×10^8 s^{-1} (10 ns). This rate is consistent with two other measurements in the literature by Nocera et al. for $acac \cdot Tb^{3+} \subset 2.2.1$ cryptate [143] and Lehn et al. for $Tb^{3+} \subset bpy.bpy.bpy$ cryptate (bpy = bipyrdine) [153], where the rates were derived to be 9.7×10^9 s^{-1} and 0.5×10^8 s^{-1}, respectively. With the addition of the data for the lanthanide chelates there are three examples where energy transfer through a bond, whether it be an adduct held together by an equilbrium or a metal ligand bond, is faster than diffusion. In the next chapter energy transfer through space will be discussed as it relates to the active site mechanism for chemosensing of PAHs and BTEXs.

CHAPTER 6

PAH AND BTX OPTICAL CHEMOSENSING BY AN ABSORPTION-ENERGY TRANSFER- EMISSION PROCESS

Introduction

Aromatic hydrocarbons such as PAHs (polycyclic aromatic hydrocarbons) and BTEXs (Benzene, Toluene, Ethylbenzene, Xylene) are environmental pollutants that are powerful mutagens and carcinogens [154-157]. The Urban Air Toxic Program (UATP) sponsored by the EPA has measured 397 benzene compounds in 14 cities, and the National Ambient Volatile Compound (NAVOC) program found 564 benzene compounds in 31 cities. These chemicals are therefore a great health risk to humans and animals, demanding that water, air and soil be monitored for these contaminants.

Many of the techniques involved in detecting and monitoring levels of PAHs and BTEXs involve time-consuming and meticulous laboratory analyses that must be performed in an off-line or indirect manner. Some of the techniques employ micoextraction-GC-FID [158], FTIR spectroscopy [159], capillary electrophoresis [160],

synchronous fluorometry [161], synchronous phosphorimetry [162], or synchronous luminescence spectroscopy [163]. One recently developed method is based on fiber optic sensors [164-167], which can be applied directly (on-line, on-site or *in-situ*). The challenge in building fiber optic sensors for aromatic hydrocarbons, especially BTEXs, is that they absorb and emit light in the ultraviolet region of the electromagnetic spectrum where it is difficult to obtain inexpensive powerful light sources, sensitive detectors and quartz fiber optics.

One fiber optic probe of BTEs (excluding xylene) based on infrared excitation uses Raman spectroscopy, with a near infrared (NIR) diode laser and a CCD detector [164]. These components and fiber optics are less expensive than those required for ultraviolet light. This fiber optic is used in quality and process control for industrial applications in petroleum fuel production [168,169]. Typical analysis of fuel products involves gas chromatography, which is time consuming and labor intensive [170]. Currently, NIR reflectance/absorbance spectroscopy is used to remotely monitor petroleum chemical composition. However, the disadvantages of NIR absorption are that the peaks are few, broad and overlapping [171-173]. Raman spectroscopy provides many peaks that are well resolved and that can yield information about the analyte. Concentrations of BTEs ranging from 1 to 16 % w/w can be measured by Raman spectroscopy, at an instrumentation cost of < $20,000.

A near-ultraviolet fiber optic absorption sensor for BTEXs has been developed for soil remediation at the Lawrence Livermore Dynamic Underground Stripping Site [166]. Both off-line laboratory analysis and on-line optical sensors were used to gain a better understanding of the dynamic stripping process, whereby resistive heating or steam

injection raises the ground temperature, causing volatilization of organic contaminants trapped in the arid soil. Direct detection of BTEXs is obtained from the absorption spectrum (230-300 nm) from moisture-saturated vapor steam via fiber optic on-line probes. Near UV absorption has advantages over infrared spectroscopy as there are no interferences from water. A flow-through cell is used to determine the absorption of the vapor, which contained aromatic hydrocarbons. All optics are made of fused silica and quartz, and a UV photodiode with a current-to-voltage amplifier was used as the detector. The optical source for the sensor is a 30 Watt deuterium lamp whose wavelengths are selected by a monochromator and modulated with a chopper. The sensor was used at temperatures ranging from 12 to 43 °C for five weeks to monitor benzene concentrations at the absorption maximum (243 nm) with a detection limit of 13 ppm [166].

A third optical sensor based on time-resolved fluorescence spectroscopy has been developed for *in situ* detection of PAHs in water. The sensor device employs a fiber length of 50 meters and a detection limit in the nanogram per liter range [167]. The apparatus consists of a 337 nm pulsed nitrogen laser light source, which is coupled to the 50 m quartz fiber optic (core diameter of 600 μm) connected to a PMT and boxcar. Thirteen environmentally relevant analytes have been detected with this instrumentation, including fluoranthene, benzo(b)fluoranthene, benzo(e)pyrene, chrysene, benzo(f)fluoranthene, indeno(1,2,3-CD)pyrene. The lifetimes of these analytes range from 5 to 33 ns, with varying emission spectra from 395 to 540 nm. This sensor is compact enough to fit into a briefcase and is very sensitive to PAHs [167].

Other portable and on-line means of measuring PAHs and BTEXs have been developed, in addition to fiber optic sensors. Compact analytical instrumentation for

benzene has also been designed with gas chromatography and mass spectrometry (GC-MS) [174,175]. These instruments are designed for operation on an electrically powered vehicle for monitoring exposure to benzene. The accuracy of measuring benzene is achieved by enrichment with deuterated benzene. Close to real-time monitoring is obtained with 4 minute inter-analysis time. The limit of detection is approximately 1 $\mu g/m^3$ for benzene and 2 $\mu g/m^3$ for toluene.

Design Strategy for Chemosensing by a Triggered Luminescent Response

Although there are many optical sensors for PAHs and BTEXs, all of the absorption and emission techniques rely on detection of ultraviolet light, which can be subject to many interferences. For our strategy of optical sensing by triggered visible luminescence, a means for converting ultraviolet light to visible light is necessary. The source of visible emission that we have selected is lanthanide ions, commonly found in phosphors in television screens. Lanthanide ions such as europium (Eu^{3+}) and terbium (Tb^{3+}) are intrinsically bright lumophores, but they show little or no luminescence under direct irradiation owing to the low absorbance ($\varepsilon < 1$ M^{-1} cm^{-1}) of the ^5D_J emitting state manifold. With regard to eq (1) in Chapter 1, the k_r of the emitting state of Ln^{3+} ions is small and hence the luminescence produced by direct irradiation is weak. Nothwithstanding, the emitting state can be indirectly excited with energy from a sensitizer. As popularized by Balzani and Lehn [153], an absorption-energy transfer-emission (AETE) process produces an emitting excited state in very high yields as long as the rate of energy transfer from the sensitizer to the photoluminescent center is efficient. We recognized that this AETE process could be useful for chemosensing if the sensitizer was an analyte possessing a large absorption cross-section with respect to that

of the active site. However, one additional problem must be solved in order to implement lanthanide-based chemosensing schemes. Even if Ln^{3+} ions are efficiently excited, their luminescence is quenched efficiently by water because the O-H bonds act as good thermal receptors of the energy of lanthanide-ion excited states [142]. This deleterious effect of water can be overcome by encapsulating the Ln^{3+} ions in supramolecular cages that exclude water.

In order for an AETE process to be effective, the distance between the sensitizer analyte and lanthanide lumophore must be short. In normal aqueous solutions, the average distance from an aromatic hydrocarbon to a lanthanide is too far for efficient energy transfer to occur. For example, using the Perrin formulation, the quenching sphere of a donor molecule in a dilute solutions (10^{-2} M) places the acceptor at a distance (R) greater than 30 Å (R = $6.5[A]^{1/3}$ where [A] is the concentration of the acceptor) [17]. This distance challenge was addressed by using a cyclodextrin cup (CD) as the molecular recognition center for the aromatic hydrocarbon. Different sizes of cyclodextrins can be used to control size selectivity for BTEXs and PAHs. Alone, a cyclodextrin is an inadequate chemosensing active site because there is no photoactive center. However, a photoactive center can be incorporated into a cyclodextrin by adding a binding site for a lumophore. Macrocyclic ligands, such as aza crown ethers or diethylentriaminepentaacetic acid (DTPA) can be tethered to the cyclodextrin at the primary side, leaving the secondary side of the cyclodextrin accessible to binding of the hydrophobic pocket by mono- and bicyclic aromatic hydrocarbons.

In our efforts to design supramolecular assemblies capable of optically detecting aromatics and polycyclic aromatics, several derivatized cyclodextrins were synthesized in

our group, specifically the aza crown swing and cradle cyclodextrins [176,177] and

diethylenetriaminepentaacetic acid (DTPA) (Figure 34) [178]. In the absence of aromatic

hydrocarbons, weak emission is observed when all three complexes, Eu^{3+} aza crown

swing cyclodextrin, Eu^{3+} cradle cyclodextrin and a Tb^{3+} triacid cyclodextrin complex, are

directly excited with ultraviolet light. When aromatic hydrocarbons are present, however,

enhanced luminescence is observed. Since aromatic hydrocarbons bind with high

affinities to the cyclodextrin cavity, they are held close to the ligand, at a distance where

energy transfer can occur to a lanthanide coordinated to the macrocyclic ligand. We

attribute the enhancement in luminescence to an absorption-energy transfer-emission

process from the aromatic that resides in the cavity to a lanthanide ion coordinated to the

aza crown and DTPA macrocycles.

We are particularly interested in sensing benzene, toluene and xylene (BTX) by

energy transfer. Tethered at only one nitrogen, the aza crown prefers a conformation that

is swung away from the hydrophobic cup; therefore the triggered luminescence response

is weak, owing to the long distance for energy transfer. Studies with the Eu^{3+} aza crown

swing cyclodextrin and benzene analyte indicated that the small binding constant

($117\ M^{-1}$) and small increase in emission intensity of Eu^{3+} could be ascribed to the long

energy transfer distance [176]. Because a shorter distance is imposed when the lanthanide

ion binding site is cradled under the CD, we suspected that the aza crown tethered to the

CD cup via its two nitrogens would show a significantly larger triggered luminescence

response. To address this issue, the distance was shortened by tethering the aza ligand at

both nitrogens [177]. However, although the distance from benzene to the lanthanide
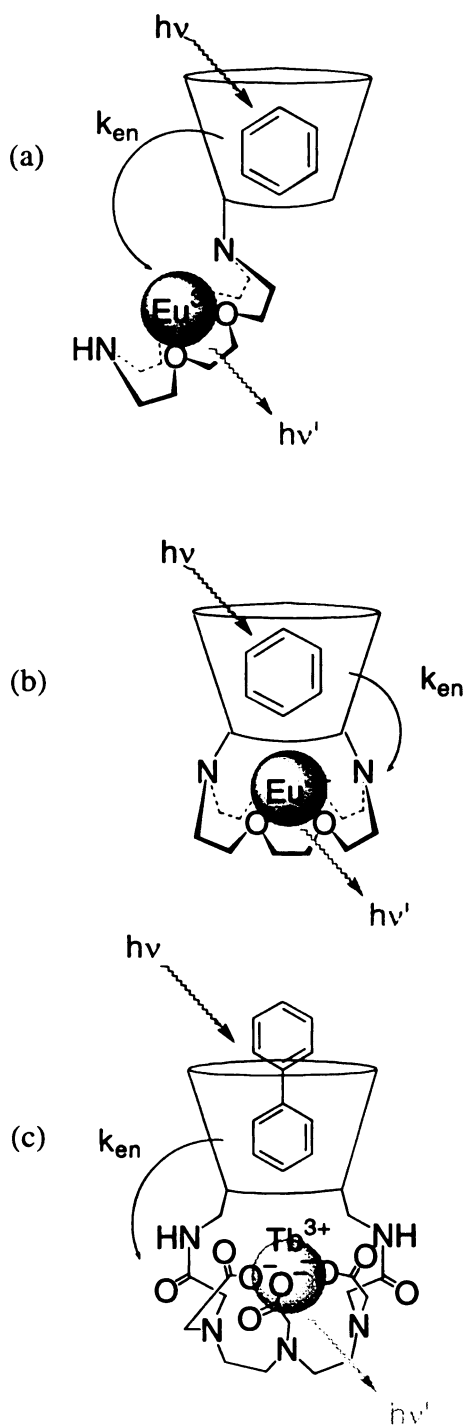
Figure 34. (a) Swing aza crown-β-cyclodextrin coordinated with Eu^{3+}. (b) Cradle aza crown-β-cyclodextrin coordinated with Eu^{3+}. (c) Diethylenetriaminepentaacetic acid-β-cyclodextrin coordinated with Tb^{3+}.

(Eu^{3+}) was closer, instead of observing an increase in lanthanide luminescence, there was little improvement. Indeed, the binding constant was smaller ($< 10 \ M^{-1}$). Apparently the 3+ charge of the appended europium cradle at the bottom of the cup makes the interior of the CD less hydrophobic and hence decreases the association of benzene in the cup. It was predicted that the hydrophobicity of the cyclodextrin cavity would remain unaltered if the overall charge of the CD supramolecular assembly could be made neutral. Neutralization of the charge is achieved by linking a tricarboxylic acid macrocyclic ligand synthesized from diethylenetriaminepentaacetic acid to the cyclodextrin. The synthesis of a CD supramolecule appended with a diethylenetriaminepentaacetic acid (DTPA) binding site that neutralizes the charge of the lanthanide ion in a cradle geometry has been reported by Mortellaro and Nocera [178]. The neutral charge of the Tb^{3+} triacid CD complex was the key to binding neutral substrates; it showed sensitivity to BTXs, and to bicyclics such as Bph [179].

The ultimate aim of the investigation reported in this chapter is to determine the mechanism of the energy transfer process leading to detection of the BTXs (aromatic hydrocarbon) to the acceptor (lanthanide ion). The rate of energy transfer, distance dependence, Förster energy transfer mechanism, and overlap integral of aromatic donor and lanthanide acceptor will be presented in this chapter. Predicting the distance of energy transfer is possible by measuring the energy transfer rate, the overlap integral of the donor emission and absorption of the acceptor, and the donor lifetime and quantum yield. These measurements and their implications on the theory of energy transfer formalisms will be discussed.

Experimental

Biphenyl (Bph) was obtained from Fischer and recrystallized from methanol. Scintillation grade naphthalene (Np) was purchased from Aldrich and used as received. $Tb(NO_3)_3 \cdot 5H_2O$ and $Eu(NO_3)_3 \cdot 5H_2O$ were obtained from Aldrich and used as received. The synthesis of the aza crown swing, cradle and diethylenetriaminepentaacetic acid (DTPA-β-CD) cyclodextrin molecules was conducted by Dr. Zoe Pikramenou [176], Dr. Mark A. Mortellaro [178] and Dr. Jude Rademacher [127]. The compounds were characterized by 300 and 500 MHz NMR, thin layer chromatography and mass spectrometry. With the assistance of Dr. Mark Mortellaro, the synthesis of the swing cyclodextrin was repeated although the compound was not fully purified by gel chromatography. Mark Mortellaro attempted the reaction under more vigorous conditions with pyridine as the solvent, at higher temperatures. These conditions did not improve the yield of the reaction and in some cases caused decomposition. Jude Rademacher has repeated the syntheses of swing and cradle cyclodextrins and improved the purification methods. He has observed that the aza crown swing CD can exhibit a pale yellow color instead of the typical white powders observed for cyclodextrin compounds.

All experiments were performed using room temperature aerated aqueous solutions unless otherwise noted. Absorption spectra were collected on double beam Hitachi U2001 or OLIS retrofitted Cary 17 spectrophotometers. To obtain data for overlap integral estimations, lanthanide absorption spectra were collected for highly concentrated aqueous 0.05 M solutions of $Tb(NO_3)_3 \cdot 5H_2O$ ($\varepsilon \sim 1$ M^{-1} cm^{-1}) or $TbCl_3 \cdot 5H_2O$ in methanol. The data were scanned at 0.2 nm intervals to match the interval of the emission spectra of aromatic hydrocarbons. The spectral overlap integral of donor

emission (Bph) and absorption of the terbium (III) acceptor was calculated using a spreadsheet format by utilizing Kaleidagraph software.

Binding constants of aromatic hydrocarbons to DTPA-β-CD coordinated with Tb^{3+} (TbDTPA-β-CD) were determined by the same technique used to determine binding of 1-BrNp to Gβ-CD described in Chapter 2. The absorption spectra of two cells saturated with aromatic hydrocarbon were measured to give a relative baseline of zero. Concentrated DTPA-β-CD solution (25 mM) was added to the sample compartment, resulting in an increase in absorption that is proportional to the concentration of complex [CD•Ar], where CD = cyclodextrin and Ar = aromatic hydrocarbon. A plot of $[A-A_0]/A_0$ versus $[CD]_{tot}$-[CD•Ar] yields K, the binding constant. To verify the binding constants, a measurement was also obtained from titrations of the emission profiles described in the next section and fit with a standard equation [124].

Excitation and emission spectra were collected under the same conditions as described in Chapter 2. Titration profiles were collected for emission at 544 nm of TbDTPA-β-CD as a function of added aromatic hydrocarbon at an excitation wavelength specific for each analyte (λ_{ex} = 266 nm for Bph and 275 nm for Np). A 2.5 x 10^{-4} M solution of TbDTPA-β-CD was made by dissolving equimolar amounts of $Tb(NO_3)_3$•$5H_2O$ and DTPA-β-CD in doubly deionized water and assuming 100% complexation. Excitation and emission spectra were collected as aliquots of 1-100 µl of a 0.02 M solution of Bph or 0.1 M Np in ethanol were titrated into a 2 ml solution of 2.5 x 10^{-4} M TbDTPA-β-CD. Quantum yields of Tb^{3+} in TbDTPA-β-CD in the presence of Bph and Np were determined by integrating the 544 nm line in the asymptotic concentration limit of Bph and Np, using a standard of degassed biacetyl in hexane [105].

Other quantum yield standards (quinine bisulfate and Ru(bpy)$_3^{2+}$) gave irreproducible results.

Luminescence lifetimes of Tb^{3+} in TbDTPACD complexed with Bph (TbDTPA-β-CD•Bph) were collected on a pulsed ns laser system. The 532 nm output of a nanosecond Quanta Ray DCR2 Nd:YAG was doubled by a WEX to obtain 266 nm light used to excite the aromatic hydrocarbons (Np and Bph). The power of ultraviolet light out of the WEX was typically 10-40 mW (10-15 % conversion). The luminescence risetime and lifetime of Tb^{3+} were collected at 544 nm, the luminescence line with the largest intensity. The slits were set at the same widths as described for the 1-BrNp lifetimes described previously.

The Stern-Volmer method of luminescence lifetimes was also used to determine the extent of static and dynamic quenching of Bph fluorescence by Tb^{3+} quencher [107]. Quenching of Bph and Np singlet excited states in DTPA by Tb^{3+} was determined by picosecond lifetime and steady state luminescence experiments. A concentrated solution of Tb(NO$_3$)•5H$_2$O (20 mM) was titrated into a solution of 3 x 10^{-4} M Bph and 2.5 x 10^{-4} M DTPA-β-CD. The emission intensity and lifetime of Bph fluorescence were measured at 320 nm with the excitation set at λ_{ex} = 266 nm. The fluorescence lifetime decays of the singlet state of Bph in the absence and presence of Tb^{3+} were fit using an instrument response function between 30-80 ps with software provided by Edinburgh Instruments (FLA 900) in a GEM platform.

Energy minimizations were run on a Silicon Graphics IRIS Elan χ^2 computer using Biosym Insight Discover. Approximations were made of the distance of energy transfer from the lanthanide acceptor at the bottom of the cyclodextrin to the donor

aromatic in the CD cavity. As lanthanide forcefields are not available on Discover, the lanthanide was excluded from the energy minimization calculation of swing and cradle CD. An ammonium ion was used to approximate the charge interactions of a cation (to replace Tb^{3+} and Eu^{3+}) with the triacid group of the DTPACD. The results of the minimization were plausible as the three negative charges formed a triangular orientation about the ammonium cation. The average distance from the center of one ring of Bph to the center of mass of the lanthanide was around 6-7 Å.

Reversed Timing and TCPC Instrumental Modifications

When lifetimes and risetimes become shorter than the pulsewidth of a nanosecond laser, it is necessary to use a picosecond laser as the excitation source, where the pulses are typically 6-8 ps FWHM. The repetition rate of the laser can be varied with a cavity dumper and external trigger from 76 MHz to 1 KHz, corresponding to 13 ns to 1 ms intervals between pulses, respectively. At a repetition rate of 76 MHz, the light pulses are arriving too quickly for the electronic detection system to respond. As a result, time-correlated single photon timing (TCPC) was developed [180]. As the name implies, only one photon can be counted at a time. Therefore, one is able to avoid excessive dead time on the detector where fluorescent photons arrive too quickly and cannot be counted. TCPC is a reverse timing mode where the start (fluorescence) light pulse is detected prior to the stop (reference) pulse. In this case the trigger or start signal is initiated by an emitted fluorescent photon at the MCP-PMT detector. The stop signal is the photon from the laser pulse that is optically and electronically delayed. Previously in our laboratory Jeonga Yu et al. [143] was able to measure fast risetimes with subsequent slow luminescent decays of $Tb^{3+} \subset 2.2.1$ with acac when the cavity dumper was externally

triggered at a repetition rate of 1 kHz. Unfortunately, this led data collection times of ~ 80 hours to collect 1000 counts. We are still investigating an alternative method to data collection.

The picosecond laser system that was used as the excitation source is a Coherent 702 dye laser. For amplification of the 702 pulse (typically ~12 nJ/pulse, 6-8 ps) a dye laser a Continuum Regenerative amplification system is used. The second harmonic of a Coherent Antares 76S (100 ps FWHM, 3W of 532 nm) was used to pump the laser dyes LDS 698, Rhodamine 6G and Pyrromethene 567 in either ethylene glycol or propylene glycol solutions. The output of the 702, which varied between 100-400 mW depending on the dye and wavelength, was doubled with a KDP crystal. The doubling efficiency was typically 10-15 %. The light that was not doubled was filtered out with a Corning 7-54 filter. Bph was excited to the first singlet state with 280 nm obtained from 560 nm (Pyrromethene 567). Stern-Volmer dynamic quenching of Bph fluorescence lifetime in DTPACD by Tb^{3+} was collected on this laser system by TCPC.

The TCPC instrument described by Bowman et al. [180] was rebuilt in order to decrease instrument response function (IRF) by eliminating the transit time spread (TTS) of the monochromator and decreasing the risetime of the detector [181]. The SPEX 1681 single grating monochromator was replaced with a subtractive double monochromator from CVI (CM112 and DK1200 controller), thereby eliminating the use of a 10 mm mask previously placed on the 1681 grating. A subtractive double monochromator eliminates the TTS between blue and red photons that the 10 mm mask previously provided. Therefore, the throughput of photons was larger. A TAC biased amplifier (Oxford, Instruments Model TC 864) replaced the TC 862, changing the range of the smallest

temporal window from 25 ns to 5 ns. The 220 ps risetime of the detector was improved to 156 ps by replacing the 12 µM R1564U/11 MCP-PMT (Hamamatsu) with a 6 µM R3809U MCP-PMT (Hamamatsu). The shortened risetime of the 6 µM detector necessitated a shortening of the 9 cm internal delay loop of the fluorescence channel of the CFD (Tennelec CFD 454). However, after an exhaustive variation of the internal delay lengths longer and shorter than 9 cm (electronics design by John Rugis), the IRF still did not improve. Therefore a picotiming discriminator (9606) and fast preamp (9607) were purchased from EG&G ORTEC. The picotiming discriminator replaces the CFD for the fluorescence channel, and the Tennelec CFD is still used for the reference channel from the laser pulse. The fast preamp was necessary for the MCP-PMT pulse shaping. A picotiming analyzer (pTA 9608) is also available from EG&G ORTEC and would replace the need for a TAC and allow longer lifetimes to be measured. Another advantage of the 9608 is that the software runs in a Windows platform. A demo model of this instrument was investigated, but due to limited funds was not purchased. As there are a finite number of bins for data, short lifetimes can be measured with high resolution; however, as the lifetimes lengthen, the resolution is poorer. Hence, for measuring short risetimes on a long exponential decay, this instrumentation is not beneficial.

Results

Binding Constants

Binding constants of mono- and bicyclic aromatic hydrocarbons to TbDTPA-β-CD were measured by absorption and independently verified by emission spectroscopy by Mark Mortellaro. The binding constant of Np to TbDTPA-β-CD is previously

reported at 18000 M^{-1} [176,178]. The binding constant measured for Bph is also 18000 M^{-1} [182]. Bicyclic aromatic hydrocarbons bind more tightly to TbDTPA-β-CD than monocyclic aromatics such as durene (4000 M^{-1}) [176,178]. The binding constants of other monocyclic aromatic hydrocarbons investigated in our studies: benzene, toluene and xylene, are too small to be measured by changes in absorption because the molar absorptivies (< 200 $M^{-1}cm^{-1}$) and the changes in the terbium luminescence upon complexation are too small.

A comparision of DTPA-β-CD to previously studied aza crown swing and cradle as seen in Table 6. reveals that a Tb^{3+} cyclodextrin complex with an overall neutral charge, TbDTPA-β-CD, binds neutral complexes more strongly than a cyclodextrin that does not neutralize the +3 charge of the lanthanide (aza crown swing and aza crown cradle). The swing cyclodextrin results demonstrate that charged carboxylate analytes have the strongest binding of all analytes examined. A more detailed study of the aza crown swing and aza crown cradle CD binding properties with neutral aromatic hydrocarbons (Bph and Np) is necessary for a direct comparison.

Titrations and Steady State Luminescence

Steady state luminescence spectra of TbDTPA-β-CD, when titrated with aromatic hydrocarbons, provide evidence of an energy transfer process. When TbDTPA-β-CD complexed with Bph is excited at 266 nm, emission from Tb^{3+} at four wavelengths, 488, 544, 585 and 620 nm, increases with increasing amounts of Bph (Figure 35). The four transitions of Tb^{3+} are from the lowest J level of the excited state J = 4, $^5D_4 \rightarrow {}^7F_6$ (488 nm), $^5D_4 \rightarrow {}^7F_5$ (544 nm), $^5D_4 \rightarrow {}^7F_4$ (585nm), $^5D_4 \rightarrow {}^7F_3$ (620 nm).

Table 6. Molar absorptivities of aromatic hydrocarbons, binding constants of cyclodextrin complexes and lanthanide luminescence quantum yields for aza swing, aza cradle and DTPA cyclodextrins and aromatic hydrocarbons [176,178].

Cyclodextrin	Aromatic Analyte	Molar Absorptivity/ $M^{-1}cm^{-1}$	Binding Constant/ M^{-1}	Quantum Yield
azaCrown Swing β-CD	benzene	196	117	-
azaCrown Swing β-CD	benzoic acid	546	36000	-
azaCrown Swing β-CD	naphthoic acid	1370	43000	-
azaCrown Cradle β-CD	benzene	196	<10	-
TbDTPA-β-CD	biphenyl	6000	18000	0.103[a]
TbDTPA-β-CD	naphthalene	5500	18000	0.029[a]
TbDTPA-β-CD	durene	692	4000	-

[a] Measured for the most intense transition $^5D_4 \rightarrow {}^7F_5$ relative to biacteyl in hexane (Φ_p = 0.05).

Bph emission from the singlet state is also present in the emission spectrum, at 320 nm, but is not shown in Figure 35.

Excitation spectra were collected by scanning the excitation monochromator while detecting at the 544 nm Tb^{3+} emission line. Figure 36 shows the excitation spectrum of the TbDTPA-β-CD complex with increasing amounts of Bph. Two excitation bands are observed, one at 220 nm, a Tb^{3+} f-d transition, and another at 266 nm, the first excited state of Bph (S_1). The Bph singlet state grows in with increasing amounts of Bph and is structureless due to the non-planar character of Bph in the ground state. The emission spectrum of Bph is slightly more structured, indicating that the excited state of Bph is more planar in character [106].

The titration profiles of Bph and Np with 2.5 x 10^{-4} M TbDTPACD are shown in Figure 37. For these measurements λ_{ex} = 275 nm for Np, λ_{ex} = 266 nm for Bph and λ_{em} = 544 nm for Tb^{3+} emission. For each case Tb^{3+} emission increases to a plateau by 1.5 x 10^{-4} M. The relative emission intensities in the asymptotic limit are 35 for Bph and 5 for Np. The factor of 7 difference can be explained in part by differences in the molar absorptivity; Bph is 6600 $M^{-1}cm^{-1}$ (266 nm), compared to 5000 $M^{-1}cm^{-1}$ for Np (275 nm). However, the ratio of the emission intensities is much larger than ratio of the molar absorptivites.

As the binding constants of Np and Bph are identical, differences in the plateau intensity must be due to another factor in addition to the molar absorptivites. Measurement of the quantum yields of emission for TbDTPACD•Bph and TbDTPACD•Nap, relative to biacetyl, yields a quantum yield for emission of 0.103 and
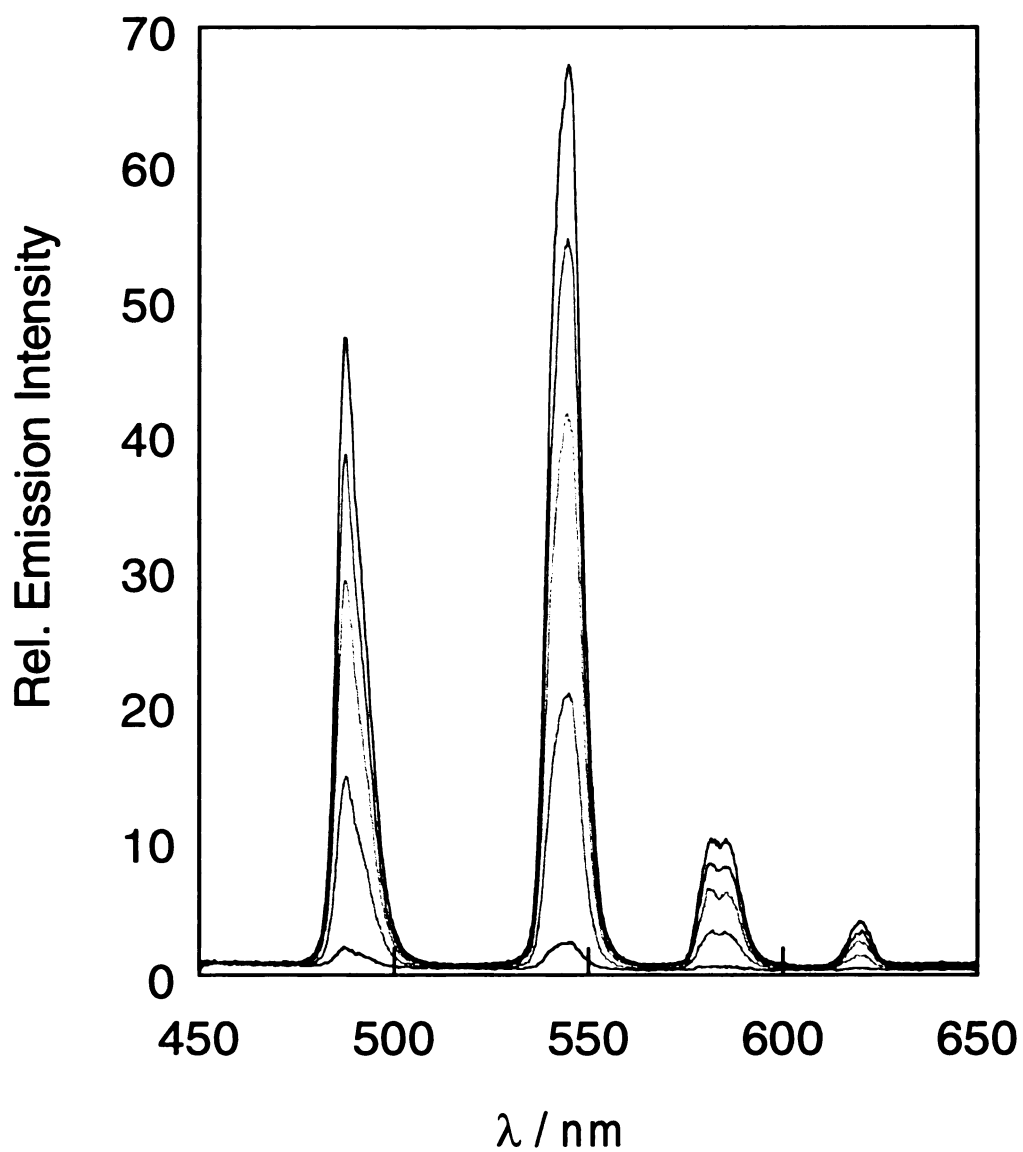
Figure 35. Emission Spectra (λ_{ex} = 266 nm) for a 2.5 x 10^{-4} M aqueous solution of TbDTPACD with increasing concentrations of Bph (data courtesy of M.A. Mortellaro [179]).
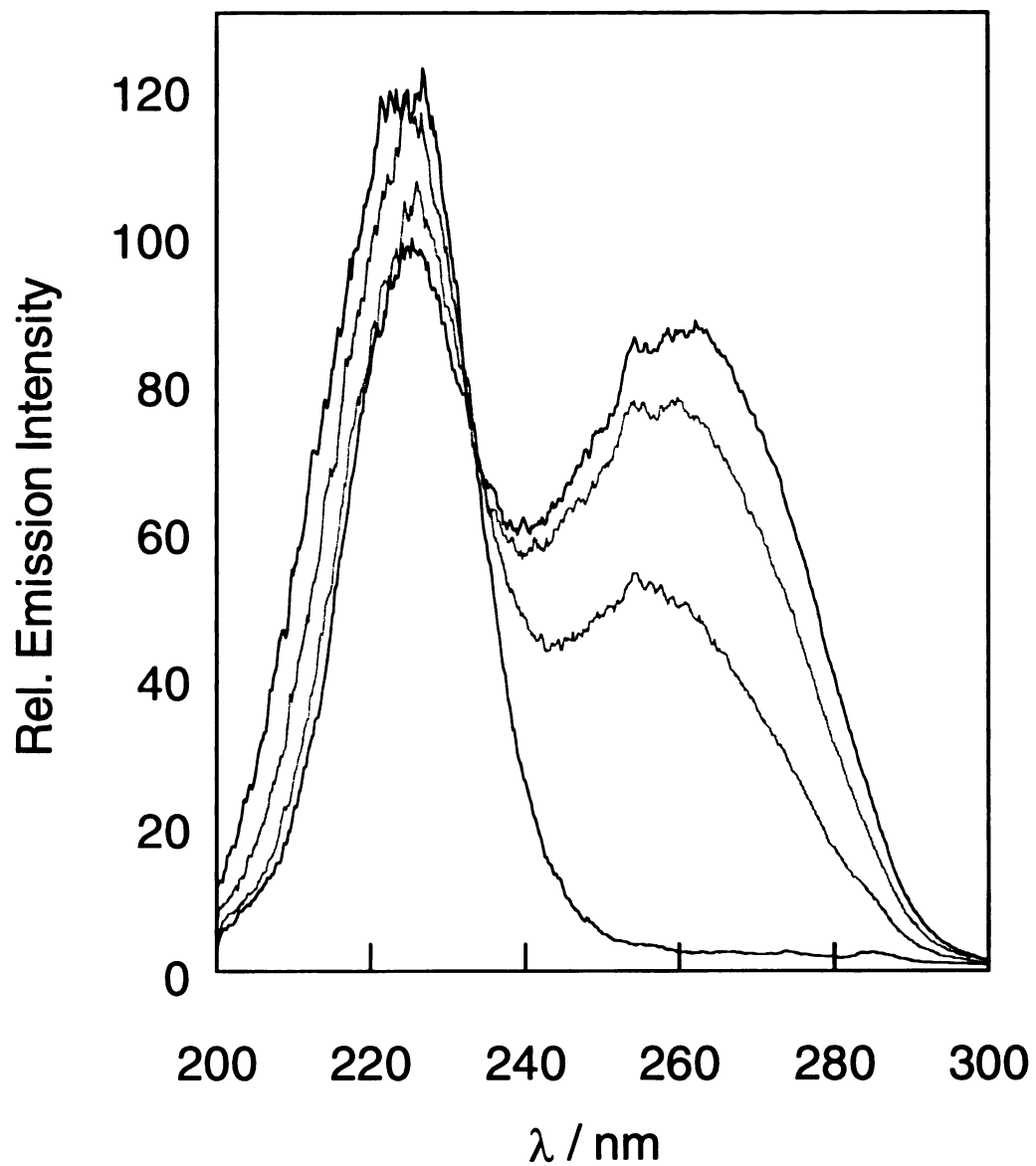
Figure 36. Excitation Spectra (λ_{em}= 544 nm) for a 2.5 x 10^{-4} M aqueous solution of TbDTPACD with increasing concentrations of Bph (data courtesy of M.A. Mortellaro [179]).
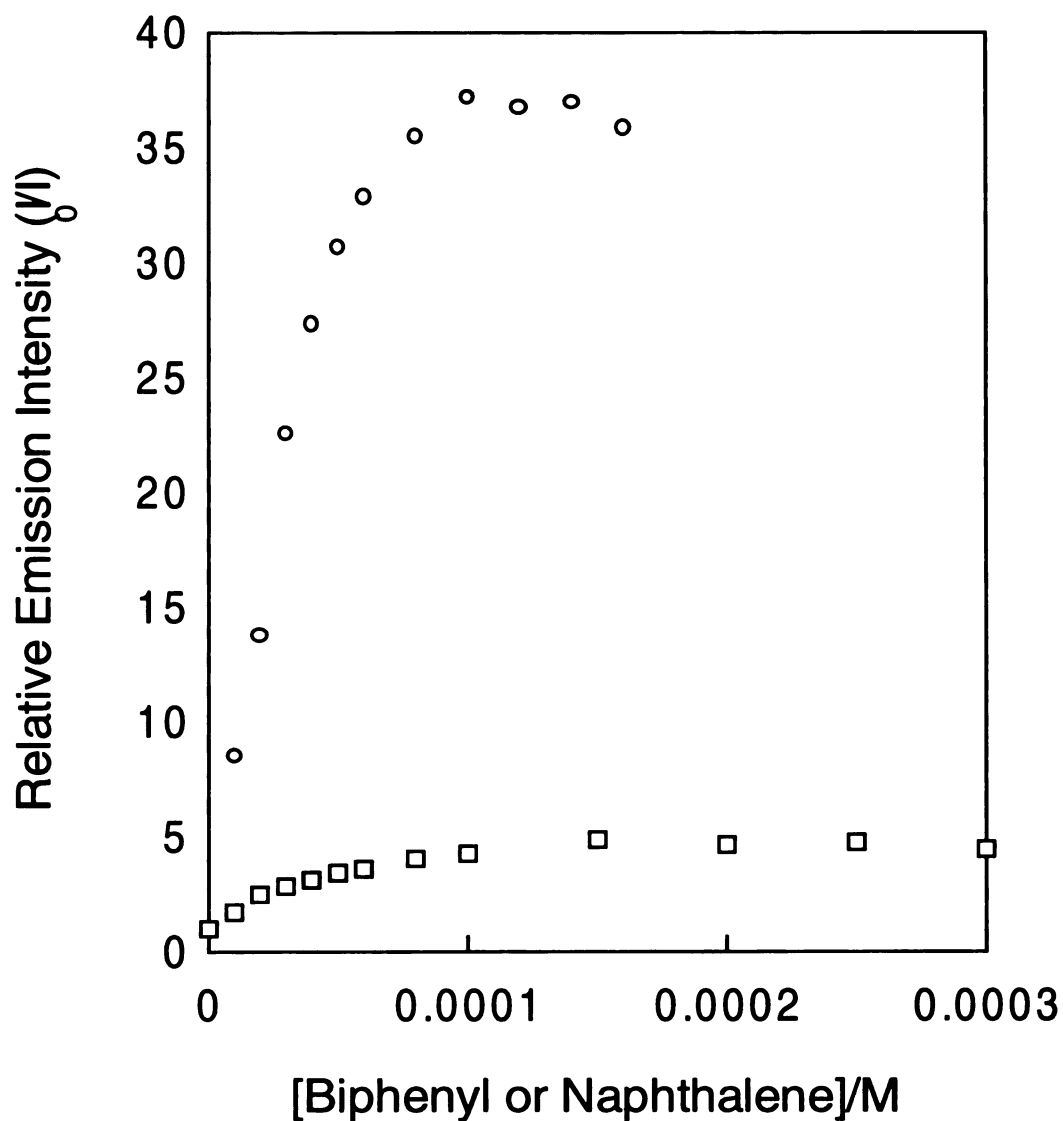
Figure 37. Relative Emission intensity from an aqueous solution of TbDTPACD (2.5 x 10^{-4} M) as a function of Bph (O) and Np (□) concentrations. The luminescence of the Tb^{3+} ion was detected at 544 nm with excitation wavelengths of 268 and 275 nm, respectively (data courtesy of M.A. Mortellaro [179]).

0.029 respectively as given in Table 6 a factor of 3.55 difference. The quantum yield reported is only for the most intense transition of Tb^{3+} the transition $^5D_4 \rightarrow ^7F_5$. This transition accounts for only 50% of the intensity of the four emission bands. Therefore if we consider all four bands the overall quantum yield should be 0.206 and 0.058 for TbDTPA-β-CD•Bph and TbDTPA-β-CD•Nap complexes respectively.

Overlap Integral and Critical Förster Energy Transfer Distance

The overlap integral is essential in ascertaining if a transition is allowed by a dipole-dipole mechanism. The overlap integral is proportional to the critical energy transfer distance by the relationship given in equation 19 and can vary from 1 x 10^{-14} to 1 x 10^{-20} M^{-1} cm^3 for a strongly and weakly overlapped donor-acceptor pair, respectively. A large value of J leads to efficient transfer over long distances (80-100 Å). A small J limits energy transfer to shorter distances. The overlap integral of Bph emission and Tb^{3+} absorption was calculated using a Kaleidagraph spreadsheet format and integrating over the product of normalized Bph emission and Tb^{3+} absorption divided by the wavenumber taken to the fourth power. The values for the overlap integral of Bph and Np with Tb^{3+} are given in Table 7. for two integration intervals, 17241 to 28703 cm^{-1} and 17241-30012 cm^{-1}. The spectral overlap as a function of wavenumber of the Bph emission and Tb^{3+} ($Tb(NO_3)_3$•$5H_2O$) absorption is shown as a bold line in Figure 38. The emission spectrum of Bph (a) shows the tail of the singlet state transition, which shows a maximum at 266 nm (37594 cm^{-1}). There is little evidence of emission from the triplet state of Bph under these conditions, which should appear at around 22900 cm^{-1} [183].

Table 7a. Overlap Integral from 17241-28703cm^{-1} and Critical Distances for Singlet (S) and Triplet (T) States of Bph and Np Donor and $Tb(NO_3)_3 \cdot 5H_2O$ Acceptor.

Aromatic Hydrocarbon	J/M^{-1}cm^3	R$_0$/Å (S)[a]	R/Å (S)[b]	Efficiency[c]	R$_0$/Å (T)[a]	R/Å (T)[b]	Efficiency[c]
Bph	2.86 x 10^{-19}	4.17	8.57	1.3 %	4.62	3.12	91 %
Np	3.99 x 10^{-19}	4.59			5.77		

Table 7b. Overlap Integral from 17241-30012 cm^{-1} .

Aromatic Hydrocarbon	J/M^{-1}cm^3	R$_0$/Å (S)[a]	R/Å (S)[b]	Efficiency[c]	R$_0$/Å (T)[a]	R/Å (T)[b]	Efficiency[c]
Bph	5.24 x 10^{-19}	4.62	14	0.13%	6.15	4.16	91%
Np	7.35 x 10^{-19}	5.08			6.39		

[a] Evaluated with $R_0=9.78 \times 10^3 (Q_D \kappa^2 n^{-4} J)^{1/6}$ with quantum yields given by the previous table, $\kappa = 2/3$ and n = 1.332 for water. Equation from Reference [131].
[b] Fit with $k_{exp} = 8.3 \times 10^4$ s^{-1} and $k = 1/\tau_D (R_0/R)^6$
[c] Efficiency= $1/1+(R/R_0)^6$
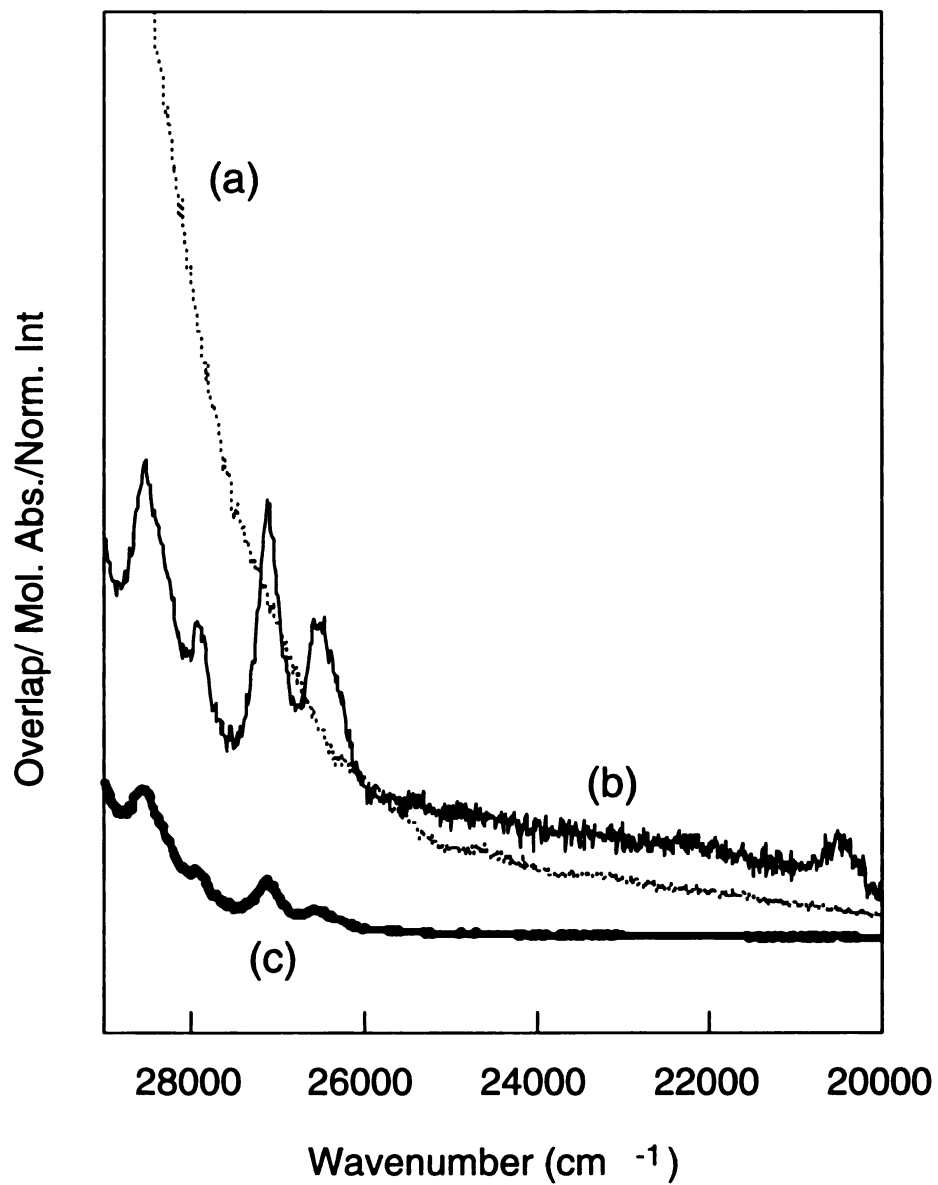
Figure 38. Overlap Integral (c) of Bph emission (a) and $Tb(NO_3)_3 \cdot 5H_2O$ absorption (b).

The absorption spectrum of $Tb(NO_3)_3$ (Figure 38b) shows 5 narrow lines at 28500 ($^7F_6 \rightarrow {}^5D_4$), 27800 ($^7F_6 \rightarrow {}^5G_5$), 27100 ($^7F_6 \rightarrow {}^5L_{10}$), 26500 ($^7F_6 \rightarrow {}^5D_3$, $^5G_6$) and 20500 cm^{-1} ($^7F_6 \rightarrow {}^5D_4$) with the transitions given in parenthesis [184]. The transition at 20500 represents direct population of the emissive excited state of Tb^{3+} at 544 nm ($^5D_4 \rightarrow {}^7F_5$). A very large absorption band from nitrate counter ions is observed above 29000 cm^{-1} and was not included in the calculation of the overlap integral.

$TbCl_3 \cdot 6H_2O$ can also be used as a source for terbium. The absorption spectrum of $TbCl_3 \cdot 6H_2O$ (Figure 39) shows 9 narrow lines from 25000 to 36000 cm^{-1}, but lacks the large absorption band observed for $Tb(NO_3)_3 \cdot 5H_2O$ around 30000 cm^{-1}. The absence of the nitrate band should decrease the overlap integral. The value of J for $TbCl_3 \cdot 6H_2O$ absorption and Bph emission yields a value of 3.15 x 10^{-19} M^{-1} cm^3 (28703 to 30012 cm^{-1}). Therefore, the difference between the overlap integral of $Tb(NO_3)_3 \cdot 5H_2O$ and $TbCl_3 \cdot 6H_2O$ is not significant.

Time-Resolved Luminescence and Stern-Volmer Quenching

The risetime and lifetime of Bph with TbDTPACD were measured at room temperature in aerated solutions with a Nd:YAG nanosecond laser. Lanthanides are notorious for their slow non-radiative deactivation in the excited state [141], and therefore it was necessary to measure the risetime when the lanthanide excited state is directly populated. The risetimes of $Tb(NO_3)_3 \cdot 5H_2O$ and $TbCl_3 \cdot 6H_2O$ ($^5D_4$ 546 nm) are < 10 ns when excited directly (λ_{ex} = 266 nm) in the absence of any added Bph light harvester, and the quantum yield of terbium luminescence is small (Figure 40 and Figure 41). This implies that internal conversions from the higher level $^5D_3$ excited state is very
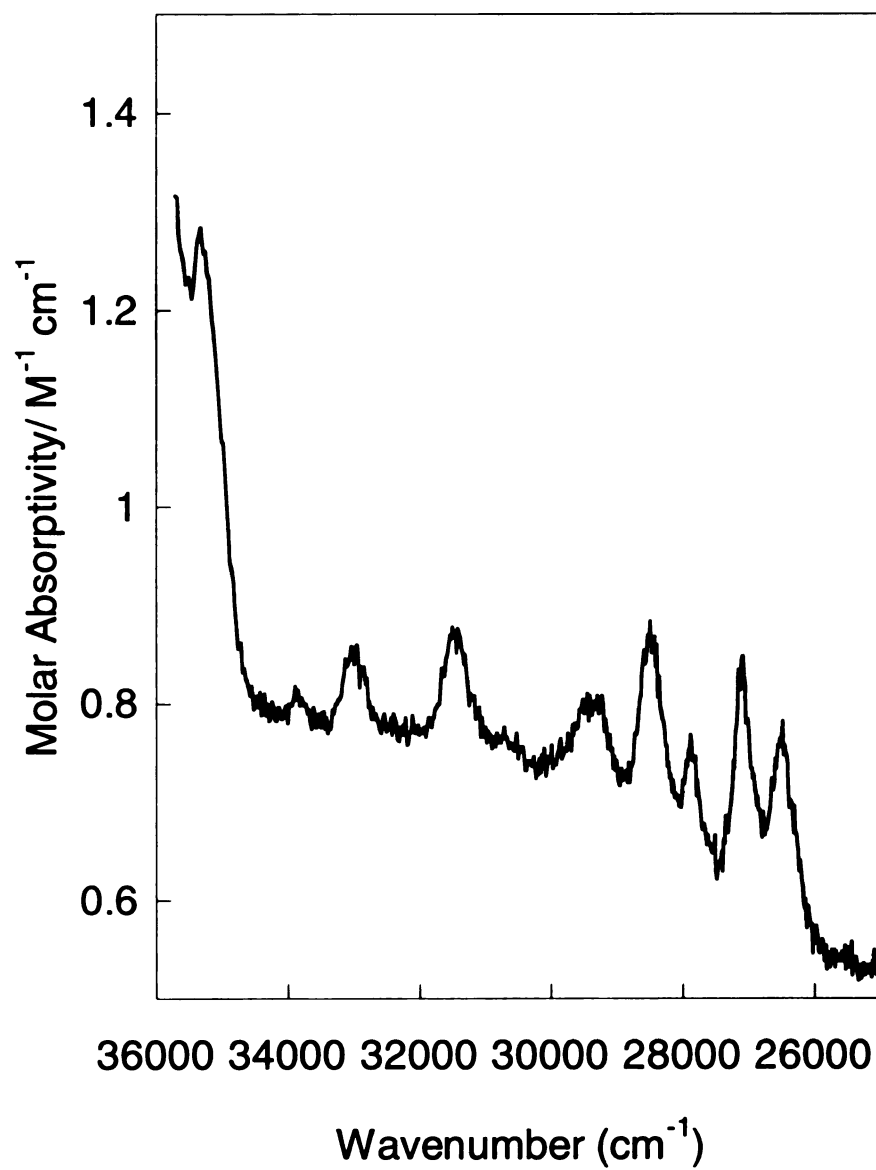
Figure 39. TbCl₃•6H₂O absorption spectrum (0.05 M in methanol).
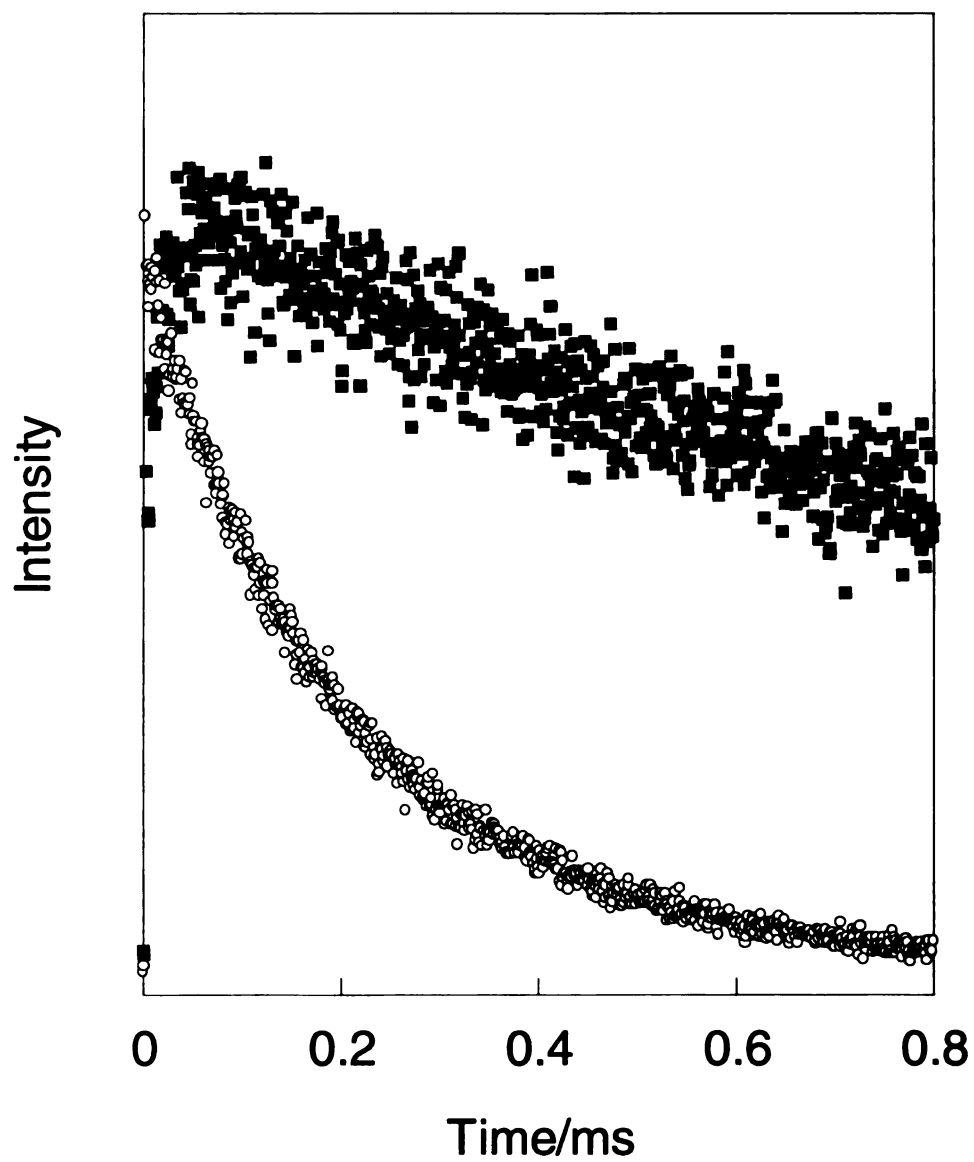
Figure 40. Time-resolved luminescence of Tb(NO₃)₃•6H₂O (open circles) and TbDTPA-β-CD (squares) at 546 nm.

Figure 41. Time-resolved luminescence of $TbCl_3 \cdot 6H_2O$ (open circles) and $TbDTPA-\beta$-CD (squares) at 546 nm.

fast leading to a fast population of the luminescent excited state $^5D_4$. Therefore slow internal conversion of the excited states of $Tb(NO_3)_3 \cdot 5H_2O$ and $TbCl_3 \cdot 6H_2O$ is not apparent at room temperature.

When 2 μl of 0.02 M Bph in ethanol is titrated in to the solution there is a dramatic change in the risetime (Figure 40 and Figure 41), which is actually very slow in the presence of Bph. Concomitant with the longer risetime is a large increase in the quantum yield of Tb^{3+} emission. A fit of the risetime of terbium luminescence at 546 nm results in a 12 μs time constant, which is consistent over the entire titration range as shown in (Figure 40). The risetime is attributable to the population buildup of the $^5D_4$ state at 20500 cm^{-1} when light harvested by Bph is transferred to the terbium excited state. This risetime is equivalent to a rate for energy transfer of 8.3 x $10^4 s^{-1}$, assuming the reaction is first order.

Time-resolved luminescence of the excited state of Tb^{3+}, $^5D_4$, was fit to a standard kinetics equation involving an exponential rise, representing the buildup of population by energy transfer in the Tb^{3+} excited state and the exponential decay of the state, representing the radiative decay. The kinetics scheme of Bph exicted state donor and $TbDTPA$-β-CD is given below, where $DTPA$-β-CD is abbreviated CD and $TbDTPA$-β-CD is represented by $TbCD$

$$^*Bph \bullet TbCD \xrightarrow{k_1} Bph \bullet TbCD + h\nu \qquad (25)$$

$$^*Bph \bullet TbCD \xrightarrow{k_2} {}^*Bph + TbCD \qquad (26)$$

$$^*Bph + TbCD \xrightarrow{k_3} {}^*Bph \bullet TbCD \qquad (27)$$

$$^{*}Bph \xrightarrow{k_4} Bph + h\nu \tag{28}$$

$$^{*}Bph \bullet TbCD \xrightarrow{k_5} Bph \bullet ^{*}TbCD + h\nu \tag{29}$$

$$Bph \bullet ^{*}TbCD \xrightarrow{k_6} Bph \bullet TbCD + h\nu \tag{30}$$
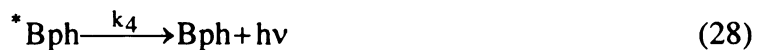
This scheme was adapted from Thomas et al. [147]. Step 1 is the phosphorescence (fluorescence) of Bph when encapsulated in the cyclodextrin cavity. Step 2 is the dissociation of excited state Bph from the CD cavity. The rate of excited state Bph association with a cyclodextrin cavity is given by the third step. In the fourth step excited state Bph radiatively decays in bulk solution. The most important steps (5) and (6) show the rate of energy transfer and the rate of terbium luminescence. The last two steps define the time evolution of the excited state of terbium(III). This luminescence time profile is given by [147]:

$$[^{*}Tb] = \frac{k_5[Bph \bullet TbCD]_i}{k_6 - \tau_p^{-1}} \left[e^{\frac{-t}{\tau_p}} - e^{-k_6 t} \right] \tag{31}$$

where τ_p is the phosphorescence lifetime of Bph and t is dependant variable, time. The data was fit to the equation given above where the decay of Bph (τ_p) is incorporated into the risetime of Tb^{3+} luminescence and k_6 represents the decay of luminescence of $^{*}Tb^{3+}$. According to this equation the energy transfer rate is given in the preexponential factor k_5. However, for our purposes we will use the risetime as the energy transfer rate. The slowness of the risetime is indicative of a slow population of the Tb^{3+} $^{5}D_4$ excited state by the triplet state of Bph. If the singlet state is involved in energy transfer then one would expect a much faster energy transfer rate with a nanosecond risetime (or picosecond) for

Tb^{3+} luminescence. Therefore the delayed buildup of Tb^{3+} verifies that the mechanism of transfer is through the triplet state of biphenyl.

The description of Bph energy transfer to TbDTPA-β-CD as a unimolecular process is tenuous. Stern-Volmer quenching of *Bph by Tb^{3+} will discriminate between a unimolecular and bimolecular process. Since we do not observe Bph phosphorescence in aerated solutions, we cannot measure quenching of Bph triplet. We therefore investigated Stern-Volmer static and dynamic quenching of Bph fluorescence by measuring the intensity and lifetime of Bph and DTPA-β-CD with increasing concentrations of $Tb(NO_3)_3 \cdot 5H_2O$. The lifetime of Bph in DTPA-β-CD was measured by TCPC to be 11 ns in the absence of Tb^{3+}. This lifetime is shorter than the literature value of 16 ns for polar solvents [183]. As the concentration of terbium increases, the lifetime and intensity of Bph emission at 320 nm (fluorescence) decreases. The Stern-Volmer plot of I_0/I and τ_0/τ of Bph fluorescence in DTPA-β-CD as a function of Tb^{3+} concentration is shown in Figure 43. The intensity and fluorescence lifetime of Np was also investigated and similar results were observed. The dynamic (bimolecular) quenching derived from the slope of the lifetime plot of both Np and Bph are roughly equivalent at 1.66×10^{10} and 2.10×10^{10} s^{-1}, respectively. These bimolecular rates are within the limit of diffusional processes.

In an attempt to obtain the static rate constant (binding constant) the I_0/I quenching data was fit with a quadratic equation. The fit failed to give a meaningful value for static quenching rate constant. However, we can conclude that the extent of static quenching is significant, given the large differences between the plots of I_0/I and
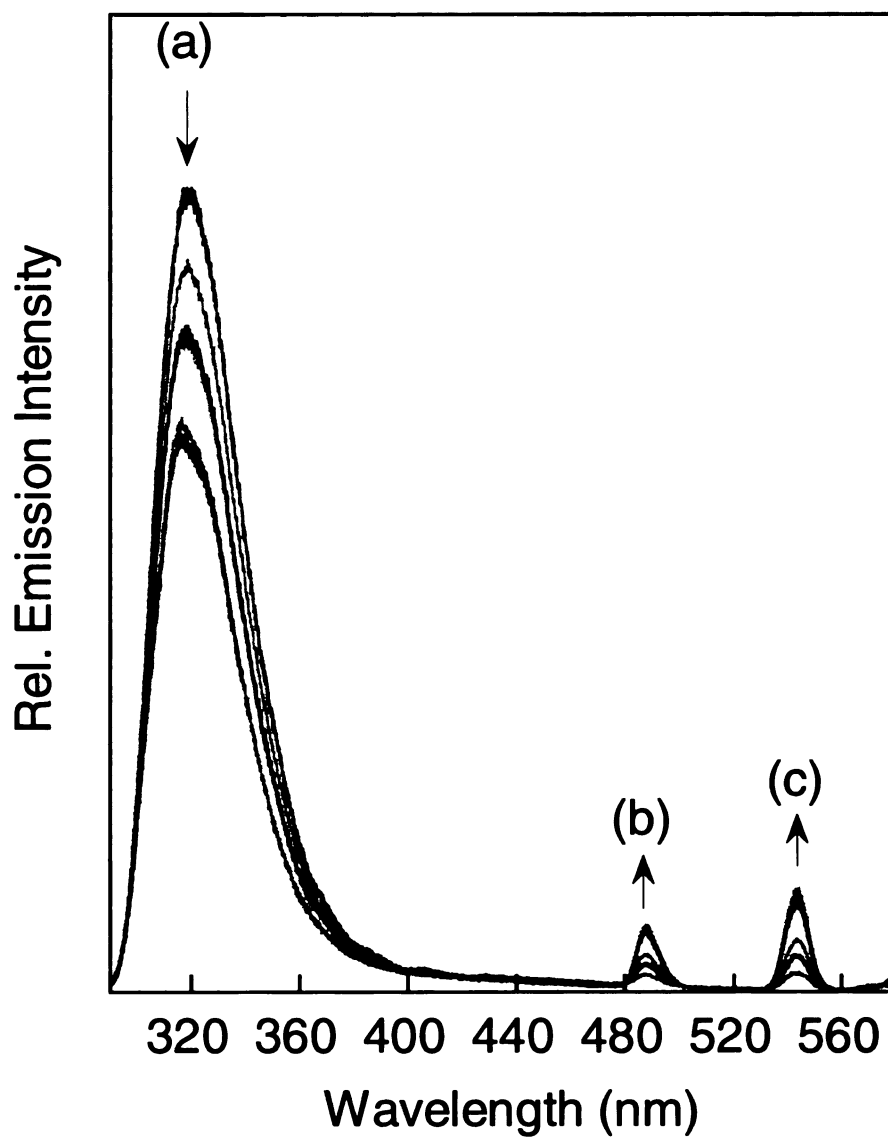
Figure 42. Bph fluorescence quenching by Tb^{3+}. Fluorescence (a) decreases upon addition of terbium(III). A concomitant increase in terbium luminescence (b,c) is observed at 488 and 544 nm.
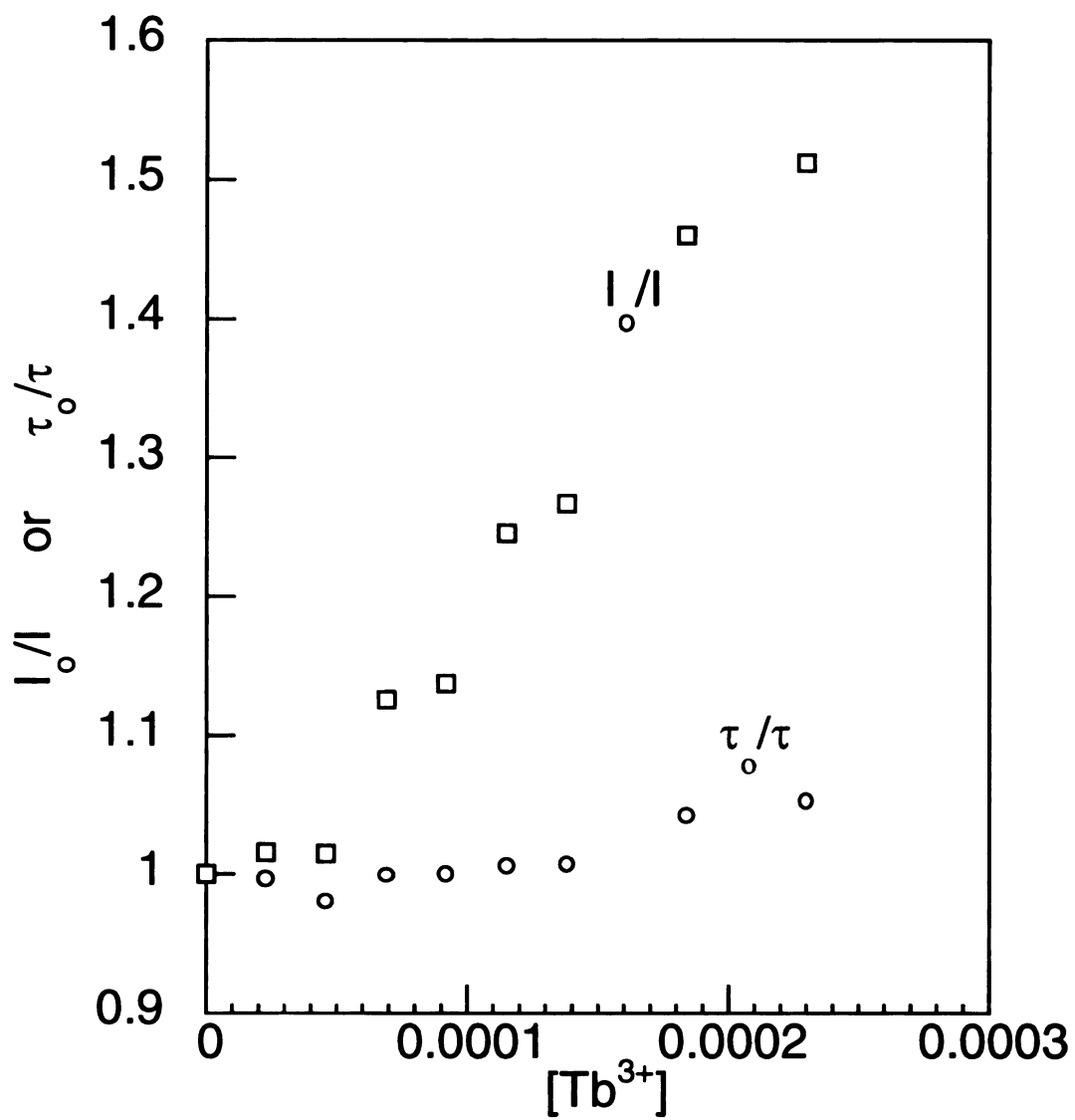
Figure 43. Stern-Volmer plot of I_0/I and τ_0/τ of Bph in DTPACD quenched with Tb^{3+}.

τ_0/τ. Therefore the value of 8.3×10^4 s^{-1} for the risetime is truly a reflection of the energy transfer rate of a bound complex of Bph in the hydrophobic cavity of TbDTPACD.

Discussion

The very slow rate of energy transfer from light harvesting aromatic hydrocarbons to luminescent lanthanide ions we observe in supramolecular cyclodextrin assemblies is precedented. Thomas and coworkers observed very slow rates of energy transfer from Np and Bph encapsulated in a micelle to lanthanide ions on the surface of the micelle [147]. In this case risetimes of ~ 20 μs were observed. Another example of a slow and inefficient rate of energy transfer was observed in a protein system studied by Horrocks where a tryptophan residue to a terbium ion residing in a calcium binding site transfers energy over a distance of 8-10 Å [185]. The very slow transfer can be accounted for by many factors. The primary factor is the exceedingly small value for the overlap integral that leads to an inefficient transfer of energy. Involvement of the triplet state will also slow down the transfer, as the decay is long-lived and the Förster rate is proportional to the inverse of the donor lifetime.

It seems evident from the magnitude of the energy transfer rate that the triplet state of biphenyl is involved. However, perhaps more proof is needed. The presence of the heavy lanthanide in close proximity to the light harvesting aromatic donor may enhance intersystem crossing to the triplet manifold of the donor. At this point we have no data to support or refute this hypothesis. Inspection of Table 8 shows that the triplet yield of Bph and Np are already very large, 0.84 and 0.75. Addition of a heavy lanthanide

Table 8. Quantum yields of fluorescence, triplet state, fluorescence lifetime and triplet lifetime for mono- and bicyclic aromatic hydrocarbons. Data taken from reference [183].

Aromatic Hydrocarbon	ϕ_{fl}	ϕ_T	τ_{fl}/ns	τ_T/μs
Bph	0.15	0.84	16	130
Np	0.19	0.75	96	175
1,2,3,4-tetramethyl benzene	0.14	-	36.2	-
Benzene	0.06	0.25	34	-
Toluene	0.14	0.53	34	-
p-Xylene	0.22	0.63	30	-

atom would increase the intersystem crossing by approximately an order of magnitude if the lanthanide were within bonding distance of the aromatic hydrocarbon [150].

Amazingly enough, there is a lack of intensity of Bph triplet observed in the overlap integral (Figure 38), which is typically observed at 22900 cm^{-1} in the emission spectra. It appears that the intensity and lifetime of the triplet state of Bph is quenched by oxygen in aerated solutions as noted by the absence of emission at 22900 cm^{-1}. An attempt was made at collecting emission spectra of degassed solutions at room temperature. This yielded inconsistent results. Gadolinium was used in place of terbium as a control experiment to test for phosphorescence of Bph at exceedingly high concentrations [186]. Some evidence of Bph triplet emission was observed when precipitation occurred. The same results were observed for solutions of Gd^{3+} and Bph in the absence of the cyclodextrin.

The conformation of Bph may play some role in determining whether the triplet or singlet excited states are involved in energy transfer. Many studies of the conformation of aromatic hydrocarbons, particularly Bph, have been published [187]. The general consensus is that more planar, rigid molecules have smaller intersystem crossing rate constants. In one study the quantum yield, phosphorescence quantum yield and phosphorescence lifetime of Bph in viscous propylene glycol were measured as a function of temperature and excitation wavelength. The intersystem crossing rate and radiative phosphorescence rate are both faster in twisted Bph in comparison to planar Bph. It is difficult to determine the extent of planarity of Bph in a cyclodextrin cavity, however molecular modeling minimizations show a twisted conformation for Bph

(Figure 44). Circular dichroism measurements may shed light on the conformation of Bph in the cyclodextrin cavity.

Approximations of the distance of energy transfer from the lanthanide acceptor at the bottom of the cyclodextrin to the aromatic donor in the CD cavity were also modeled on the Silicon Graphics system using Insight Discover Biosym. As lanthanide forcefields are not available on Discover, the lanthanide was excluded from the energy minimization calculation of swing and cradle CD. An ammonium ion was used to approximate the charge interactions of a cation (to replace Tb^{3+} and Eu^{3+}) with the triacid group of the DTPACD. The results of the minimization were realistic, as the three negative charges formed a triangular orientation about the ammonium cation. The average distance was around 6-7 Å.

Table 7 lists the values of the critical energy transfer distance (R_0) and the actual distance calculated with the experimental rate and lifetime of the donor. Two different values of the overlap integral give similar results. An accurate measurement of the overlap integral is pivotal to determining the validity of the dipole-dipole mechanism for this type of energy transfer. The values of R were evaluated for using equation 20, with the values for R_0 from measurement of the overlap integral and k from the risetime. The singlet state of Bph gives a distance of 8-14 Å between the Bph and Tb^{3+} ion and a very low efficiency of 1% or less. Distances of 3-4 Å are approximated for the triplet state with larger efficiencies of 91%. The slow rate along and the measurements of the efficiency are a convincing argument for a triplet state mechanism. The small efficiency of energy transfer from the singlet state coupled with the longer distances for energy
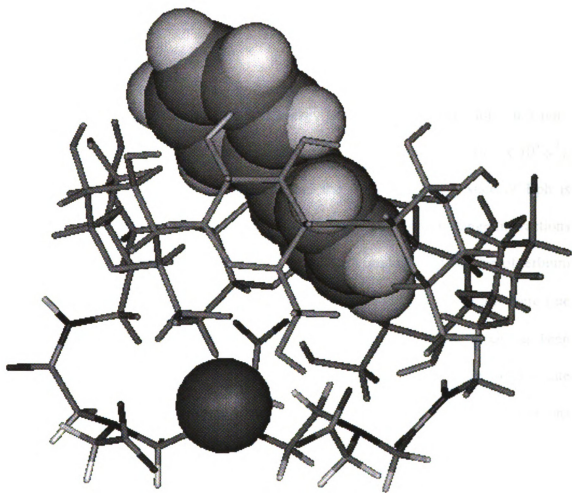
Figure 44. Molecular modeling showing twisted Bph in the cavity of TbDTPA-*β*-cyclodextrin. The lanthanide ion is the shaded ball, the DTPA-*β*-cyclodextrin is shown as a stick and Bph in CPK rendering. The distance from the center of the closest Bph aryl ring to the center of the lanthanide is 6-7 Å.

transfer make it unlikely that energy will flow directly through this state to the lanthanide excited state.

Summary and Future Work

The rate of absorption of Bph and energy transfer to lanthanide ions in a non-covalent supramolecular cyclodextrin assembly is slower than diffusion, $(8.3 \times 10^4 \text{ s}^{-1})$. Two issues that remain unresolved are whether the triplet or singlet state of Bph is involved in energy transfer and if a significant contributions from exchange interactions are also possible. To address the first point, it seems very unlikely that buildup of terbium population is arriving by population from Bph singlet state ($\tau = 11$ ns). If this were true one should observe a risetime that is orders of magnitude faster than what has been measured. Inspection of the values of R_0 and R for energy transfer from the singlet state (Table 7) the efficiency is 1%. Since all experiments were performed in aerated solutions at room temperature, the quantum yield and lifetime of Bph triplet state will be very small. Despite the apparent absence of Bph triplet state emission and extremely small overlap of Bph emission and terbium absorption, an energy transfer efficiency of 91% is estimated.

Balzani and coworkers have measured the triplet-triplet transient absorption of $[\text{Ln} \subset \text{bpy.bpy.bpy}]^{3+}$ cryptand where $\text{Ln} = \text{Gd,Tb}$ and Eu. They observed a very large triplet state absorption for the bipyridine ligands having a ΔOD of 0.4 and a non-exponential decay in the μs time scale. The transient triplet signal was quenched by oxygen with a rate of $5 \times 10^8 \text{ M}^{-1} \text{ s}^{-1}$. In our laboratory, attempts at measuring the transient absorption of Bph, GdDTPACD with Bph and TbDTPACD with Bph yielded

inconclusive results. The pump pulse was set at 266 nm and the monochromator scanned from 280-400 nm. Degassing of a solution of Bph in ethanol also failed to produce a transient signal at moderate slit widths. A possible false signal was observed when the slits were opened to nearly 8 mm. If the proper set of optics coated for 266 nm were employed excitation power of the laser pulse and overlap with the probe white light could be greatly improved.

Preliminary energy transfer studies of the risetime of Tb^{3+} in TbDTPACD in the presence of 4-bromobiphenyl and 3-bromobiphenyl donor show that the rate of buildup is also very slow (20-50 μs) adding further evidence that the triplet state of the aromatic is involved [62]. Although intersystem crossing is enhanced by attachment of bromine, energy transfer is still limited by the decay of the triplet state. Small changes in the conformation of Bph by using various 2-, 3-, 4- substituted derivatives may prove essential in determining whether the route of energy transfer flows through the singlet or triplet state by providing an assessment of how the extent of twisting increases intersystem crossing rates.

The second issue concerning the proof or disproof of an exchange mechanism is difficult to undertake until a way to systematically varying the distance is found. Also, it is not possible to completely eliminate the possibility of contributions from Dexter energy transfer. A general rule of thumb for the rate dependence of Dexter energy transfer as a function of distance is, $k = k_0 \exp{\frac{-2R}{2.3}}$ where k_0, the limiting rate at collisional distance (R = 0) is 10^{13} s^{-1} [17]. This crude model gives an estimate of the rate to be ~10^4 s^{-1} when R = 10 Å. One control experiment would be a measurement of the

rate of a covalent system of Tb^{3+} and biphenyl where the distance is set between 6-7 Å. This would give a value for a through bond rate.

Although the exchange mechanism is typically viewed as a through bond mechanism, there is no reason not to believe that a through space mechanism is impossible. Farran and Deshayes have demonstrated that exchange energy transfer can occur bimolecularly on the extremities of a hemicarcerand to a biacetyl molecule trapped in the cavity over a distance of around 7 Å [136]. One possible solution is to choose a series of donors where the triplet/singlet state is varied over a region where a Marcus curve can be measured. One is limited by sizes of donor aromatic hydrocarbons that will fit in the cavity of the cyclodextrin and by the energy of the triplet state. Experiments with pyrene and anthracene donors show that no energy transfer occurs due to the low energy of the triplet state [188]. Possible molecules in the a Marcus curve series are substituted biphenyls and naphthalenes. Table 9 lists substituted Bphs whose triplet states vary from 2.5-2.79 eV. Other potential donors that have triplet energies above the Tb^{3+} $^5D_4$ (20500 cm^{-1}) are fluorene ($E_{triplet}\sim$ 23000 cm^{-1}), triphenylene ($E_{triplet}\sim$ 23400 cm^{-1}), benzophenone ($E_{triplet}\sim$ 24200 cm^{-1}), xanthone ($E_{triplet}\sim$ 25905 cm^{-1}) and xanthene ($E_{triplet}\sim$ 27700 cm^{-1}), to name a few. Xanthene has previously been used as a light harvester for terbium complexes [189].

In conclusion, we have succeeded in designing a sensor that is optimized for neutral aromatic hydrocarbons. Other supramolecular AETE systems exist (Figure 45), however, in these systems the chromophore is built into the backbone of the molecule. The bipyridine calixarene complexes with Tb^{3+} synthesized by Sabbatini, Ungaro and

Table 9. Energy levels of substituted Bphs for a Dexter Marcus curve study.

Bph Donor	Energy of Triplet State/eV
4,4'-dinitro	2.50
4,4'-dibenzoyl	2.50
2-nitro	2.57
2-iodo	2.73
4,4-dichloro	2.73
4,4'-dihydroxy	2.73
4,4'-dimethoxy	2.74
4-chloro	2.75
3-chloro	2.76
4,4'-difluoro	2.76
4-hydroxy	2.78
3,3'-dichloro	2.79
4,4'dimethyl	2.79

(a)

(b)

(c)
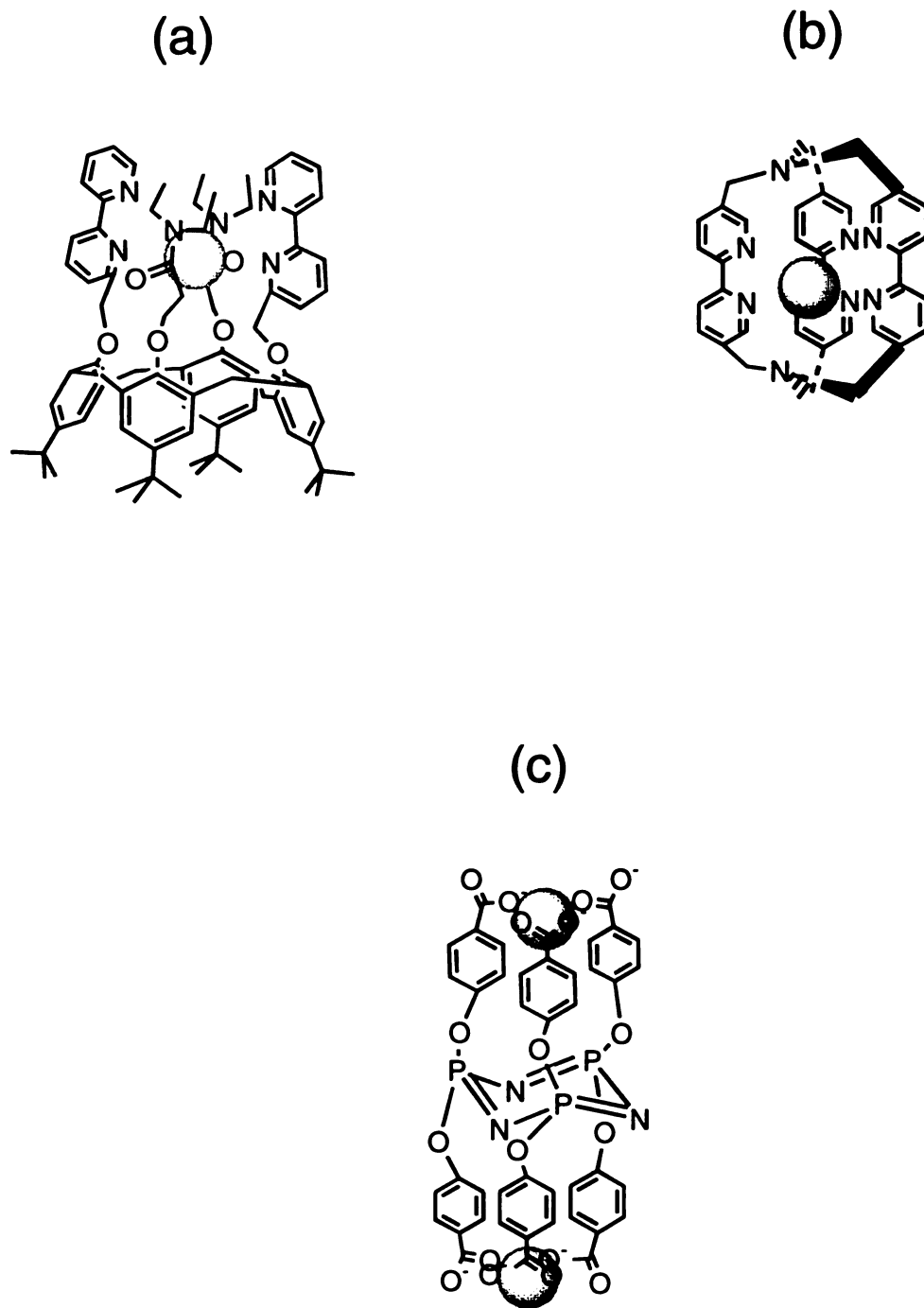
Figure 45. Three supramolecular antenna lanthanide complexes (a) bipyridine cryptand
(b) hexakis(4-carboxyphenoxy)cyclotriphosphazine (c) [Ln ⊂ bpy.bpy.bpy.]$^{3+}$.

coworkers has a quantum yield of 0.12 [190]. Matusumoto has created a complex with a quantum yield of 0.30 [191]. Lanthanide bipyridine cryptates ($Ln \subset bpy.bpy.bpy$) have large lanthanide quantum yields from between 0.01 to 0.10 in H_2O and D_2O [153]. These values are comparable to the quantum yields of 0.10 and 0.03 obtained for Bph•TbDTPA-β-CD and Np•TbDTPA-β-CD. The rate of energy transfer from the bipyridine triplet state through the bonds of the cryptate cage to the $^5D_4$ of Tb in $Tb \subset bpy.bpy.bpy$ is derived from a kinetics scheme involving decay of the transient absorption triplet state and of the $^5D_4$ state [153]. The solution to a best fitting procedure gives an energy transfer rate of 0.5×10^8 s^{-1}.

In our systems the chromophore is bound to the supramolecule by an equibrium process, allowing us to turn bright visible lanthanide luminescence on and off. There are very few cases of lanthanide luminescence used in optical sensing by this type of technique. The only other example is the work by Shinkai [192]. In this AETE sensor binding of saccharides to a boronic acid inhibits quenching by a tertiary amine and bright luminescence of a lanthanide ion is observed. The challenge that we face with our system is fine tuning the properties of the AETE supramolecule to enhance the luminescence response for benzene and other weakly absorbing monocyclic aromatic hydrocarbons. As we can see from Figure 42 the luminescence intensity of the donor molecule is still very large relative to terbium luminescence.

There are many potential future directions for this research project. Several possibilities are outlined in Figure 46. One control experiment (Figure 46a) is to make a covalent AETE complex with Bph, Np and benzene covalently bound to the secondary side of the primary side linked DTPA-β-CD. This experiment will define a measurable

156
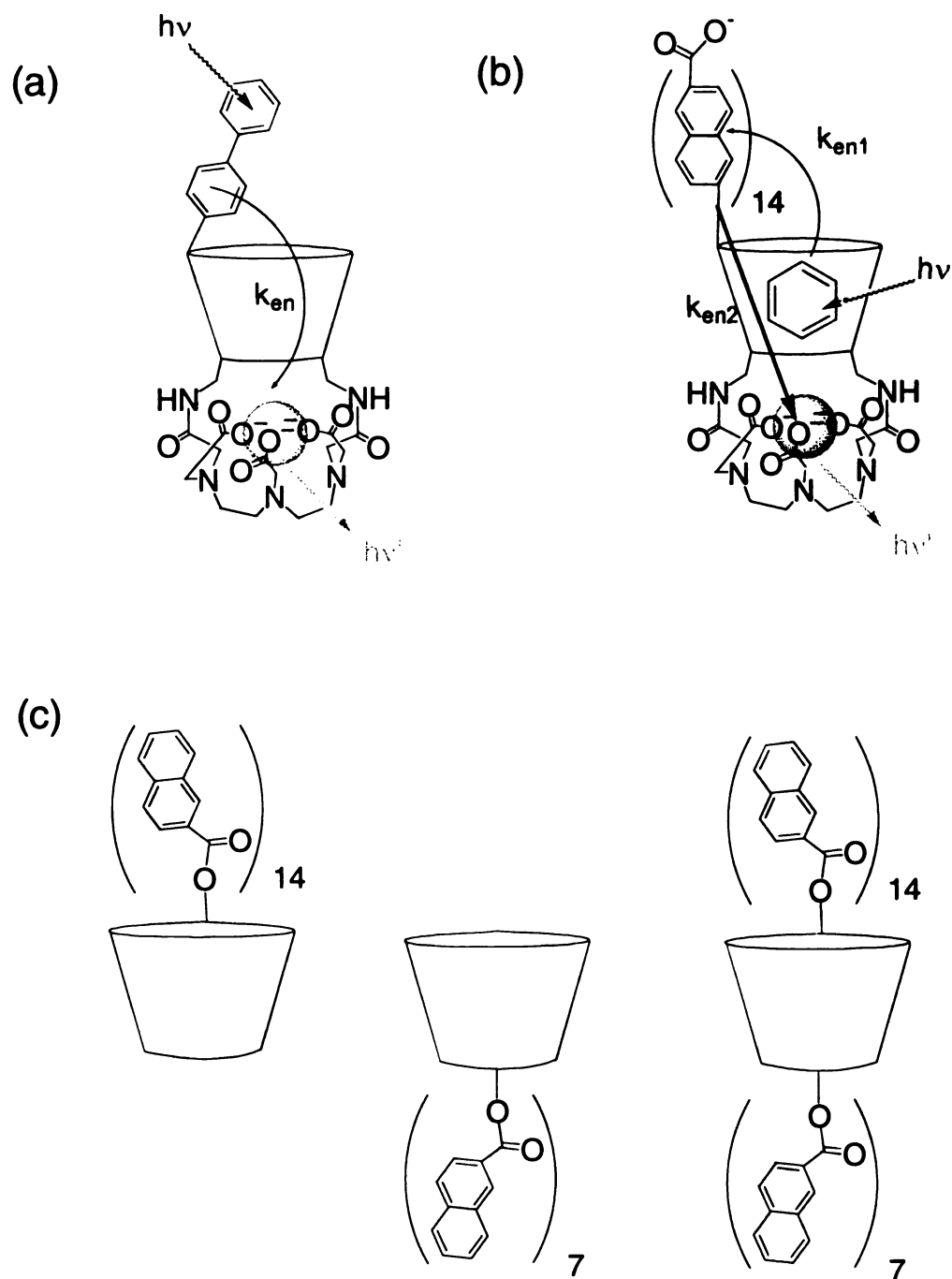
Figure 46. (a) Covalent Bph-CD-lanthanide AETE system. (b) Potential new scheme for sensing benzene by an antenna amplification of the signal. (c) Multichromomorphic cyclodextrins (see reference [132])

distance and reveal if energy can transfer from the upper rim of the CD through the bonds to the lanthanide ion on the secondary side.

A second possibility is to make a DTPACD with multichromophore antenna molecules on the secondary side (Figure 46b). The light harvesting backbone on this cyclodextrin may significantly magnify the luminescent signal from benzene by cascading the energy down a light collecting channel of two short distance steps (k_{en1} and k_{en2}) to the lanthanide ion, akin to the way that energy is funneled to the reaction center in photosynthetic units. We may be able to convert high energy light absorbed by benzene to lower energy by using smaller energy gaps to transfer the energy from benzene to the lanthanide ion. Addition of through bond step may yield more efficient transfer and faster rates.

LIST OF REFERENCES

1. (a) Silkworth, J.B.; Lipinskas, T.; Stoner, C.R. *Toxicology*, **1995**, *105*, 375. (b) Johnson, B.L. *Chemosphere* **1995**, *31*, 2415. (c) Ahlfeld, D.P.; Page, R.H.; Pinder, G.F. *Groundwater* **1995**, *33*, 58. (d) Pascoe, G.A.; Dalsoglio, J.A. *Environmental Toxicology and Chemistry*, **1994**, *13*, 1943. (e) Kamrin, M.A.; Fischer, L.J.; Suk, W.A.; Fouts, J.R.; Pellizzari, E.; Thornton, K. *Environmental Health Perspectives* **1994**, *102*, 221. (f) Royer, M.D.; Selvakumar, A.; Gaire, R. *Journal of the Air & Waste Management Association* **1992**, *42*, 970.

2. Reisch, M.; Johnson, S.L.; Bearden, D.M. Congression Research Service Report for Congress, Superfund Fact Book, Environment and Natural Resources Policy Devision, **1994**, 94-464 ENR.

3. Jones, K. in *Sensors, A Comprehensive Survey*; Göpel, W.; Hesse, J.; Zemel, J.N. Eds.; VCH: Weinheim, 1990; Vol. 8, Ch 16.

4. Soloman, S. *Sensors and Control Systems in Manufacturing*, McGraw-Hill: New York, 1994.

5. Westbrook, M.H.; Turner, J.D. *Sensors Series: Automotive Sensor*s Jones, B.E. (ed.) Institute of Physics Publishing: Philadelphia, 1994.

6. Shulman, M.A.; Hamburg, D.R. *Society of Automotive Engineers Paper* 1980, 800018,.

7. Pfeifer, J.L; Wertheimer, H.P. *Proc. 5th Int. Automotive Electronics Conf. (ImechE Conf. Publication 1985-12)*, 1985, 357.

8. Norton, H.N. *Sensor and Analyzer Handbook*; Englewood Cliffs, NJ: Prentice Hall, 1982.

9. Göpel, W.; Hesse, J.; Zemel, J.N. (eds.) *Sensors: A Comprehensive Survey. Fundamentals and General Aspects*, VCH: New York, 1988, Vol. 1.

10. Janata, J. *Principles of Chemical Sensors*, Plenum Press, New York 1988, Ch. 5.

11. Wolfbeis, O.S. (ed.) *Fiber-Optic Chemical Sensors and Biosensors*, CRC Press: Boca Raton, FL, 1991, Vol. 1.

12. Wagner, E.; Dändliker, R.; Spenner, K. (eds.) *Sensors: A Comprehensive Survey. Optical Sensors*, VCH: New York, 1991, Vol. 6.

13. Rogers, A.J. in W. Gopel, J. Hesse and J.N. Zemel (eds.), *Sensors: A Comprehensive Survey. Fundamentals and General Aspects, Optical Sensors* Plenum Press: New York, 1992, Vol. 6, Ch. 15.

14. Goldberg, M.C. (ed.) *Luminescence Applications in Biological, Chemical, Environmental and Hydrological Scineces*, ACS Symposium Series 383, Amcerican Chemical Society, Wasington, D.C.

15. Wolfbeis, O.S. (ed.) *Fluorescence Spectroscopy, New Methods and Applications*, Springer-Verlag, Berlin.

16. (a) Balzani, V.; Carassiti, V. *Photochemistry of Coordination Compounds*, Academic Press: New York, 1970. (b) Wayne, R.P. *Principles and Applications of Photochemistry*, Oxford University Press: New York, 1988.

17. Turro, N.J. *Modern Molecular Photochemistry*, University Science Books: Mill Valley, 1991.

18. Ferraudi, G.J. *Elements of Inorganic Photochemistry*, Wiley-Interscience: New York , 1988, Ch. 1.

19. Balzani, V.; Moggi, L.; Manfrin, M.F.; Bolletta, F.; *Coord. Chem. Rev.* **1975**, *15*, 321.

20. Mortellaro, M.A.; Nocera, D.G. ChemTech, 1996, 26, 17. (b) Nocera, D.G. *New Scientist*, 1996, 149, 24. (c) Pikramenou, Z.; Yu, J.-a; Lessard, R.B.; Ponce, A.; Wong, P.A.; Nocera, D.G. *Coord. Chem. Rev.* **1994**, *132*, 181.

21. McGlynn, S.P.; Azumi, T.; Kinoshita, M. *Molecular Spectroscopy of the Triplet State*; Prentice-Hall: Englewood Cliffs, 1969; Chapter 5 and Appendix 1.

22. (a) Lehn, J.-M. *Supramolecular Chemistry: Concepts and Perspectives*; VCH: New York, 1995. (b) Lehn, J.-M. in *Frontiers in Supramolecular Organic Chemistry and Photochemistry* Schneider, H.-J.; Dürr, H. (eds.) VCH: New York, 1991, Ch. 1. (c) Lehn, J.-M. *Angew. Chem. Int. Ed. Engl.* **1988**, *27*, 89.

23. Odell, B.; Reddington, M.V.; Slawin, A.M.Z.; Spencer, N.; Stoddart, J.F.; Williams, D.J. *Angew. Chem. Int. Ed. Engl.* **1988**, *27*, 1547.

24. El Khalifa, M.; Pétillon, F.Y.; Saillard, J.Y. and Talarmin, J. *Inorg. Chem.* **1989**, *28*, 3849.

25. Gutsche, C.D. *Calixarenes* Royal Society of Chemistry: Cambridge, 1989.

26. Cram, D.J.; Karbach, S.; Kim, Y.H.; Baczynskyj, L. Marti, K.; Sampson, R.M.; Kalleymeyn, G.W. *J. Am. Chem. Soc.* **1988**, *110*, 2554.

27. Cram, D.J.; Karbach, S.; Kim, Y.E.; Knobler, C.B.; Maverick, E.F.; Ericson, J.L.; Helgeson, R.C. *J. Am. Chem. Soc.* **1988**, *110*, 2229.

28. Rebek, J., Jr. *Science*, **1987**, *235*, 1478.

29. Pedersen, C.J. *Science*, **1988**, *241*, 536.

30. Dietrich, B.; Lehn, J.M. Sauvage, J.P *Tetrahed. Lett.* **1968**, 2285.

31. Dietrich, B. *Angew. Chem. Int. Ed. Engl.* **1988**, *27*, 362

32. Kroto, H.W. *Nature*, **1987**, *329*, 529.

33.   Vinod, T.K.; Hart, H. *J. Am. Chem. Soc.* **1988**, *110*, 6574.

34.   Hamilton, A.D.; Van Engen, D. *J. Am. Chem. Soc.* **1987**, *109*, 5035.

35.   Barr, D.; Clegg, W.; Hodgson, S.M.; Lamming, G.R.; Mulvey, R.E.; Scott, A.J.; Snaith, R.; Wright, D.S. *Angew. Chem. Int. Ed. Engl.* **1989**, *28*, 1241.

36.   Hyatt, J.A. *J. Org. Chem.* **1978**, *43*, 1808.

37.   Fessner, W.D.; Sedelmeier, G.; Spurr, P.R.; Rihs, G.; Prinzbach, H. *J. Am. Chem. Soc.* **1987**, *109*, 4626.

38.   Pallavicini, P.S.; Perotti, A.; Poggi, A.; Seghi, B.; Fabbrizzi, L. *J. Am. Chem Soc.* *187*, **109**, 5139.

39.   Sargeson, A.M. *Chem. Brit.* **1979**, *15*, 23.

40.   Canceill, J.; Collet, A.; Gabard, J.; Kotzyba-Hilbert, F.; Lehn, J.M. *Helv. Chim. Acta*, **1982**, *65*, 1894.

41.   Cram, D.J. *Angew. Chem. Int. Ed. Engl.* **1986**, *25*, 1039.

42.   Bell, T.W.; Firestone, A.; Ludwig, R.; *J. Chem. Soc., Chem. Commun.* **1989**, 1902.

43.   Leppkes, R.; Vögtle, F. *Angew. Chem. Int. Ed. Engl.* **1981**, *20*, 396.

44.   Zimmerman, S.C.; Wu,W. *J. Am. Chem. Soc.* **1989**, *111*, 8054.

45.   Arrhenius, T.S.; Blanchard-Desce, M.; Dvolaitzky, M.; Lehn, J.M. Malthete, J. *Proc. Natl. Acad. Sci.*, *1986*, **83**, 5355.

46.   (a) Schierbaum, K.D.; Weiss, T.; Thoden van Velzen, E.U.; Engbersen J.F.J; Reinhoudt, D.N; Göpel, W. *Science*, **1994**, *265*, 1413. (b) Göpel, W. *Sens. Actuators B.*, **1994**, *18-19*, 1. (c)Weimar, U.; Vaihinger, S.; Schierbaum, K.D.; Göpel, W. *Chemical Sensor Technology*, Kodansha: Tokyo, **1991**, *3*, 51. (c) Hierlemann, A.; Weimar, U. Kraus, G.; Gauglitz, G.; Göpel, W. *Sensors and Materials*, 1995.

47. (a) Reinhoudt, D.N.; Sudholter. E. J.R. *Adv. Mater.* **1990**, *2*, 23. (b) Cobben, P.L.H.M.; Egberink, R.J.M.; Bomer, J.G.; Bergveld, P. Verboom, W.; Reinhoudt, D.N. *J. Am. Chem. Soc.* **1992**, *114*, 10573.

48. Hafeman, G.; Parce, J.W. McConnell, H.M. *Science*, **1988**, *240*, 1182.

49. Wenz, G. *Angew. Chem. Int. Ed. Engl.* **1994**, *33*, 803.

50. (a) Saenger, W. *Angew. Chem. Int. Ed. Engl.* **1980**, *19*, 344. (b) Saenger, W. *Inclusion Compounds* **1984**, *2*, 231.

51. Breslow, R. *Acc. Chem. Res.* **1995**, *28*, 146.

52. Tabushi, I. *Acc. Chem. Res.* **1982**, *15*, 66.

53. Szejtli, J. *Cyclodextrins and Their Inclusion Compounds*, Aladémiai Kiadó: Budapest, 1982.

54. Bender, M.L.; Komiyama, M. *Cyclodextrin Chemistry* Springer Verlag: New York 1978.

55. Okada, Y.; Kubota, Y.; Koizumi, K.; Hizukuri, S.; Ohfuji, T.; Ogata, K. *Chem. Pharm. Bull.* **1988**, *36*, 2176.

56. Broser, W. *Z. Naturforsch.* **1953**, *8b*, 722.

57. Sakurai, M.; Kitagawa, M.; Hoshi, H. *Chem. Lett.* **1988**, 895.

58. Cramer, F. *Chem. Ber.* **1951**, *84*, 851.

59. Broser, W.; Lautsch, W. *Naturwiss.*, **1953**, *40*, 220.

60. Cramer, F. *Chem. Ber.*, **1953**, *86*, 1582.

61. Kinoshita, F.; Iinuma, F.;Tsuji, A. *Biochem. Biophys. Res. Commun.* **1973**, *51*, 666.

62. Cramer, F.; Hettler, H. *Naturwiss.* **1967**, *54*, 625.

63. Labianco, D.A. *J. Chem. Ed.* **1990**, *67*, 259.

64. Wisemann, A. *Trends Anal. Chem.* **1988**, *7*, 5.

65. Ruz, J.; Fernandez, A.; Luque de Castro, M.D.; Valcarcel, M.J. *Pharm. Biomed. Anal.* **1986**, *4*, 559.

66. Völkl, K.-P.; Opitz, N.; Lübbers, D.W. *Fresenius' Z. Anal. Chem.* **1980**, *301*, 162.

67. Wolfbeis, O.S.; Posch, H.E. *Fresenius' Z. Anal. Chem.* **1988**, *332*, 255.

68. Schirmer, R.E.; Zetter, M. *Adv. Instrum.* **1987**, *42*, 173.

69. Maeder, G.; Veuthey, J.-L.; Pelletier, M.; Haerdi, W. *Anal. Chim. Acta* **1990**, *231*, 115.

70. Walters, B.S.; Nielson, T.J.; Arnold, M.A. *Talanta* **1988**, *35*, 151.

71. Scheper, T.; Buckmann, A.F *Biosens. Bioelectron.,* **1990**, *5*, 125.

72. Gautier, S.M.; Blum, L.J.; Coulet, P.R. *Biolum. Chemilumin.* **1990**, *5*, 57.

73. (a) Borkenstein, R.F. U.S. Patent 2 824 789, 1958. (b) Borkenstein, R.F.; Smith, H.W. *Med. Sci. Law* **1961**, *2*, 13.

74. Intoximeters Inc. 1994-1995 http://www.intox.com

75. Stafford, D.T. "Investigation of the Response of Fuel Cell Based Alcohol Breath Test Instruments to Substances Other than Ethanol:" 1993, Tennessee: University of Tennessee Toxicology Laboratory.

76. Hayes, E.T.; Galal, A.; Mark, H.B, Jr. *Talanta,* **1995**, *42*, 873.

77. Stiller, M. *Anal. Chim. Acta* **1961**, *25*, 85.

78. Tanaka, M. *Talanta* **1960**, *5*, 162.

79. Seiler, K.; Wang, K.; Kuratli, M.; Simon, W. *Anal. Chim. Acta* **1991**, *244*, 151.

80. Kurauchi, Y.; Yanai, T. Ohga, K. *Chem. Lett.* **1991**, 1411.

81. Orellana, G.; Gómez-Carneros, A.M.; de Dios, C.; García-Martínez, A.A.; Moreno-Bondi, M.C. *Anal. Chem.* **1995**, *67*, 2231.

82. Zeng, H.-H.; Wang, K.-M.; Dong, L.; Yu, R.-Q. *Talanta*, **1994**, *41*, 969.

83. Woflbeis, O.S. *Fresenius' Z. Anal. Chem.* **1986**, *325*, 387.

84. Ueno, A. In *Photochemistry in Organized and Contrained Media*; Ramamurthy, V., Ed. ; VCH: New York, 1991.

85. Balzani, V.; Scanola, F. *Supramolecular Photochemistry*; Ellis Horwood: West Sussex, England, 1991; Chapter 10.

86. Kalyanasundaram, K. *Photochemistry in Microheterogenous Systems*; Academic: Orlando, FL, 1987.

87. Eaton, D.F. *Tetrahedron* **1987**, *43*, 1551.

88. Schuette, J.M.; Ndou, T.T.; Muñoz de la Peña, A.; Mukundan, S., Jr.; Warner, I.M. *J. Am. Chem. Soc.* **1993**, *115*, 292 and references therein.

89. (a) Patonay, G.; Fowler, K. Shapira, A.; Nelson, G.; Warner, I.M. *J. Inclusion Phenom.* **1987**, *5*, 717. (b) Nelson, G.; Patonay, G.; Warner, I.M. *Anal. Chem.* **1988**, *60*, 274. (c) Zung, J.B.; Muñoz de la Peña, A.; Ndou, T.T.; Warner, I.M. *J. Phys. Chem.* **1991**, *195*, 6701. (d) Muñoz de la Peña, A.; Ndou, T.T.; Zung, J.B.; Greene, K.L.; Live, D.H.; Warner, I.M. *J. Am. Chem. Soc.* **1991**, *113*, 1572.

90. Nakajim, A. *Bull. Chem. Soc. Jpn.* **1984**, *57*, 1143.

91. Ueno, A.; Takahashi, K.; Hino, Y.; Osa, T *J. Chem. Soc., Chem. Commun.* **1981**, 194.

92.　Hamai, S. *J. Am. Chem. Soc.* **1989**, *111*, 3954. (b) Hamai, S. *J. Phys. Chem.* **1989**, *93*, 2074.

93.　Bergmark, W.R.; Davis, A.; York, C.; Macintosh, A.; Jones, G., II *J. Phys. Chem.* **1990**, *94*, 5020.

94.　(a) Nelson, G.; Warner, I.M. *J. Phys. Chem.* **1990**, *94*, 576. (b) Nelson, G.; Neal, S.L.; Warner, I.M. *Spectroscopy* **1988**, *3*, 24.

95.　(a)Scypinski, S.; Love, L.J.C. *Anal. Chem.* **1984**, *56*, 322. (b) Femia, F.A.; Love, L.J.C. *J. Phys. Chem.* **1985**, *89*, 1897.

96.　(a) Turro, N.J.; Bolt, J.D.; Kuroda, Y.; Tabushi, I. *Photochem. Photobiol.*, **1982**, *35*, 69 (b) . Turro, N.J.; Cox, G.S.; Li, X. *Photochem. Photobiol.*, **1983**, *37*, 149.

97.　Alak, A.M.; Vo-Dinh, T. *Anal. Chem.* **1988**, *60*, 596.

98.　Richmond, M.D.; Hurtubise, R.J. *Anal. Chem.* **1989**, *61*, 2643.

99.　Turro, N.J.; Okubo, T.; Chung, C.-J. *J. Am. Chem. Soc.* **1982**, *104*, 1789.

100.　Ponce, A.; Way, J.J.; Wong, P.A.; Nocera, D.G *J. Phys. Chem.* **1994**, *97*, 11137.

101.　Mortellaro, M.A.; Hartmann, W.K.; Nocera, D.G. *Angew. Chem. Int. Ed. Engl.* **1996**, *35*, 1945.

102.　Mussel, R.D.; Nocera, D.G. *J. Am. Chem. Soc.* **1988**, *110*, 2864.

103.　Saari, E. Ph.D. Thesis, M.S.U.

104.　(a)Muñoz de la Peña, A.; Ndou, T.T; Zung, J.B.; Greene, K.L; Live, D.H.; Warner, I.M. *J. Am. Chem. Soc.* **1991**, *113*, 1572. (b)Hamai, S. *J. Phys. Chem.* **1988**, *92*, 6140. (c)Hamai, S. *J. Phys. Chem.* **1989**, *93*, 2047.

105.　Eaton, D.F. in *Handbook of Photochemistry*; Scaiano, J.C. Ed.; CRC: Boca Raton, 1989; Vol 1, Chapter 4.

106. Lakowicz, J.R. *Principles of Fluorescence Spectroscopy*; Plenum Press: New York, 1983.

107. Jackson, J.A.; Turro, D.; Newsham, M.D.; Nocera, D.G. *J. Phys. Chem.* **1990**, *94*, 4500.

108. Muñoz de la Peña, A.; Ndou, T.T.; Zung, J.B.; Warner, I.M. *J. Phys. Chem.* **1991**, *95*, 3330.

109. (a) Muñoz de la Peña, A.; Ndou, T.T.; Zung, J.B.; Greene, K.L.; Live, D.H.; Warner, I.M. *J. Am. Chem. Soc.* **1991**, *113*, 1572. (b) Hamai, S. *J. Phys. Chem.* **1988**, *92*, 6140 (c) Hamai, S. *J. Phys. Chem.* **1989**, *93*, 2074.

110. Turro, N.J.; Bolt, J.D.; Kuroda, Y.; Tabushi, I. *Photochem. Photobiol.* **1982**, *35*, 69.

111. Hamai, S. *J. Am. Chem. Soc.* **1989**, *111*, 3954.

112. (a)Harata, K.; Uedaira, H. *Bull. Chem. Soc. Jpn.* **1975**, *48*, 375. (b)Hamai, S. *Bull. Chem. Soc. Jpn.* **1982**, *55*, 2721. (c)Yorozu, T.; Hoshino, M. Imamura, M.; Shizuka, H. *J. Phys. Chem.* **1982**, *86*, 4422. (d)Hashimoto, S.; Thomas, J.K. *J. Am. Chem. Soc.* **1985**, *107*, 4655. (e)Nelson, G.; Warner, I.M. *J. Phys. Chem.* **1990**, *94*, 546. (f)Pitchumani, K. Vellayappan, M. *J. Incl. Phenom.* **1992**, *14*, 157.

113. Liao, Y.; Frank, J.; Holzwarth, J.F; Bohne, C.J. *J. Chem. Soc. Chem. Commun.* **1995**, 199.

114. (a) Ravi, M.; Soujanya, A.; Samanta, A.; Radhakrishnan, T.P. *J. Chem. Soc. Faraday Trans.*, **1995**, *91*, 2739. (b) Ravi, M.; Smanata, A.; Radhakrishnan *J. Phys. Chem.* **1994**, *98*, 9133. (c) Abe, T. *Bull. Chem. Soc. Jpn.* **1991**, *64*, 3224.

115. (a)Bissel, R.A.; de Silva, A.P. *J. Chem. Soc. Chem. Commun.* **1991**, 223. (b)Beecroft, R.A.; Davidson, R.S.; Goddwin, Pratt, J.E.; Luo, X.J. *J. Chem. Soc., Faraday Trans. 2*, **1986**, *82*, 2393. (c)Yip, R.W.; Loutfy, R.O.; Chow, Y.L.; Magdzinski, L. *Can. J. Chem.* **1972**, *50*, 3426.

116. Park, J.H.; Nah, T.H. *J. Chem. Soc. Perkin Trans. 2* **1994**, 1359.

117. (a)Breslow, R.; Czarnik, A.W. *J. Am. Chem. Soc.* **1983**, *105*, 1390 (b) Breslow, R.; Hammond, M.; Lauer, M. *ibid.* **1980, 102**, 421.

118. Martin, K.A.; Mortellaro, M.A.; Sweger, R.W.; Fikes, L.E.; Winn, D.T.; Clary, S.C.; Johnson, M.P.; Czarnik, A.W. *J. Am. Chem. Soc.* **1995**, *117*, 10443.

119. Rao, K.R.; Srinivasan, T.N.; Bhanumathi, N.; Sathur, P.B. *J. Chem. Soc. Chem. Commun.* **1990**, 10 (b) Cramer, F.; Mackensen, G. *Angew Chem. Int. Ed. Engl.* **1966**, *5*, 601.

120. Fabbrizzi, L.; Poggi, A. Chem. Soc. Rev. 1995, 197 (b) Czarnik, A.W. *Acc. Chem. Res.* **1994**, *27*, 302. (c) *Fluorescent Chemosensors for Ion and Molecular Recognition* (*ACS Symp. Ser.* **1993**, 538).

121. Pikramenou, Z; Yu, J.A.; Lessard, R.B.; Ponce, A.; Wong, P.A.; Nocera, D.G. *Coord. Chem. Rev.* **1994**, *132*, 181.

122. Ueno, A.; Suzuki, I.; Osa, T. *J. Am. Chem. Soc.* **1989**, *111*, 6391.

123. Park, J.W.; Park, K.H. *J. Inclusion Phenom. Mol. Recog. Chem.* **1994**, *17*, 277.

124. Connors, K.A. *Binding Constants*; Wiley: New York, 1987.

125. van Dienst, E.; Snellink, B.H. M.; von Piekartz, I.; Engbersen, J.F.J.; Reinhoudt, D.N. *J. Chem. Soc. Chem. Commun.* **1995**, 1151.

126. Turro, N.J.; Okube, T.; Chung, C.-J. *J. Am. Chem. Soc.* **1982**, *104*, 1789.

127. Rademacher, J.T.; Nocera, D.G., unpublished results.

128. Harata, K.; Uedaira, H. *Bull. Chem. Soc. Jpn.* **1975**, *48*, 375.

129. van Grondelle, R; Dekker, J.P.; Gilbro, T.; Sundstrom, V. *Biochem. et. Biophys. Acta* **1994**, *1187*, 1.

130. (a)Förster, Th. *Annalen der Physik* **1948**, *2*, 55; English translation in *Biological Physics* Mielczarek, E.V., Greenbaum, E., and Knox, R. S., Eds.; American

Institue of Physics: New York, 1993; p.148-60. (b)Förster, Th. *Discuss. Faraday Soc.* **1959**, *27*, 7. (c)Förster, Th. *Z. Naturforsch.* **1949**, *4a*, 321.

131. Van Der Meer, W.B.; Coker, G.; Chen, S.S.-Y. *Resonance Energy Transfer Theory and Data*; VCH: New York, 1994.

132. (a)Berberan-Santos, M.N.; Canceill, J.; Brochon, J.C.; Jullien, L.; Lehn, J.-M.; Pouget, J.; Tauc, P.; Valeur, B. *J. Am. Chem. Soc.* **1992**, *114*, 6427. (b)Berberan-Santos, M.N.; Pouget, M.; Valeur, B.; Canceill, J.; Jullien, L.; Lehn, J.M. *J. Phys. Chem.* **1993**, *97*, 11376. (c)Berberan-Santos, M.N.; Canceill, J.; Gratton, E.; Jullien, L.; Lehn, J.-M.; So, P.; Sutin, J.; Valeur *J. Phys. Chem.* **1996**, *100*, 15. (d)Jullien, L.; Canceill, J.; Valeur, B.; Bardez, E.; Lefèvre, J-P.; Lehn, J.-M.; Marchi-Artzner, V.; Pansu, R. *J. Am. Chem. Soc.* **1996**, *118*, 5432.

133. Daschak, D.M.; Mallouk, T.E. *J. Am. Chem. Soc.* **1996**, **118**, 4222.

134. Dexter, D.L. *J. Chem. Phys.* **1953**, *21*, 836.

135. (a)Closs, G.L.; Piotrowiak, P.; MacInnis, J.M.; Fleming, G.R. *J. Am. Chem. Soc.* **1988**, *110*, 2652. (b)Closs, G.L; Johnson, M.D.; Miller, J.D.; Piotrowiak, P. *J. Am. Chem. Soc.* **1989**, *111*, 3751. (c) Sigman, M.E.; Closs, G.L. *J. Phys. Chem.* **1991**, *95*, 5012.

136. Farran, A.; Deshayes, K.D. *J. Phys. Chem.* **1996**, *100*, 3305.

137. (a)Farhoosh, R.; Chynwat, V.; Gebhard, R.; Lugtenburg, J.; Frank, H.A. *Photosyn. Res.* **1994**, *42*, 157. (b)Wasielewski, M.R.; Liddell, P.A.; Barrett, D.; Moore, T.A; Gust, D. *Nature*, **1986**, *322*, 570.

138. Bunzli, J.-C.G. in *Lanthanide Probes in Life, Chemical and Earth Sciences*; J.-C.G. Bunzli and G.R. Choppin Eds.; Elsevier: Amsterdam, 1988; Ch. 7, p. 219.

139. (a)Judd, B.R. *Phys. Rev.* **1962**, *127*, 750. (b)Ofelt, G.S. *J. Chem. Phys.* **1962**, *73*, 511. (c)Ofelt, G.S. *J. Chem. Phys.* **1963**, *38*, 2171.

140. (a)Fong, F.K.; Naberhuis, S.L.; Miller, M.M. *J. Chem. Phys.* **1972**, *56*, 4020. (b)Miller, M.M. *Chem. Phys. Lett.* **1971**, *10*, 408. (c)Tallant, D.R.; Miller, M.R.; Wright, J.C. *J.Chem. Phys.* **1976**, *65*, 510.

141.   Richter-Lusting, H.; Ron, A.; Speiser, S. *Chem. Phys. Lett.* **1982,** *85,* 576.

142.   (a)Horrocks, W.D.; Albin, M. in *Prog. Inorg. Chem.* S.J. Lippard Ed.; Wiley: New York, 1984; Vol. 31, p. 1. (b)Horrocks, W.D.; Sudnick, D.R. *J. Am. Chem. Soc.* **1979,** *101,* 335.

143.   Yu, J.-a.; Lesarard, R.B.; Bowman, L.E.; Nocera, D.G. *Chem. Phys. Lett.* **1991,** *187,* 263.

144.   (a) Crosby, G.A.; Watts, R.J.; Westlake, S.J.; *J. Chem. Phys.* **1971,** *55,* 4663. (b) Sahbari, J.J.; Bomben, K.D; Tinti, D.S. *J. Am. Chem. Soc.* **1983,** *105,* 5577. (c) Marciniak, B.; Buono-Core, G.E. *J. Photochem. Photobiol. A* **1990,** *52,* 1.

145.   (a)Crosby, G.A. *Molecular Crystals* **1966,** *1,* 37. (b)Freeman, J.J.; Crosby, G.A. *J. Phys. Chem.* **1963,** *67,* 2717. (c)Whan, R.E.; Crosby, G.A. *J. Mol. Spectry.* **1962,** *8,* 315. (d)Crosby, G.A.; Whan, R.E.; Alire, R.M. *J. Chem. Phys.* **1961,** *34,* 743.

146.   Brown, A.; Wilkinson, F. *J. Chem. Soc. Faraday Trans. 2* **1979,** *75,* 880.

147.   Almgren, M.; Thomas, J.K. *J. Am. Chem. Soc.* **1979,** *101,* 2021.

148.   (a)Rudkevich, D.M.; Verboom, W.; van der Tol, E.; van Staveren, C.J.; Kaspersen, F.M.; Verhoeven, J.W. Reinhoudt, D.N. *J. Chem. Soc. Perkin Trans. 2,* **1995,** 131. (b)Steemers, F.J.; Verboom, W.; Reinhoudt, D.N.; van Der Tol, E.B.; Verhoeven, J.W. *J. Am. Chem. Soc.,* **1995,** *117,* 9408.

149.   Buono-Core, G.E.; Li, H.; Marciniak, B.; *Coord. Chem. Rev.* **1990,** *99,* 55.

150.   Tobita, S.; Arakawa, M.; Tanaka, I. *J. Phys. Chem.* **1985,** *89,* 5649.

151.   Bhaumik, M.L.; El Sayed, M.A. *Appl. Opt. Supp.* **1965,** *2,* 214.

152.   Wagner, P.J.; Schott, H.N. *J. Phys. Chem.* **1968,** *72,* 3702.

153.   Alpha, B.; Ballardini, R.; Balzani, V.; Lehn, J.-M.; Perathoner, S.; Sabbatini, N. *Photochem. Photobiol.* **1990,** *52,* 299.

154. Onuska, F.I. in B.K. Afghan and A.S.Y. Chau (Eds.) *Analysis of Trace Organics in the Aquatic Environment*, CRC: Boca Raton, F. 1990, 205.

155. Neff, J.M. *Polycyclic Aromatic Hydrocarbons in the Aquatic Environment*, Applied Science: Barking, 1979.

156. Vo-Dinh, T. in Vo-Dinh (Ed.) *Chemical Analysis of Polycyclic Aromatic Hydrocarbons*, Wiley: New York, 1990, 1.

157. Futoma, D.J.; Smith, S.R.; Smith T.E.; Tanaka, J. *Polycyclic Aromatic Hydrocarbons in Water Systems*, CRC: Boca Raton, FL, 1981.

158. Thomas, S.P.; Ranjan, R.; Webster, G.R.B.; Sarna, L.P. *Environmental Science and Technology* **1996**, *30*, 1521.

159. C.E. Anson, C.S. Creaser, G.R. Stephenson, *Spectrochimica Acta A* **1996**, *52*, 1183.

160. Brown, R.S.; Luong, J.H.T.; Szolar, O.G.J.; Halasz, A.; Hawari, J. *Anal. Chem.* **1996**, *68*, 287.

161. Ariese, F.; Kok, S.J.; Verkaik, M.; Gooijer, C.; Velthorst, N.H.; Hofstraat, J.W. *Aquatic Toxicology*, **1993**, 275.

162. Carretero, A.S.; Blanco, C.C.; Gutiérrez, A.F. *Anal. Chim. Acta* **1996**, *329*, 165.

163. Alarie, J.P.; Vo-Dinh, T.; Miller, G.; Ericson, M.N.; Eastwood, D.; Lidberg R.; Dominguez, M. *Rev. Sci. Instrum.* **1993**, *64*, 2541.

164. Fletcher, P.E.; Cooper, J.B.; Vess, T.M.; Welch, W.T. *Spectrochimica Acta Part A* **1996**, *52*, 1235.

165. M.T. Tena, M.D. Luque de Castro, M. Valcárcel, *Anal. Chem.* **1996**, *68*, 2386.

166. Barber, T.E.; Fisher, W.G.; Wachter, E.A. *Environ. Sci. Technol.* **1995**, *29*, 1576.

167. Niessner, R.; Panne, U.; Schröder, H. *Anal. Chim. Acta* **1991**, *255*, 231.

168. Weiss, M. *Today's Chemist at Work* **1995**, *4*, 25.

169. Owen, H. *Proc SPIE-Int. Soc. Opt. Eng. (Opt. Based Methods Process. Anal.)*, **1992**, *1681*, 128

170. Pauls, R.E.; Weight, F.J.; Munowitz, P.S. *J. Chromatogr. Sci*, **1992**, *30*, 32.

171. Schirmer, R.E.; Fopulk, S. *Adv. Instrum. Control*, **1990**, *45*, 1529.

172. Maggard, S.M. *Am. Chem. Soc. Div. Fuel Chem.*, **1990**, *35*, 95.

173. Parisi, A.F.; Nogueiras, H.P. *Anal. Chim. Acta*, **1990**, *283*, 95.

174. Davoli, E.; Cappellini, L.; Moggi, M.; Ferrari, S.; Fanelli, R. *Internal Archives of Occupation and Environmental Health* **1996**, *68*, 262.

175. Riedel, K.; Ruppert, T.; Conze, C.; Scherer, G.; Adlkofer, F. *J. of Chromatography A* **1996**, *719*, 383.

176. Pikramenou, Z.; Nocera, D.G. *Inorg. Chem.* **1992**, *31*, 532.

177. Pikramenou, Z.; Johnson, K.M.; Nocera, D.G. *Tetrahedron Lett.* **1993**, *34*, 3531.

178. Mortellaro, M.A.; Nocera, D.G. *J. Am. Chem. Soc.* **1996**, *118*, 7414.

179. Hartmann, W.K.; Mortellaro, M.A.; Nocera, D.G.; Pikramenou, Z. *Chemosensors of Ion and Molecule Recognition, NATO ASI series*; Kluwer Academic: Dordrecht, 1997, in press.

180. (a)Bowman, L.E.; Berglund, K.A.; Nocera, D.G. *Rev. Sci. Instr.* **1993**, *64*, 338. (b)Bowman, L.E. M.S.U. Ph.D. Thesis, 1991.

181. Kim, J.; Hartman, W.K.; Schock, H.J.; Golding, B.; Nocera, D.G. *Chem Phys. Lett.* **1997**, *267*, 323.

182. Mortellaro, M.A.; Nocera, D.G., unpublished results.

183. Murov, S.L; Carmichael, I.; Hug, G.L. *Handbook of Photochemistry*; Marcel Dekker: New York, 1993.

184. Carnall, W.T.; Fields, P.R.; Rajnak, K. *J. Chem. Phys.* **1968**, *49*, 4447.

185. Horrocks, W.D. ACS Meeting, San Francisco, 1997

186. Rudzinski, C.K.; Nocera, D.G., unpublished results.

187. (a)Fujii, T.; Suzuki, A.; Komatsu, S. *Chem. Phys. Lett.* **1978**, *57*, 175. (b)Nijegorodov, N.I.; Downey, W.S. *J. Phys. Chem.* **1994**, *98*, 5639.

188. Hartmann, W.K., Nocera, D.G., unpublished results.

189. Suzuki, Y.; Morozumi, T.; Kakizawa, Y.; Bartsch, R.A.; Hayashita, T.; Nakamura, H.; *Chem. Lett.* **1996**, 547.

190. Casnati, A.; Fischer, C.; Guardigli, M.; Isernia, A.; Manet, I.; Sabbatini, N.; Ungaro, R. *J. Chem. Soc. Perkins Trans. 2* **1995**, 395.

191. Itaya, T.; Sasaki, Y.; Tanigaki, T.; Matsumoto, A.; Inoue, K. *Chem. Lett.* **1996**, 305.

192. Matsumoto, H.; Ori, A.; Inokuchi, F.; Shinkai, S. *Chem. Lett.,* **1996**, 301.